

NONLINEAR DYNAMIC INVERSION AUTOPILOT DESIGN FOR AN AIR  
DEFENSE SYSTEM WITH AERODYNAMIC AND THRUST VECTOR  
CONTROL

A THESIS SUBMITTED TO  
THE GRADUATE SCHOOL OF NATURAL AND APPLIED SCIENCES  
OF  
MIDDLE EAST TECHNICAL UNIVERSITY

BY

RABIYA BIYIKLI

IN PARTIAL FULFILLMENT OF THE REQUIREMENTS  
FOR  
THE DEGREE OF MASTER OF SCIENCE  
IN  
AEROSPACE ENGINEERING

FEBRUARY 2022



Approval of the thesis:

**NONLINEAR DYNAMIC INVERSION AUTOPILOT DESIGN FOR AN  
AIR DEFENSE SYSTEM WITH AERODYNAMIC AND THRUST  
VECTOR CONTROL**

submitted by **RABİYA BIYIKLI** in partial fulfillment of the requirements for the degree of **Master of Science in Aerospace Engineering, Middle East Technical University** by,

Prof. Dr. Halil Kalıpçılar  
Dean, Graduate School of **Natural and Applied Sciences** \_\_\_\_\_

Prof. Dr. Serkan Özgen  
Head of the Department, **Aerospace Engineering** \_\_\_\_\_

Assoc. Prof. Dr. İlkay Yavrucuk  
Supervisor, **Aerospace Engineering Dept., METU** \_\_\_\_\_

Dr. Raziye Tekin  
Co-Supervisor, **TMS Dept., Roketsan Missiles Inc.** \_\_\_\_\_

**Examining Committee Members:**

Prof. Dr. Kemal Leblebicioğlu  
Electrical and Electronics Engineering Dept., METU \_\_\_\_\_

Assoc. Prof. Dr. İlkay Yavrucuk  
Aerospace Engineering Dept., METU \_\_\_\_\_

Assist. Prof. Dr. Ali Türker Kutay  
Aerospace Engineering Dept., METU \_\_\_\_\_

Assist. Prof. Dr. Kutluk Bilge Arıkan  
Mechanical Engineering Dept., TEDU \_\_\_\_\_

Assist. Prof. Dr. Yakup Özkazanç  
Electrical and Electronics Engineering Dept., HACETTEPE U. \_\_\_\_\_

Date: 07.02.2022

**I hereby declare that all information in this document has been obtained and presented in accordance with academic rules and ethical conduct. I also declare that, as required by these rules and conduct, I have fully cited and referenced all material and results that are not original to this work.**

Name Last name : Rabiya Bıyıklı

Signature :

## **ABSTRACT**

### **NONLINEAR DYNAMIC INVERSION AUTOPILOT DESIGN FOR AN AIR DEFENSE SYSTEM WITH AERODYNAMIC AND THRUST VECTOR CONTROL**

Bıyıklı, Rabiya  
Master of Science, Aerospace Engineering  
Supervisor: Assoc. Prof. Dr. İlkey Yavrucuk  
Co-Supervisor: Dr. Raziye Tekin

February 2022, 109 pages

The study proposes complete attitude and acceleration autopilots in all three channels of a highly agile air defense missile by utilizing a subcategory of nonlinear feedback linearization methods Nonlinear Dynamic Inversion (NDI). The autopilot design includes cross-coupling effects enabling bank-to-turn (BTT) maneuvers and a rarely touched topic of control in the boost phase with hybrid control which consists of both aerodynamic fin control and thrust vector control. This piece of work suggests solutions to exclusive challenges of a system, such as non-minimum phase characteristics and mechanical coupling, which can also be referred to as the integrated mechanic design of TVC jet vanes and aerodynamic fins. A physically inspired solution to a non-minimum phase of a tail-controlled system is offered by performing output redefinition on the center of percussion of the missile. A cascaded two-loop structure is established with the fast loop inside and the slower loop outside. The thesis further analyses these designs with certain commands to create a highly coupled environment. In addition, the effects of uncertainties observed on the system with a selection of realistic uncertainty levels on parameters. Moreover, a realistic guided scenario in a 6-DOF simulation

environment with the implementation of realistic sensor models and available feedbacks in real life for such air defense systems is inspected.

Keywords: Nonlinear Dynamic Inversion, Air Defense Missile, Non-minimum Phase, Thrust Vector Control, Output Redefinition

## ÖZ

### **AERODİNAMİK VE İTKİ VEKTÖR KONTROLLÜ BİR HAVA SAVUNMA SİSTEMİ İÇİN DOĞRUSAL OLMAYAN DİNAMİK TERSLEMEYLE OTOPILOT TASARIMI**

Bıyıklı, Rabiya  
Yüksek Lisans, Havacılık ve Uzay Mühendisliği  
Tez Yöneticisi: Doç. Dr. İlkay Yavrucuk  
Ortak Tez Yöneticisi: Dr. Raziye Tekin

Şubat 2022, 109 sayfa

Bu çalışma, çevik bir hava savunma füzesinin her üç kanaldaki ivme ve açı otopilotları için doğrusal olmayan geri besleme doğrusallaştırma yöntemlerinin alt bir kategorisi olan Doğrusal Olmayan Dinamik Tersine Çevrim yöntemini önermektedir. Otopilot tasarımı, çapraz bağlaşım etkilerini dahil ederek yatarak dönme ve yüksek ivme komutlu manevralara olanak sağlamakla birlikte, nadiren değinilen yanma fazında hem aerodinamik kanatçık kontrolü hem de itki vektör jet kanadı kontrolü içeren hibrit bir kontrolü kapsamaktadır. Bu çalışma, sistemin kuyruk kontrollü olması, farklı fiziksel prensiplerle çalışan kontrol yüzeylerinin olması ve bu yüzeylerin bu tarz sistemlerde entegre tasarlanabilmesi gibi sisteme özel zorluklara çözümler üretmektedir. Bu sorunlar için fiziksel bir temele dayandırılarak füzenin perküsyon merkezine göre yeniden çıktı tanımlama yapılmıştır. İç içe iki döngü yapısı içeride hızlı döngü, dışarıda yavaş döngü olacak şekilde kurgulanmıştır. Tasarlanan yapı belirli komutlarla altı serbestlik dereceli simülasyon ortamında test edilmiş, analizlere hassasiyet analiziyle, gerçekçi bir güdümlü senaryo da dahil edilmiştir.

Anahtar Kelimeler: Doğrusal Olmayan Dinamik Tersine Çevrim, Hava Savunma Füzesi, Aerodinamik Kuyruk Kontrolü, İtke Vektör Kontrolü, Yeniden Çıktı Tanımlama

To people who care about little things in life

## ACKNOWLEDGMENTS

I would like to express my sincere acknowledgements to my supervisor Assoc. Prof. Dr. İlkey Yavrucuk for his belief in me and his supervision.

And, I would like to express my deepest gratitudes to my co-supervisor Dr. Raziye Tekin for her guidance, endless support, and precious comments.

I would like to extend my acknowledgments to thesis committee members for their insightful comments.

I would like to express my appreciation to all of my colleagues for their unwavering help, especially Suzan Kale Güvenç for her kindness, encouragement and understanding.

My special thanks to Doğa Akgün and Ceren Cansu Esmek for standing by me no matter what and never withholding their love.

Last but not least, I would like to thank my mother Sibel Bıyıklı, my father Ahmet Bıyıklı and my sisters Nesibe Ölger and Zeynep Bıyıklı for their everlasting love, patience and support.

## TABLE OF CONTENTS

ABSTRACT .....	v
ÖZ.....	vii
ACKNOWLEDGMENTS .....	x
TABLE OF CONTENTS.....	xi
LIST OF TABLES.....	xiii
LIST OF FIGURES .....	xiv
LIST OF ABBREVIATIONS .....	xvii
1 INTRODUCTION .....	1
1.1 Motivation .....	3
1.2 Contribution of Thesis.....	3
1.3 Outline .....	4
2 LITERATURE REVIEW.....	5
3 PRELIMINARIES .....	9
3.1 Plant Model.....	9
3.1.1 Reference Frames and Transformation Matrices .....	9
3.1.2 Kinematic Relations .....	11
3.1.3 Dynamic Relations .....	11
3.1.4 Subsystem Models.....	14
3.2 Review of Nonlinear Feedback Linearization .....	23
3.2.1 Basic Idea of Nonlinear Feedback Linearization .....	23
3.2.2 Input-Output Feedback Linearization.....	26
3.2.3 Necessary Conditions and Formal Definitions.....	29

3.3	Review of Baseline Autopilot Design.....	30
4	AUTOPILOT DESIGN WITH NONLINEAR FEEDBACK LINEARIZATION.....	33
4.1	Attitude Autopilot .....	33
4.1.1	Problem Formulation .....	33
4.1.2	Inner Loop Design.....	34
4.1.3	Outer Loop Design .....	44
4.1.4	Evaluation of Nominal Attitude Autopilot.....	47
4.2	Acceleration Autopilot .....	51
4.2.1	Problem Formulation .....	52
4.2.2	Minimum Phase Output Definition .....	53
4.2.3	Inner Loop Design.....	56
4.2.4	Outer Loop Design .....	56
4.2.5	Evaluation of Nominal Acceleration Autopilot.....	64
4.3	Sensitivity Analysis.....	75
4.3.1	Sensitivity Analysis for Attitude Autopilot .....	77
4.3.2	Sensitivity Analysis for Acceleration Autopilot .....	80
4.4	Realistic Nonlinear Simulation Scenario .....	83
5	DISCUSSION AND CONCLUSION.....	89
	REFERENCES .....	91
A.	Non-minimum Phase Inspection with Linear Analysis .....	97
B.	Solution for Mechanically Coupled Control Surfaces .....	103

## LIST OF TABLES

### TABLES

Table 1 CAS Parameters .....	22
Table 2 IMU Parameters .....	23
Table 3 Uncertainties for Sensitivity Analysis.....	76

## LIST OF FIGURES

### FIGURES

Figure 1 Body Fixed and Earth Fixed Coordinate Frames .....	10
Figure 2 Generic Thrust Profile (Peterson, 1992) .....	16
Figure 3 TVC Rear View and Side View .....	17
Figure 4 Angle of Attack and Angle of Side Slip .....	19
Figure 5 Reference Model.....	39
Figure 6 Inner Loop Schematic for the Coast Phase .....	40
Figure 7 Perfect Dynamic Inversion Visualization .....	40
Figure 8 Virtual Input Allocation to AC and TVC.....	43
Figure 9 Attitude Autopilot Scheme .....	46
Figure 10 Normalized Euler Angle Tracking Performance of Attitude Autopilot..	48
Figure 11 Normalized Angular Rate Tracking Performance of Attitude Autopilot	49
Figure 12 Normalized Effective Fin Deflections with Attitude Autopilot .....	50
Figure 13 Normalized Values of Mach Number, Angle of Attack and Angle of Sideslip with Attitude Autopilot.....	51
Figure 14 Acceleration Autopilot Scheme .....	63
Figure 15 Normalized Acceleration Tracking Performance for Scenario 1 .....	65
Figure 16 Normalized Angular Rate Tracking Performance for Scenario 1 .....	66
Figure 17 Normalized Effective Fin Deflections for Scenario 1 .....	67
Figure 18 Normalized Values of Mach Number, Angle of Attack, and Angle of Sideslip for Scenario 1 .....	68
Figure 19 Normalized Acceleration Tracking Performance in Comparison with the Baseline Autopilot for Scenario 1 .....	69
Figure 20 Normalized Effective Fin Deflections in Comparison with Baseline Autopilot for Scenario 1.....	70
Figure 21 Normalized Acceleration Tracking Performance for Scenario 2 .....	71
Figure 22 Normalized Angular Rate Tracking Performance for Scenario 2 .....	72
Figure 23 Normalized Effective Fin Deflections for Scenario 2.....	72

Figure 24 Normalized Values of Mach Number, Angle of Attack and Angle of Sideslip for Scenario 2 .....	73
Figure 25 Normalized Acceleration Tracking Performance in Comparison with the Baseline Autopilot for Scenario 2 .....	74
Figure 26 Normalized Effective Fin Deflections in Comparison with Baseline Autopilot for Scenario 2.....	75
Figure 27 Normalized Euler Angle Tracking Performance of Attitude Autopilot under Uncertainties .....	77
Figure 28 Normalized Angular Rates of Attitude Autopilot under Uncertainties ..	78
Figure 29 Normalized Effective Aerodynamic Fin Deflections with Attitude Autopilot under Uncertainties .....	79
Figure 30 Normalized Effective Jet Vane Deflections with Attitude Autopilot under Uncertainties.....	79
Figure 31 Normalized Acceleration Tracking Performance for Scenario 2 under Uncertainties.....	80
Figure 32 Normalized Angular Rates for Scenario 2 under Uncertainties .....	81
Figure 33 Normalized Effective Aerodynamic Fin Deflections for Scenario 2 under Uncertainties.....	82
Figure 34 Normalized Effective Jet Vane Deflections for Scenario 2 under Uncertainties.....	83
Figure 35 Normalized Trajectories of the Missile, and Target for Guided Scenario ( $R_0$ : initial range between missile and target).....	84
Figure 36 Normalized Acceleration Tracking Performance for Guided Scenario ..	85
Figure 37 Normalized Angular Rates for Guided Scenario .....	86
Figure 38 Normalized Effective Fin Deflections for Guided Scenario .....	86
Figure 39 Normalized Values of Mach Number, Angle of Attack and Angle of Sideslip for Guided Scenario.....	87
Figure 40 Pole-Zero Map for the Transfer Function from $\delta e$ to $acgz$ .....	99
Figure 41 Pole-Zero Map for the Transfer Function from $\delta e$ to $apz$ .....	100
Figure 42 Center of Percussion on the Missile .....	101

Figure 43 Movements of Zeros on Pole-Zero Maps with Normalized Location of $x_p$ .....	101
Figure 44 Conversion of Effective Deflections to Real Deflections .....	104
Figure 45 Algorithm Scheme for Imposing Mechanical Coupling to Autopilot Design .....	105
Figure 46 Normalized Acceleration Tracking Performance Comparison for Case 1 and Case 2 .....	106
Figure 47 Normalized Effective Fin Deflection Comparison for Case 1 and Case 2 .....	107
Figure 48 Normalized Elevator Deflection Comparison for Case 1 and Case 2...	107
Figure 49 Normalized Euler Angle Tracking Performance Comparison for Case 1 and Case 2 for Attitude Autopilots .....	108
Figure 50 Normalized Effective Fin Deflection Comparison for Case 1 and Case 2 for Attitude Autopilot .....	108

## LIST OF ABBREVIATIONS

### ABBREVIATIONS

AC: Aerodynamic Control

BTT: Bank-To-Turn

CAS: Control Actuation System

cg: Center of Gravity

cop: Center of Percussion

DOF: Degree of Freedom

IMU: Inertial Measurement Unit

INDI: Incremental Nonlinear Dynamic Inversion

LHP: Left Half Plane

MFC: Model Following Control

MIMO: Multi Input Multi Output

MRAC: Model Reference Adaptive Control

NDI: Nonlinear Dynamic Inversion

NFL: Nonlinear Feedback Linearization

PI: Proportional Integral

RHP: Right Half Plane

SISO: Single Input Single Output

TPN: True Proportional Navigation

TVC: Thrust Vector Control

UAV: Unmanned Aerial Vehicle

VTOL: Vertical Take-off and Landing Vehicle

## LIST OF SYMBOLS

### SYMBOLS

$\phi, \theta, \psi$ : Euler roll, pitch, yaw angles

$p, q, r$ : Roll, pitch, yaw rates of the body

$\omega$ : Angular rates of the body. (A vector consists of  $p, q, r$ )

$u, v, w$ : Translational velocity of the body

$X, Y, Z$ : Aeropropulsive forces on  $x_B, y_B, z_B$  respectively

$L, M, N$ : Moments with respect to  $x_B, y_B, z_B$

$\hat{C}^{(e,b)}$ : Coordinate transformation matrix from vehicle carried frame to body fixed frame

$\vec{F}_B$ : Forces on the body

$\vec{G}_B$ : Moments on the body

$m$ : Mass

$I$ : Inertia matrix

$\vec{g}$ : Gravity vector in vehicle carried coordinate system

$\vec{L}_B$ : Linear momentum of the body

$\vec{H}_B$ : Angular momentum of the body

$\vec{a}_{B/I}^B$ : Acceleration vector of the body with respect to inertial frame written in body frame

$\vec{V}_{B/I}^B$ : Velocity vector of the body with respect to inertial frame written in body frame

$\vec{\omega}_{B/I}^B$ : Angular Velocity vector of the body with respect to inertial frame written in body frame

$T$ : Temperature

$P$ : Pressure

$\rho$ : Air Density

$a$ : Speed of sound

$Ma$ : Mach Number

$Q$ : Dynamic pressure

$F_{Tx}, F_{Ty}, F_{Tz}$ : Thrust forces on  $x_B, y_B, z_B$  respectively

$M_{Tx}, M_{Ty}, M_{Tz}$ : Thrust moments on  $x_B, y_B, z_B$  respectively

$\theta_T, \psi_T$ : Deflection angles of thrust with respect to body in polar coordinates, elevation and azimuth respectively.

$\alpha$ : Angle of attack

$\beta$ : Angle of sideslip

$\delta_{1,2,3,4}$ : Applied fin deflections for general use

$\delta_{A1,2,3,4}$ : Applied aerodynamic fin deflections

$\delta_{T1,2,3,4}$ : Applied jet vane deflections

$\delta_e, \delta_r, \delta_a$ : Effective elevator, rudder aileron inputs respectively for general use

$\delta_{Ae}, \delta_{Ar}, \delta_{Aa}$ : Effective aerodynamic elevator, rudder aileron inputs respectively

$\delta_{Te}, \delta_{Tr}, \delta_{Ta}$ : Effective thrust vector control elevator, rudder aileron inputs respectively

$\delta_A, \delta_T$ : Effective aerodynamic and jet vane deflections respectively

$C_X, C_Y, C_Z$ : Non-dimensional aerodynamic force coefficients in  $x_B, y_B, z_B$  respectively

$C_l, C_m, C_n$ : Non-dimensional aerodynamic moment coefficients in  $x_B, y_B, z_B$  respectively

$\omega_{cas}$ : Natural frequency of CAS

$\zeta_{cas}$ : Damping ratio of CAS

$\omega_{rm}$ : Natural frequencies of reference models

$\zeta_{rm}$ : Damping ratios of reference models

$\sigma$ : Variance

$v$ : Virtual control input

$K_P$ : Proportional gain

$K_I$ : Integral gain

$E$ : Effectiveness ratio of the thrust vector control to aerodynamic control



## CHAPTER 1

### INTRODUCTION

Air defense missiles anticipated fulfilling their task over a spectrum of flight and target conditions. Therefore, these systems are expected to perform agile maneuvers in nonlinear time-varying environments to get their movable targets. Furthermore, to ensure the precise attainment of a target, equipping missiles with different control tools may be seen as a requirement at the system design level, as in this thesis, an air defense missile with aerodynamic control fins and jet vanes for thrust vector control at its tail is considered.

Control design plays an essential role in making maximum use of these systems. As the capabilities, maneuverability, and speed increase, corresponding control problems become more challenging. An apparent reason for this is that using conventional linear controllers on such a system may limit systems' skills besides their tiresome process of gain scheduling.

In contemplation of making the most of the capabilities of the designed system, a Nonlinear Feedback Linearization (NFL) technique is discussed here. In brief, the basic idea of NFL is to cancel nonlinearities and impose the desired dynamics by a coordinate transformation of the nonlinear system into a linear form. Nonlinear Dynamic Inversion (NDI) is a particular form of feedback linearization put in application for many flight control problems since the late 20th century. A very early application is provided in [28]. After recasting the dynamical system in linear form, this method allows design controllers based on linear theory. A proportional-integral (PI) controller with a second-order reference model is preferred in this study.

One disadvantage of NDI is that it is not applicable to non-minimum phase systems due to the direct inversion process, which may cause instability in the closed-loop

system. Aerodynamic tail-controlled missiles are also one of the non-minimum phase systems. To guarantee the stability of the internal dynamics with the transformed system, output redefinition is introduced. In order to avoid the need for accurate information of aerodynamic angles, a physically inspired output redefinition is utilized with a two-time scale cascaded structure as it is proposed in [33].

Another drawback of NDI is known as the robustness issue. It is usually assumed as precise information of state variables, flight parameters, physical and aerodynamic data are essential for NDI-based controllers. This issue is addressed in literature with adaptive additions to controllers. Although this study does not focus on robustness and these adaptive augmentations, example cases are investigated with quite uncertainties concerning to display this dependency in aforementioned parameters. This study applies the described method for designing attitude autopilot and acceleration autopilots, including boost and coast phases. The missile design considered here has hybrid control, as mentioned before. The control in the boost phase is handled in two ways regarding this issue. One solution is to allocate to control between aerodynamic control (AC) and thrust vector control (TVC) depending on the effectiveness of the corresponding control type, which changes with dynamic pressure. The other solution is given for an integrated mechanical design of these controls which is also preferred in missile designs to save space.

Even though introduced autopilots do not require a gain scheduling process, a reference model is adapted for the varying flight conditions such that a faster model is used for the higher dynamic pressure. The results of acceleration autopilots are also compared with a baseline autopilots, which are designed using model following control (MFC). Finally, a realistic guided scenario with realistic measurement models is inspected, and all the results are tabulated within this thesis.

## **1.1 Motivation**

The motivation of this thesis is proposing a nonlinear fully coupled autopilot for all pitch, yaw, and roll channels of missile airframe in boost phase and aerodynamic tail control for all over the flight envelope in order to allow system capabilities as much as possible such as highly coupled maneuvers and BTT maneuvers, and making observations on the robustness of the system with this control scheme. Furthermore, since the missile systems are unmanned and relatively have a faster production process than other aerial vehicles, it motivates studying design schemes that could fasten the system design process.

## **1.2 Contribution of Thesis**

The contribution of this study may be stated as such:

- Detailed implementation of attitude and acceleration autopilots in pitch, yaw, and roll axes of an air defense system using NDI and two-time scale cascaded structure using aerodynamic tail controls and thrust vector controls over a flight envelope including boost and coast phases and designing PI controllers with a reference model.
- Addressing non-minimum phase issue for acceleration control of an aerodynamic tail-controlled missile with output redefinition idea that built on a physically grounded idea unlike many applications in this area and comparison with a baseline autopilot designed with MFC.
- Carrying on a sensitivity analysis of NDI autopilots for the particular missile system and investigating an example-guided case for real-life applications
- Discussion on the applied techniques for the particular airframe described in this content.

### 1.3 Outline

The thesis is composed of five chapters. The first chapter presents the general idea of the dissertation.

Chapter 2 summarizes the recent studies on autopilots in the literature by specifically focusing on nonlinear autopilot approaches on missile systems. The missile autopilots for both attitude and acceleration controls are skimmed. Moreover, studies on thrust vector control are extracted from literature since it is an important feature of the system studied here.

Chapter 3 focuses on outlining the key features of the method applied, i.e., the chapter recapitulate the NFL. Also, in this chapter the baseline autopilot, which is used for comparing the results of acceleration autopilots, is introduced.

Chapter 4 demonstrates the adaptation of the NDI to the attitude and acceleration autopilots of the missile in details. It also includes the assessment of the autopilot's performance in nominal cases. In this chapter, a section that consists of sensitivity analysis of the autopilots with uncertainties is added. Lastly, a realistic scenario is scrutinized at the end of the chapter.

Chapter 5 discusses the results and concludes the thesis.

## CHAPTER 2

### LITERATURE REVIEW

Autopilot of a missile mainly aims to realize guidance commands by turning them into fin deflections via blending sensor information with dynamic knowledge of the physical system. Linearizing a nonlinear system around a trim point and making controller design then extending the design along with a flight envelope with the corresponding selection of gains, which is also a well-known strategy called gain scheduling, has taken its place for many years due to its reliability and widely known analysis tools. However, to model a nonlinear system with a linear approach, increasing the number of design points as much as possible may become necessary, which is time-consuming. Nevertheless, the classical approaches may cause some information and performance loss.

Air defense systems considered in this context are known for their agility and are expected to minimize the deviation from intercept point. Therefore, nonlinear control approaches might be more suitable for such a system to exploit the system capabilities and minimize the performance degradation. Nonlinear dynamic inversion is one of the novel applications of the feedback linearization technique. The essence of the technique roots the idea of mapping a nonlinear system to a linear one and designing controllers based on linear methods then mapping to the nonlinear system again. NDI is known for its ease of application because it adapts the flight condition without gain scheduling.

One of the drawbacks of NDI is that it is not applicable for non-minimum phase systems, including tail-controlled missiles as in this study. This issue is mainly overcome using one of these strategies. The first one is changing the state variables. One example of changing the state variables might be choosing the angle of attack as a state variable for pitch channel rather than the acceleration and

implementing a third loop to control the acceleration. The examples of this application might be found in [23], [31] and [45]. The second strategy is to redefine the output. In literature, these output redefinitions mainly include aerodynamic angles and angular velocity terms. However, this may require excellent feedback measurements or observation of these values or other augmentations to the system to ensure robustness. In [33] and [34] a physically motivated output is redefined without requirement on precise information of aerodynamic angles. This strategy is also adopted in this study. Another drawback of NDI is known as the requirement for accurate information of plant model likewise in linear control strategies except that linear robust control tools are also not available. Therefore, many studies suggest integrating adaptive control methods into the design procedure to guarantee stability and robustness. Model Reference Adaptive Control and its some kind of improved form adaptive control originates from the idea of adapting a control signal that the system can follow in the presence of uncertainties.

Another approach frequently encountered in the literature is using neural networks to cancel nonlinearities adaptively. For instance, [5] and [30] utilize neural networks on different plants. Also, a hybrid controller study using adaptive sliding mode control and NDI was proposed in [9]. The stability of NDI structures is a topic that has been studied since many years ago, as the case in [36]. A variation on NDI is grounded on sensors is so-called incremental nonlinear dynamic inversion (INDI). It is also implemented for various aerospace vehicles, and there exist studies that show the robustness enhancement of systems with these methods, as in [46] and [48]. In addition, observation of the disturbances plays a crucial role in rejecting the disturbance in many applications of NDI as stated in [10].

Concerning the attitude control, several studies were implemented based on space vehicles as in [1]. Also, many studies were carried out for VTOL systems as in [5] and [47].

When the studies inspected about the TVC which is a part of this study also, it is seen that most of the studies focus on TVC apart from the aerodynamic control as

in [16], [40]. The authors of [24] and [29] propose a nonlinear control scheme that applied with a new output redefinition according to wind frame to provide a holistic control both in and out of the atmosphere. On the other hand, boost-phase missile control with TVC combined with aerodynamic control as it is the case in this study, does not have much research on, but one example is [41], where this hybrid control is studied with linear analysis tools.

As [7] discusses on a broad collection of recent control algorithms, a trendy robust control tool for nonlinear systems is sliding mode control. The error caused by the imperfect inversion due to modeling inaccuracy and perturbation of parameters is aimed to be overcome with this method. A comprehensive review of this method could be found in [17] and an example application on a BTT system similar to the system concerned here in [25].

Another nonlinear control approach studied numerous in literature is backstepping, in which control command of the system is drawn from the designed virtual control input. In order to prevent disruption, this method is usually integrated with robust techniques such as in [20].

Besides model-based linear and nonlinear controllers with robust controllers, stochastic, optimization-based, integrated guidance control, data-driven, and artificial intelligence based approaches are also popular these days. Those interested in these subjects, could refer to [7].



## CHAPTER 3

### PRELIMINARIES

#### 3.1 Plant Model

##### 3.1.1 Reference Frames and Transformation Matrices

In this study, a missile performing an atmospheric flight is considered. In order to follow a suitable system notation, the following frames of reference are described as they are addressed in [13] comprehensively.

**Body Fixed Reference Frame ( $\mathcal{F}_B$ ):** The origin of the frame is fixed to the rigid body's center of gravity, and the frame moves with the body. The x-axis of the body frame ( $x_B$ ) points towards the nose of the missile while the y-axis ( $y_B$ ) and the z-axis ( $z_B$ ) form a right-handed coordinate system coherently by keeping the z-axis on symmetry plane of the missile.

**Earth Fixed Reference Frame ( $\mathcal{F}_E$ ):** The origin of this reference frame is attached to the Earth which is assumed flat and nonrotating in this content. Therefore, this frame can also be referred as NED (north-east-down) frame in addition, it is used interchangeably with the inertial frame ( $\mathcal{F}_I$ ). The z-axis ( $z_E$ ) of the frame aligned with the local gravity vector, the x-axis ( $x_E$ ) chosen towards the north, and the y-axis ( $y_E$ ) points to the east as a right-handed coordinate system is formed.

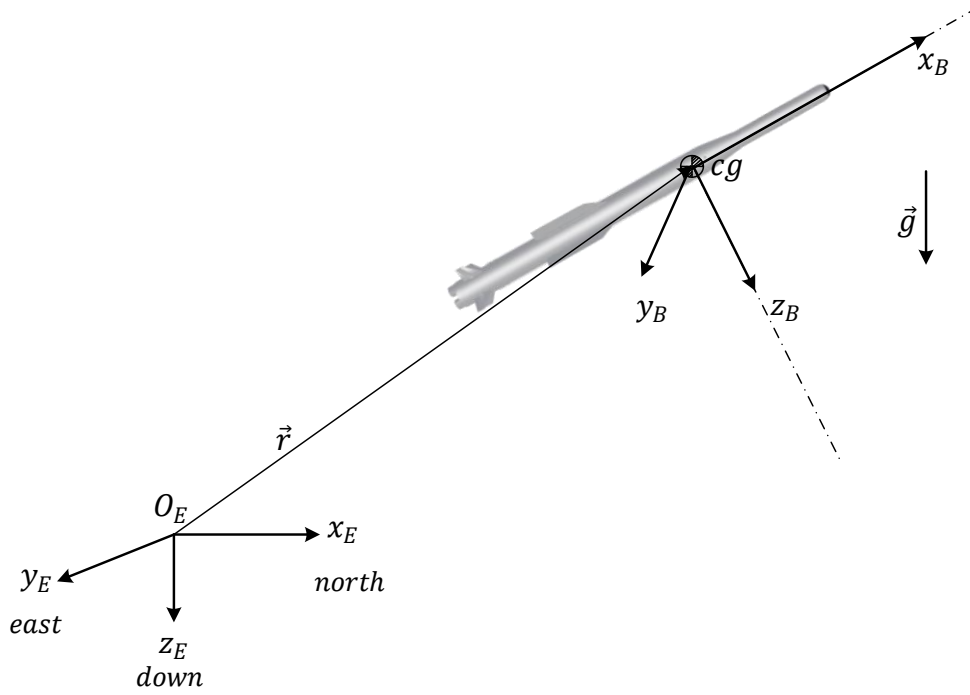


Figure 1 Body Fixed and Earth Fixed Coordinate Frames

The transformation of earth fixed frame to the body fixed frame is done here with 3-2-1 sequence rotating as described in [32]. The consecutive rotations around  $z_B$ ,  $y_B$   $x_B$  are called Euler yaw pitch yaw angles ( $\psi$ ,  $\theta$ ,  $\phi$ ) relatively and the rotations convert earth fixed frame, intermediate frames, and body frame  $\mathcal{F}_B$  respectively. So that, this transformation can be carried out with the following matrix.

$$\hat{C}^{(e,b)} = \begin{bmatrix} c\theta c\psi & c\theta s\psi & -s\theta \\ s\phi s\theta c\psi - c\phi s\psi & s\phi s\theta s\psi + c\phi c\psi & s\phi c\theta \\ c\phi s\theta c\psi + s\phi s\psi & c\phi s\theta s\psi - s\phi c\psi & c\phi c\theta \end{bmatrix} \quad (3.1)$$

### 3.1.2 Kinematic Relations

With the help of reference frame transformation, a kinematic relationship between angular rates of the body and Euler angles can be found. Derivation of these relations can be found at [13].

$$\begin{bmatrix} p \\ q \\ r \end{bmatrix} = \begin{bmatrix} \dot{\phi} - \dot{\psi} \sin \theta \\ \dot{\theta} \cos \phi + \dot{\psi} \sin \phi \cos \theta \\ -\dot{\theta} \sin \phi + \dot{\psi} \cos \phi \cos \theta \end{bmatrix} \quad (3.2)$$

$$\begin{bmatrix} \dot{\phi} \\ \dot{\theta} \\ \dot{\psi} \end{bmatrix} = \begin{bmatrix} p + (q \sin \phi + r \cos \phi) \tan \theta \\ q \cos \phi - r \sin \phi \\ (q \sin \phi + r \cos \phi) \sec \theta \end{bmatrix} \quad (3.3)$$

### 3.1.3 Dynamic Relations

In order to simulate the unsteady motion of the missile, dynamic equations of it are written within the framework of the following assumptions.

- i. The missile is a rigid body.
- ii. Earth is fixed and nonrotating.
- iii. The center of gravity is a radial vector.
- iv. The atmosphere is still relative to the Earth.
- v.  $xz$  is a plane of symmetry.

The derivation of the equations of motion is given in much detail in [13]. The equations are summarized as translational and rotational dynamics as necessary in this study.

### 3.1.3.1 Translational Dynamics

The translational motion of the missile's center of gravity (cg) is written by applying Newton's second law of motion. In (3.4)  $\vec{F}_B$  represents body force vector,  $\vec{L}_B$  is linear momentum vector,  $\vec{a}_{B/I}^B$  is body's acceleration with respect to inertial frame written in inertial frame,  $m$  is mass, and  $t$  stands for time.

$$\sum \vec{F}_B = \left. \frac{d\vec{L}_B}{dt} \right|_I = m\vec{a}_{B/I}^B \quad (3.4)$$

In (3.5) the velocity of the body with respect to inertial frame written in body frame  $\vec{V}_{B/I}^B$  and its components  $u, v, w$  on  $x_B, y_B, z_B$  are given as well as the angular velocities about these respective axis also known as roll, pitch, yaw  $p, q, r$  are defined as  $\vec{\omega}_{B/I}^B$  which is again observed from inertial frame.

$$\vec{V}_{B/I}^B = \begin{bmatrix} u \\ v \\ w \end{bmatrix}, \vec{\omega}_{B/I}^B = \begin{bmatrix} p \\ q \\ r \end{bmatrix} \quad (3.5)$$

After those definitions, kinematic relation between them is given in (3.6) by referring to [13].

$$\vec{a}_{B/I}^B = \dot{\vec{V}}_{B/I}^B + \vec{\omega}_{B/I}^B \times \vec{V}_{B/I}^B = \begin{bmatrix} \dot{u} \\ \dot{v} \\ \dot{w} \end{bmatrix} + \begin{bmatrix} p \\ q \\ r \end{bmatrix} \times \begin{bmatrix} u \\ v \\ w \end{bmatrix} \quad (3.6)$$

The forces on a flying object in the air consist of aero propulsive forces  $X, Y, Z$  on body frame and and gravitational force. These are explicitly written in (3.7) where  $\vec{g}$  represents local gravity vector.

$$\vec{F}_B = \begin{bmatrix} X \\ Y \\ Z \end{bmatrix} + \hat{c}^{(e,b)} \begin{bmatrix} 0 \\ 0 \\ m\vec{g} \end{bmatrix} \quad (3.7)$$

By composing (3.6) and (3.7), linear accelerations of the body in three axes are expressed as in (3.8).

$$\begin{aligned}
\dot{u} &= rv - qw + \frac{X}{m} - g \sin \theta \\
\dot{v} &= pw - ru + \frac{Y}{m} + g \cos \theta \sin \phi \\
\dot{w} &= qu - pv + \frac{Z}{m} + g \cos \theta \cos \phi
\end{aligned} \tag{3.8}$$

### 3.1.3.2 Rotational Dynamics

The rotational motion of the rigid body is written in (3.9) by using the Newton-Euler equations. The moments on the body shown in vector  $\vec{G}_B$ , whose each element in respective  $x_B, y_B, z_B$  axes  $L, M, N$  are given in (3.10) as well as the inertia matrix  $I$ . In (3.9)  $\vec{H}_B$  represents angular momentum vector of the body. The other parameters are used as described before.

$$\sum \vec{G}_B = \left. \frac{d\vec{H}_B}{dt} \right|_I = I \dot{\vec{\omega}}_{B/I} + (\vec{\omega}_{B/I} \times I \vec{\omega}_{B/I}) \tag{3.9}$$

$$\vec{G}_B = \begin{bmatrix} L \\ M \\ N \end{bmatrix}, I = \begin{bmatrix} I_{xx} & -I_{xy} & -I_{zx} \\ -I_{xy} & I_{yy} & -I_{yz} \\ -I_{zx} & -I_{yz} & I_{zz} \end{bmatrix} \tag{3.10}$$

Due to rigid body's symmetry axis  $I_{xy} = 0$  and  $I_{yz} = 0$ . So that, the calculations in (3.9) leads to (3.11).

$$\begin{aligned}
L &= I_{xx}\dot{p} - I_{zx}\dot{r} + qr(I_{zz} - I_{yy}) - I_{zx}pq \\
M &= I_{yy}\dot{q} + rp(I_{xx} - I_{zz}) + I_{zx}(p^2 - r^2) \\
N &= I_{zz}\dot{r} - I_{zx}\dot{p} + pq(I_{yy} - I_{xx}) + I_{zx}qr
\end{aligned} \tag{3.11}$$

From above equation rates of angular velocities can be drawn as in (3.12).

$$\begin{aligned}
\dot{p} &= \frac{L + I_{zx}\dot{r} - qr(I_{zz} - I_{yy}) + I_{zx}pq}{I_{xx}} \\
\dot{q} &= \frac{M - rp(I_{xx} - I_{zz}) - I_{zx}(p^2 - r^2)}{I_{yy}} \\
\dot{r} &= \frac{N + I_{zx}\dot{p} - pq(I_{yy} - I_{xx}) - I_{zx}qr}{I_{zz}}
\end{aligned} \tag{3.12}$$

### 3.1.4 Subsystem Models

#### 3.1.4.1 Atmosphere Model

The standard atmosphere model is implemented as explained in [50], in which more items on the subject are presented.

Temperature ( $K$ ): The flight here takes place in the troposphere; therefore, the temperature can be approximated as the following function of altitude ( $h$ ).

$$T = 288.15 - 0.0065h \tag{3.13}$$

Pressure ( $Pa$ ): Another primary variable as the temperature is pressure. It can also be expressed as a function. ( $P_0$ : Sea level pressure,  $T_0$ : Sea level temperature)

$$P = P_0 \left( \frac{T}{T_0} \right)^{5.2559} \tag{3.14}$$

Air Density ( $kg/m^3$ ): It is defined as the mass of air per unit volume and modeled using the ideal gas law. ( $R$ : gas constant)

$$\rho = \frac{P}{RT} \quad (3.15)$$

Speed of Sound ( $m/s$ ): It is derived from the adiabatic flow formula, and specific heat for air ( $\gamma$ ) is used as 1.4.

$$a = \sqrt{\gamma RT} \quad (3.16)$$

Mach Number: Represents the ratio of airspeed ( $V_\infty$ ) to the speed of sound.

$$Ma = \frac{V_\infty}{a} \quad (3.17)$$

Dynamic Pressure ( $kg/ms^2$ ): It can be thought of as the fluid's kinetic energy per unit volume. It is created by the dynamic motion of the body.

$$Q = \frac{1}{2} \rho V_\infty^2 \quad (3.18)$$

#### 3.1.4.2 Gravity Model

The mathematical calculation of the gravitational acceleration on a rotating oblate spheroid is given in [35].

$$g(\lambda) = g_c(1 + \alpha \sin^2 \lambda + \beta \sin^4 \lambda) \quad (3.19)$$

In this study for the model of Earth's gravity, the above formula is put into practice with the terms defined as,  $g_c = 9.780319 \text{ m/s}^2$ ,  $\alpha = 0.005278895$ ,  $\beta = 0.000023462$ , and  $\lambda$  stands for latitude.

### 3.1.4.3 Propulsion System Model

The solid propellant rocket motor concept is used for the boost phase as it is widely used in missile technologies due to its superior acceleration capability to air breathing propulsion. The thrust profile of such a system depends on burn area, throat area, grain placement shape, propellant type, and density, etc., which in turn affects the Mach profile and directly the performance of the missile. Therefore, it is an all-inclusive design process and those concerned may refer to [15].

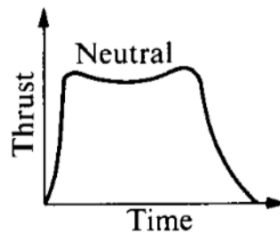


Figure 2 Generic Thrust Profile (Peterson, 1992)

A generic, typical thrust profile depending on time is implemented for the boost phase as in [22]. In addition, the autopilot design is considered with regard to the thrust change throughout the flight.

#### 3.1.4.3.1 Thrust Vector Control

Thrust vector control is based on the idea of creating moment by rotating the main thrust from the centerline of the body. Thrust vector control technologies are reviewed in [41]. In this study same jet vane system from [41] is chosen only by changing the configuration to cross-configuration since it is emphasized at the

reference that mechanically moving the jet vanes and aerodynamic fins together is preferable. Mathematical modeling of thrust vector control by jet vanes is summarized in the advancing parts.

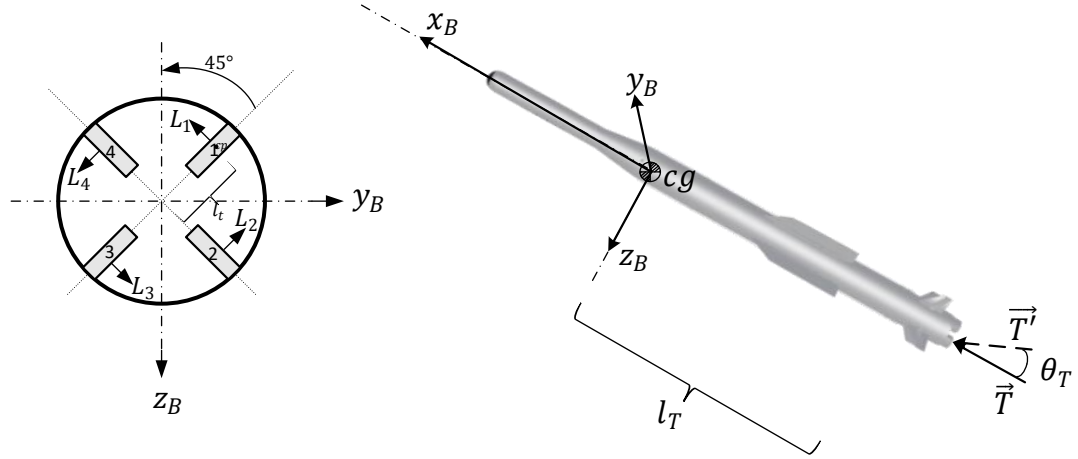


Figure 3 TVC Rear View and Side View

Each jet vane produces lift ( $L_{1,2,3,4}$ ) and drag ( $D_{1,2,3,4}$ ) due to the flow passing by. The forces  $F_{T_x}$ ,  $F_{T_y}$ ,  $F_{T_z}$  and moments  $M_{T_x}$ ,  $M_{T_y}$ ,  $M_{T_z}$  produced by these vanes on  $x_B$ ,  $y_B$ ,  $z_B$  axes can be calculated as in (3.20) and (3.21). In these equations,  $l_T$  stands for the moment arm along missile x axis whereas  $l_t$  stands for the distance between nozzle radius and center of pressure of the jet vanes.

$$\begin{bmatrix} F_{T_x} \\ F_{T_y} \\ F_{T_z} \end{bmatrix} = \begin{bmatrix} -1 & -1 & -1 & -1 \\ 0 & 0 & 0 & 0 \\ 0 & 0 & 0 & 0 \end{bmatrix} \begin{bmatrix} D_1 \\ D_2 \\ D_3 \\ D_4 \end{bmatrix} + \cos(45^\circ) \begin{bmatrix} 0 & 0 & 0 & 0 \\ -1 & 1 & 1 & -1 \\ -1 & -1 & 1 & 1 \end{bmatrix} \begin{bmatrix} L_1 \\ L_2 \\ L_3 \\ L_4 \end{bmatrix} \quad (3.20)$$

$$\begin{bmatrix} M_{T_x} \\ M_{T_y} \\ M_{T_z} \end{bmatrix} = \begin{bmatrix} -l_t(L_1 + L_2 + L_3 + L_4) \\ -l_T \cos(45^\circ) (-L_1 - L_2 + L_3 + L_4) \\ l_T \cos(45^\circ) (L_1 - L_2 - L_3 + L_4) \end{bmatrix} + l_t \cos(45^\circ) \begin{bmatrix} 0 \\ (D_1 - D_2 - D_3 + D_4) \\ (D_1 + D_2 - D_3 - D_4) \end{bmatrix} \quad (3.21)$$

The deflection angle of the thrust from the centerline of the body can be calculated as in (3.22) the elevation ( $\theta_T$ ) and in (3.23) azimuth ( $\psi_T$ ) of the deflection. The forces created by each the jet vane depend on the lift and drag as it is mentioned

previously. Those forces are generated in accordance with the angle of attack of the jet vanes which in this case corresponds to jet vane deflection angles  $\delta_{T_{1,2,3,4}}$ . Moreover, since the jet vanes are in cross configuration to use the effective deflections  $\delta_{T_{e,r,a}}$  are found more useful rather than  $\delta_{T_{1,2,3,4}}$ . One can convert one to another easily as it is described in the following section. Therefore, thrust deflection angles are estimated as functions of effective deflection angles.

$$\theta_T(\delta_{T_e}) = \text{atan}\left(\frac{F_{T_z}}{F_{T_x}}\right) \quad (3.22)$$

$$\psi_T(\delta_{T_r}) = \text{atan}\left(\frac{F_{T_y}}{F_{T_x}}\right) \quad (3.23)$$

The total thrust forces ( $\vec{F}_T^B$ ) and moments ( $\vec{M}_T^B$ ) of propulsion system is calculated in (3.24) and (3.25) added to aerodynamic forces in (3.32).

$$\vec{F}_T^B = \begin{bmatrix} T \cos \theta_T(\delta_{T_e}) \cos \psi_T(\delta_{T_r}) \\ T \sin \psi_T(\delta_{T_r}) \\ -T \sin \theta_T(\delta_{T_e}) \cos \psi_T(\delta_{T_r}) \end{bmatrix} \quad (3.24)$$

$$\vec{M}_T^B = \begin{bmatrix} -Tl_y \sin \theta_T(\delta_{T_e}) \cos \psi_T(\delta_{T_r}) - Tl_z \sin \psi_T(\delta_{T_r}) \\ Tl_z \cos \theta_T(\delta_{T_e}) \cos \psi_T(\delta_{T_r}) + Tl_x \sin \theta_T(\delta_{T_e}) \cos \psi_T(\delta_{T_r}) \\ -Tl_y \cos \theta_T(\delta_{T_e}) \cos \psi_T(\delta_{T_r}) + Tl_x \sin \psi_T(\delta_{T_r}) \end{bmatrix} \quad (3.25)$$

The components of moment arm vector  $\vec{l}$  is given in (3.26).

$$\vec{l} = \begin{bmatrix} l_x \\ l_y \\ l_z \end{bmatrix} \quad (3.26)$$

In addition, the roll moment component of the thrust vector ( $M_{T_x}$ ) is assumed as a linear function of  $\delta_{T_\alpha}$  compatible with the (3.21).

#### 3.1.4.4 Aerodynamic Model

In order to propagate linear and angular acceleration equations, aerodynamic forces and moments should be calculated. For a specific rigid body, aerodynamic forces and moments are generally modeled as non-dimensional parameters which depend on flight conditions and parameters. Therefore, firstly those parameters are defined.

**Angle of Attack:** It is the angle between the body x-axis and the vector, obtained by projecting the local air velocity ( $V_\infty$ ) onto the aircraft's symmetry plane. It can be calculated as in (3.27).

$$\alpha = \tan^{-1} \left( \frac{w}{u} \right) \quad (3.27)$$

**Angle of Sideslip:** The usual definition of the sideslip is the angle between local air velocity ( $V_\infty$ ) and the  $xz$ -plane of the body. However, to take full advantage of the physical symmetries of a missile airframe, angle of sideslip is defined similarly to the angle of attack as it is given in (3.28).

$$\beta = \sin^{-1} \left( \frac{v}{u} \right) \quad (3.28)$$

Aerodynamic angles are shown in Figure 4.

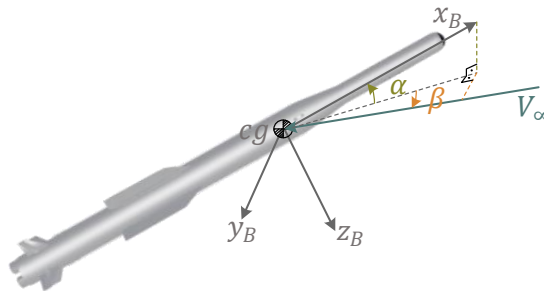


Figure 4 Angle of Attack and Angle of Side Slip

Control Surface Deflection: Control surfaces are the fins located at the tail of the missile. Aerodynamic forces are modeled in terms of effective deflections which, are referred as elevator ( $\delta_{A_e}$ ), rudder ( $\delta_{A_r}$ ), and aileron ( $\delta_{A_a}$ ) angles. However, the missile has four fins located in cross-configuration. Therefore, there is a relation between the effective deflection angles and the actual deflection angles. It is important to note that this relation does not have to be unique. In this study since a dual control is a matter of subject, effective AC fin deflections are referred as elevator ( $\delta_{A_e}$ ), rudder ( $\delta_{A_r}$ ), and aileron ( $\delta_{A_a}$ ) angles, whereas effective TVC jet vane deflections are referred as elevator ( $\delta_{T_e}$ ), rudder ( $\delta_{T_r}$ ), and aileron ( $\delta_{T_a}$ ) angles. In addition, when talking about effective control surface deflections in general, elevator ( $\delta_e$ ), rudder ( $\delta_r$ ), and aileron ( $\delta_a$ ) angles are meant. After clarifying this, the way preferred in the scope of the study for the conversion from the actual deflections to the effective deflections is described in (3.29) and the reverse is given in (3.30).

$$\begin{bmatrix} \delta_e \\ \delta_r \\ \delta_a \end{bmatrix} = \begin{bmatrix} 0.25 & 0.25 & -0.25 & -0.25 \\ 0.25 & -0.25 & -0.25 & 0.25 \\ 0.25 & 0.25 & 0.25 & 0.25 \end{bmatrix} \begin{bmatrix} \delta_1 \\ \delta_2 \\ \delta_3 \\ \delta_4 \end{bmatrix} \quad (3.29)$$

$$\begin{bmatrix} \delta_1 \\ \delta_2 \\ \delta_3 \\ \delta_4 \end{bmatrix} = \begin{bmatrix} 1 & 1 & 1 \\ 1 & -1 & 1 \\ -1 & -1 & 1 \\ -1 & 1 & 1 \end{bmatrix} \begin{bmatrix} \delta_e \\ \delta_r \\ \delta_a \end{bmatrix} \quad (3.30)$$

Some critical parameters to generate the aerodynamic model are defined until this point. In light of this information, aerodynamic moments and forces are modeled using the pre-described parameters at the beginning of the chapter and the nondimensionalized parameters obtained for the specific rigid body by using DATCOM. The idea of modeling aerodynamics by some non-dimensional parameters originated from small perturbation theory.

Small perturbation theory suggests that the motion of the air vehicle is composed of minor deviations from reference steady state condition. From this point forth, it is stated in [14] that writing the aerodynamic forces as a linear function of state variables is quite accurate and practical for engineering purposes. The longitudinal and lateral state variables and the aerodynamic forces and moments depending on them are specified in [14] with further explanations on the nondimensionalization process using Buckingham's  $\pi$  theorem.

$$\begin{aligned}
C_X &= C_X(Ma, \alpha, \beta, \delta_{A_e}, \delta_{A_r}, \delta_{A_a}) \\
C_Y &= C_Y(Ma, \alpha, \beta, \delta_{A_e}, \delta_{A_r}, \delta_{A_a}) + \frac{C_{Y_r} r l_{ref}}{2V} \\
C_Z &= C_Z(Ma, \alpha, \beta, \delta_{A_e}, \delta_{A_r}, \delta_{A_a}) + \frac{C_{Z_q} q l_{ref}}{2V} \\
C_l &= C_l(Ma, \alpha, \beta, \delta_{A_e}, \delta_{A_r}, \delta_{A_a}) + \frac{C_{l_p} p l_{ref}}{2V} \\
C_m &= C_m(Ma, \alpha, \beta, \delta_{A_e}, \delta_{A_r}, \delta_{A_a}) + \frac{C_{m_q} q l_{ref}}{2V} + \frac{C_{m_a} \dot{\alpha} l_{ref}}{2V} \\
C_n &= C_n(Ma, \alpha, \beta, \delta_{A_e}, \delta_{A_r}, \delta_{A_a}) + \frac{C_{n_r} r l_{ref}}{2V} + \frac{C_{n_\beta} \dot{\beta} l_{ref}}{2V}
\end{aligned} \tag{3.31}$$

The dimensional form of aerodynamic forces, added with propulsive forces, generates aero-propulsive forces and moments to be used in (3.8) and (3.11) and the final equation of motion equation can be summarized as in (3.32).

$$\begin{aligned}
X &= Q C_X S_{ref} + F_{T_x} \\
Y &= Q C_Y S_{ref} + F_{T_y} \\
Z &= Q C_Z S_{ref} + F_{T_z} \\
L &= Q C_l S_{ref} l_{ref} + M_{T_x} \\
M &= Q C_m S_{ref} l_{ref} + M_{T_y} \\
N &= Q C_n S_{ref} l_{ref} + M_{T_z}
\end{aligned} \tag{3.32}$$

### 3.1.4.5 Missile Avionics Model

#### 3.1.4.5.1 Actuator Model

After the control command is delegated to four fins as described in (3.30), the control actuation system (CAS) cuts into mechanization to bring the deflection angles to their respective values. In missile systems, an electrical motor actuates the fin deflections, and the autopilot design needs to take into consideration the capabilities of this unit. Therefore, a representation of this unit is included in the Simulink model as a second-order transfer function as shown in (3.33) where the related parameters are as described in Table 1.

$$\frac{\delta}{\delta_{com}} = \frac{\omega_{cas}^2}{s^2 + 2\zeta_{cas}\omega_{cas}s + \omega_{cas}^2} \quad (3.33)$$

Table 1 CAS Parameters

CAS Parameters	Representation	Value	Unit
Natural frequency	$\omega_{cas}$	25	Hz
Damping ratio	$\zeta_{cas}$	0.6	—
Angle limit	$\delta_{max}$	30	°
Angular rate limit	$\dot{\delta}_{max}$	500	°/s

#### 3.1.4.5.2 Inertial Measurement Unit Model

Autopilots proposed in this context require the missile's linear and angular acceleration information as feedback. In applications, this information comes from Inertial Measurement Unit (IMU) to on-board missile computer where the algorithms run. IMU generates this information with sensors, i.e., accelerometer and gyroscope. The design process is carried out as feedbacks are measured

perfectly, but in the preceding parts, more realistic results are tabulated by implementing an IMU model using the specifications of Honeywell Aerospace’s tactical grade MEMS IMU named HG1930. Also, a misalignment error is assumed in the IMU measurements.

The IMU model mentioned is assumed with errors as in Table 2 using [21] and [26].

Table 2 IMU Parameters

Error Type	Accelerometer Channels			Gyro Channels		
	Units	Measure	Value	Units	Measure	Value
<b>Bias</b>	<i>mg</i>	$1\sigma$	5	$^{\circ}/h$	$1\sigma$	20
<b>Bias in run stability</b>	<i>mg</i>	$1\sigma$	0.3	$^{\circ}/h$	$1\sigma$	1
<b>Scale Factor</b>	<i>ppm</i>	$1\sigma$	300	<i>ppm</i>	$1\sigma$	300
<b>Random Walk</b>	<i>fps/<math>\sqrt{h}</math></i>	<i>max</i>	0.3	$^{\circ}/\sqrt{h}$	<i>max</i>	0.125
<b>Misalignment</b>	<i>mrad</i>	–	1	<i>mrad</i>	–	1

### 3.2 Review of Nonlinear Feedback Linearization

#### 3.2.1 Basic Idea of Nonlinear Feedback Linearization

Nonlinear feedback linearization differs from the conventional linearization method in the sense that via feedback linearization, a one-to-one representation of a dynamical system is being obtained rather than an approximation [38]. It is a usual experience that the representation of a dynamical system may have different complexity depending on the choice of coordinates. Likewise, the NFL strategy aims to characterize a nonlinear system into a more manageable form, meaning that it cancels the nonlinear terms without loss of any information.

From linear systems theory, a dynamical system has different state-space realizations and an important one is the controllable canonical form (or companion form). For a given linear time-invariant system, companion form with state transformation can be written as in (3.34) referring to [37].

$$\begin{aligned} \dot{x} &= Ax + Bu \\ z &= z(x) \end{aligned}$$

$$\dot{z} = \begin{bmatrix} 0 & 1 & \cdots & 0 \\ 0 & 0 & \ddots & \vdots \\ 0 & 0 & \cdots & 1 \\ -a_0 & -a_1 & \cdots & -a_{n-1} \end{bmatrix}_{n \times n} z + \begin{bmatrix} 0 \\ 0 \\ \vdots \\ 0 \\ 1 \end{bmatrix}_{n \times 1} u \quad (3.34)$$

In the above representation  $x$  is  $n$  dimensional state vector,  $u$  is control input,  $A$  and  $B$  are linear time-invariant matrices,  $z$  is transformation matrix and finally,  $a_0, a_1, \dots, a_n$  are coefficients of characteristic polynomial of this system, i.e., they hold the information of poles. From (3.34), the transformation vector  $z$  can be written in terms of first element of  $z$  by taking derivatives of each element as in (3.35).

$$z = [z_1 \quad z_2 \quad \cdots \quad z_n]^T = [z_1 \quad \dot{z}_1 \quad \cdots \quad z_1^{(n-1)}]^T \quad (3.35)$$

Also, from the last line of the companion form, the relation between input  $u$  vector  $z$  can be stated.

$$z_1^{(n)} + a_{n-1}z_1^{(n-1)} + \cdots + a_0z_1 = u \quad (3.36)$$

It is seen that companion form leads a representation of the system, such that the state vector is defined by only the first state  $z_1$ , and  $n^{th}$  order state equation is replaced by one scalar differential equation (3.36) from which the related control input can be calculated for the desired state.

NFL tries to extend this idea also for nonlinear systems. A unique form of a system is companion form such that the derivatives of the states seem to be in the equation without derivatives of input term. A single input nonlinear system is considered in [38], and in order to put it into a similar form given as (3.34), vector transformation of  $z = z(x)$  is performed.

$$\begin{aligned} \dot{x} &= f(x) + g(x)u \\ z^{(n)} &= \underbrace{f(z, \dot{z}, \dots, z^{(n-1)}, t) + g(z, \dot{z}, \dots, z^{(n-1)}, t)u}_{\triangleq v} \end{aligned} \quad (3.37)$$

In the above equation  $f$  and  $g$  are nonlinear functions of states,  $x$  is  $n$  dimensional state vector,  $u$  is a scalar input.

If the right-hand side of the whole nonlinear equation above is lumped to one variable  $v$  then the state equation will result in linear form, which allows performing linear control theory. However, to find the corresponding input  $u$ , perfect knowledge of  $f$  and  $g$  would be required. Although this idea seems complementary to robust control theory, this issue is left aside for the time being.

$$\begin{aligned} z^{(n)} &= v \\ u &= g^{-1}(v - f) \end{aligned} \quad (3.38)$$

Now,  $v$  depends on the controller design of this transformed linear system. As an example, a linear controller approach can be made such that the characteristic equation will have stable roots,  $v = -[K_1 \ K_2 \ \dots \ K_n]^T$  and  $K_{1,\dots,n}$  symbolize the controller gains. One may design them to characterize the decay rate etc.

The nonlinear state equation seems to be linear with respect to input  $u$  in the above explanations, however, it may depend on some nonlinear function of input ( $\alpha(u)$ ) as well, as long as  $u = \alpha^{-1}$  is exists.

The state equation can be fully linearized, or only the part of it can be linearized, i.e., input-output map [27]. Since the latter is involved in this study, that concept will be detailed in the upcoming part.

### 3.2.2 Input-Output Feedback Linearization

In this part, the intuitive idea of input-output feedback linearization will be explained since the application investigated in this thesis is originated from this intuition. The narration proceeded through the SISO system, and much of the details can be found in [27].

An  $n^{th}$  order state variable equation with state vector  $x$  and output  $y$  is defined.

$$\begin{aligned}\dot{x} &= f(x) + g(x)u \\ x &= [x \quad \dot{x} \quad \dots \quad x^{n-1}]^T \\ y &= h(x)\end{aligned}\tag{3.39}$$

Vector fields  $f$ ,  $g$ ,  $h$  map subdomain  $D$  into the real space  $R$  with related dimension.

$$\begin{aligned}f: D &\rightarrow R^n, & g: D &\rightarrow R^{n \times 1}, & h: D &\rightarrow R \\ D &\subset R^n\end{aligned}\tag{3.40}$$

As it is described in the previous section, the nonlinear equation is linearized using the input, more precisely by redefining it. Then, the linear form of the system is controlled. Therefore, while designing feedback linearization based on the output equation, its derivative is taken repeatedly until the order in which input appears. If the system is well defined, the input  $u$  will eventually appear in  $r^{th}$  order derivative of output  $y$ , where  $r$  is the relative degree of the nonlinear system. Relative degree of a such system might be equal or less than the full order of the system ( $r \leq n$ ).

Assuming  $h$  is a sufficiently smooth function in a domain  $D \subset R^n$  so we can take its derivative as expressed in the (3.41).

$$\begin{aligned}
 y &= h(x) = \psi_1 \\
 \dot{\psi}_1 = \dot{y} &= \frac{\partial h(x)}{\partial x} \dot{x} = \frac{\partial h(x)}{\partial x} f(x) + \frac{\partial h(x)}{\partial x} g(x) u = \psi_2 \\
 &\vdots \\
 \dot{\psi}_{r-1} &= y^{n-1} = \frac{\partial \psi_{r-1}}{\partial x} f(x) = \psi_r \\
 \dot{\psi}_r &= y^r = \underbrace{\frac{\partial \psi_r}{\partial x} f(x) + \frac{\partial \psi_r}{\partial x} g(x) u}_{\triangleq v}
 \end{aligned} \tag{3.41}$$

If we take the derivative of the output equation given in (3.39) until input comes insight at its relative degree, and by defining a new input  $v$  that linearizes system an equivalent system until the order of  $r$  with new linear representation can be written with new state vector  $\zeta$  [12].

$$\begin{aligned}
 \zeta &= [\psi_1 \quad \psi_2 \quad \cdots \quad \psi_r]^T \\
 A_c &= \begin{bmatrix} 0 & 1 & \cdots & 0 \\ 0 & 0 & \ddots & \vdots \\ 0 & 0 & \cdots & 1_{(r-1) \times (r-1)} \\ 0 & 0 & 0 & 0 \end{bmatrix}_{r \times r} \\
 b_c &= \begin{bmatrix} 0 \\ 0 \\ \vdots \\ 0 \\ 1 \end{bmatrix}_{r \times 1} \\
 \dot{\zeta} &= A_c \zeta + b_c v
 \end{aligned} \tag{3.42}$$

The remaining part is internal dynamics by definition with order  $n - r$ . Those will be collected at another state vector  $\eta$  with similar steps described above as in (3.43).

$$\zeta = [\phi_1 \quad \phi_2 \quad \cdots \quad \phi_r]^T \tag{3.43}$$

$$\begin{aligned}\dot{\eta} &= \frac{\partial \eta}{\partial x} \dot{x} = \frac{\partial \eta}{\partial x} f(x) + \frac{\partial \eta}{\partial x} g(x)u \\ \frac{\partial \phi_i}{\partial x} g(x) &= 0, \quad \text{where } i = 1, \dots, r \\ \dot{\eta} &= f(\eta, \zeta)\end{aligned}$$

A diffeomorphism that transforms the system from  $x$  to  $z$  coordinates is found by defining the new system as in (3.44).

$$\begin{aligned}T(x) &= \begin{bmatrix} \phi_1 \\ \vdots \\ \phi_{n-r} \\ \psi_1 \\ \vdots \\ \psi_r \end{bmatrix} = \begin{bmatrix} \eta_1 \\ \vdots \\ \eta_{n-r} \\ \zeta_1 \\ \vdots \\ \zeta_r \end{bmatrix} = z \\ \dot{\zeta} &= A_c \zeta + b_c v \\ \dot{\eta} &= f(\eta, \zeta) \\ y &= C^T \zeta \\ C &= \begin{bmatrix} 1 \\ 0 \\ \vdots \\ 0 \\ 0 \end{bmatrix}\end{aligned}\tag{3.44}$$

The matrices in state variable equations are in companion form. In addition, by setting  $\zeta = 0$  zero dynamics of the system can be obtained. Zero dynamics is defined as the internal dynamics of the system when the output is kept zero by a unique choice of the input signal. Before a controller for this system is designed, internal stability has to be checked since the leftover dynamics are also subjected to the same input. These remaining dynamics will be stable if and only if all the zeros of the original system, which are poles of that remaining part at the same time, are in the left half-plane. It implies that a minimum phase system is required. If the zero dynamics is stable, then the system will be locally stable but, this gives no conclusion about global stability.

In the above progress, when  $r = n$  then  $\eta$  terms vanish and the mapping can be done seamlessly.

### 3.2.3 Necessary Conditions and Formal Definitions

After intuition of input-output linearization is addressed, the conditions for a system to be input-output linearizable are presented in compact mathematical form in this part. For this purpose, some differential geometry concepts, such as Lie derivative and Lie brackets are introduced based on the definitions of variables (3.40) for system in (3.39). The following explanations are all adapted from [27] and [11].

The Lie derivative of the scalar function  $h$  with respect to vector field  $f$  is defined as follows:

$$\mathcal{L}_f h(x) = \left. \begin{array}{c} \frac{\partial h(x)}{\partial x} \\ \text{row vector} \end{array} \right\} \underbrace{f(x)}_{\text{column vector}} \rightarrow \text{scalar} \quad (3.45)$$

Where  $\frac{\partial h(x)}{\partial x}$  is differential of scalar  $h$ ;  $dh$  which is actually the gradient of  $h$ .

The Lie bracket, also called as adjoint, is defined for vector fields  $f$  and  $g$  as follows:

$$[f, g] = ad_f g(x) = \left. \begin{array}{c} \frac{\partial g}{\partial x} \quad f - \frac{\partial f}{\partial x} \quad g \\ \text{Jacobian Matrix} \quad \text{Jacobian Matrix} \end{array} \right\} \rightarrow \text{vector} \quad (3.46)$$

One can see that Lie derivative results in a scalar, whereas the Lie bracket is a vector.

A continuously differentiable map with a continuously differentiable inverse is known as a diffeomorphism [27]. When a system in (3.39) is considered with

smooth functions  $f, g$  and  $h$  in  $D \subset R^n$  then theorem of input-output linearization says that, If  $r = n$  then for every  $x_0 \in D$ , a neighborhood  $N$  of  $x_0$  exists such that the map  $T(x)$  given as in (3.47) is restricted to  $N$  is a diffeomorphism.

$$T(x) = \begin{bmatrix} h(x) \\ \mathcal{L}_f h(x) \\ \vdots \\ \mathcal{L}_f^{n-1} h(x) \end{bmatrix} \quad (3.47)$$

Moreover, If  $r < n$ , then for every  $x_0 \in D$ , a neighbourhood  $N$  of  $x_0$  and smooth functions  $\phi_1(x), \dots, \phi_{n-r}(x)$ , which reflects the internal dynamics of the system, exist such that the condition in (3.43) is satisfied for all  $x \in N$  and the map  $T(x)$  given in (3.48) is a diffeomorphism on  $N$ .

$$T(x) = \begin{bmatrix} \phi_1(x) \\ \vdots \\ \phi_{n-r}(x) \\ h(x) \\ \vdots \\ \mathcal{L}_f^{r-1} h(x) \end{bmatrix} \quad (3.48)$$

Above, formal definition and necessary conditions for I/O linearization are mentioned for a SISO system given as in (3.39) for the sake of simple expression. Furthermore, these explanations can be extended for a MIMO system with a nonlinear state variable equation in terms of input. One may refer [27] for details of this issue.

### 3.3 Review of Baseline Autopilot Design

As a baseline, an autopilot designed with the model following control method is used. These controllers eliminate the errors between feedback and set point by forcing the control variable to reach the set point with a specified trend. The desired transient response used for designing the reference model is decided by

considering the performance specifications. The reference model calculates its control input and output. This input is corrected by the autopilot, which tries to match the model output with the system output. If the process is successful, then the output variable is achieved with desired reference model trajectory. The mathematical expression of this approach is summarized briefly. Note that, the following generalized procedure applied separately for roll, pitch, and yaw channels and coupled effects are ignored while designing the baseline autopilot.

The system is expressed in a state-space form such that states  $x_s(t) \in R^n$ , control input  $u(t) \in R^m$ ,  $A_s$  is system matrix,  $B_s$  control input matrix, and all the states are assumed measurable.

$$\dot{x}_s = A_s x_s + B_s u \quad (3.49)$$

Then a reference model for each channel is designed with the following state variable model with the reference input  $r(t)$ . An example of designing a reference model can be found in [18]. By following the approach given in [39] augmented state  $x_{sr} = [x_s \quad x_r]^T$  is defined, and the augmented system is written.

$$\begin{aligned} \dot{x}_{sr} &= \begin{bmatrix} A_s & 0_{nxn} \\ 0_{nxn} & A_r \end{bmatrix} x_{sr} + \begin{bmatrix} B_s \\ 0_{nx1} \end{bmatrix} u_c + \begin{bmatrix} 0_{nx1} \\ B_r \end{bmatrix} r \\ \dot{x}_{sr} &= A_{sr} x_{sr} + B_{sru} u_c + B_{srr} r \end{aligned} \quad (3.50)$$

In this study, the above augmented system is generated with the control outputs defined as Euler angles, normal and lateral accelerations for roll, pitch, and yaw dynamics. In order to minimize the steady state error in these outputs, the integral of the error is also fed to the system. In order to generalize the equations here, these output variables are assumed to be the first state variable for design in each corresponding axis.

$$x_i = \int_{t=0}^t (x_r(1) - x_s(1)) \quad (3.51)$$

After appending the integral state, the overall system is expressed in terms of state variable  $\bar{x}$ , input command  $u_c$ , state variable matrix  $A_o$ , state input vector  $B_{ou}$ , and reference matrix  $B_{or}$ .

$$\dot{\bar{x}} = \begin{bmatrix} \dot{x}_{sr} \\ \dot{x}_i \end{bmatrix} = \begin{bmatrix} A_{sr} & 0_{2n \times 1} \\ [-1 \ 0_{1 \times (n-1)} \ 1 \ 0_{1 \times (n-1)}] & 0 \end{bmatrix} \begin{bmatrix} x_{sr} \\ x_i \end{bmatrix} + \begin{bmatrix} B_{sru} \\ 0 \end{bmatrix} u_c + \begin{bmatrix} B_{srr} \\ 0 \end{bmatrix} r \quad (3.52)$$

$$\dot{\bar{x}} = A_o \bar{x} + B_{ou} u_c(t) + B_{or} r(t)$$

Then, a performance vector  $z(t)$  is selected, and a positive definite matrix  $Q_z$  is defined such that weighting in this matrix penalize the corresponding state variable.

$$J = \frac{1}{2} \int_{t=0}^{\infty} (z^T(t) Q_z z(t)) dt \quad (3.53)$$

The cost function below is minimized by transforming it to the well-known linear quadratic regulation cost function. This process is expressed in details in [18] where optimal control law is obtained with  $H_2$  synthesis.

$$u_c = -K \bar{x}(t), \quad K \in R^{1 \times (2n+1)} \quad (3.54)$$

The gains are found by solving the Ricatti equation by means of MATLAB. An application of MFC for roll angle control can be found in [19]. The details of the baseline autopilot design are not substantial in the context of this study. The thing that matters in the scope of this study is, a structure was already available that allows the control of the relevant parameters in many conditions. However, it should be emphasized that while designing this structure, the coupled dynamic effects in the system are ignored as well as the nonlinear dynamics are expressed in linear state-space format.

## CHAPTER 4

### AUTOPILOT DESIGN WITH NONLINEAR FEEDBACK LINEARIZATION

#### 4.1 Attitude Autopilot

Attitude autopilot of the missile implies the control of Euler angles, the coupling effects of the missile dynamics is taken into account for the design process. Also, the autopilot has to be valid during the boost phase as well as the coast phase. The idea of attitude control with two loop NDI structure is originated from the kinematic link between Euler angles and body angular rates, as one can refer 3.1.2 for this relation.

##### 4.1.1 Problem Formulation

Attitude mathematical model is described in 3.1. The state vector in (3.39) consists of rotation rates in three axes  $(p, q, r)$ , Euler angles  $(\phi, \theta, \psi)$  with the angle of attack  $(\alpha)$  and the sideslip angle  $(\beta)$ . The control vector is effective fin deflections  $(\delta_e, \delta_r, \delta_a)$ , from which one can allocate control to four fins as described in 3.1.4.4. The output vector is chosen as control variables directly, i.e., Euler angles.

The attitude control problem can be formulated according to the two time-scale separation approach. The angular rate dynamics constitute the inner loop with fast states  $(\vec{x}_i)$ , and Euler angle dynamics generate the outer loop with slow states  $(\vec{x}_o)$ .

$$\vec{x}_i = \begin{bmatrix} p \\ q \\ r \end{bmatrix}, \vec{x}_o = \begin{bmatrix} \alpha \\ \beta \\ \phi \\ \theta \\ \psi \end{bmatrix}, \vec{y} = \begin{bmatrix} \phi \\ \theta \\ \psi \end{bmatrix}, \vec{u} = \begin{bmatrix} \delta_e \\ \delta_r \\ \delta_a \end{bmatrix} \quad (4.1)$$

$$\begin{aligned}\dot{\omega} &= f(\omega) + g(\omega, u) \\ y &= h(x, \omega)\end{aligned}\tag{4.2}$$

The output function  $h$  is given in (3.3). The dynamic inversion process can be done by inverting the output function in order to find the angular rate commands and then inverting the angular rate dynamic to control the inner loop.

$$\begin{aligned}\omega_c &= h^{-1}(x, \omega) \\ \dot{\omega} &= I^{-1}G - I^{-1}(\omega \times I\omega)\end{aligned}\tag{4.3}$$

This approach summarized above is inspected in much more detail throughout the following sections.

#### 4.1.2 Inner Loop Design

Angular rates are controlled in the inner loop. In order to express the autopilot in the most generic form such that it includes boost and coast phases with the coupled effects (3.12) organized by adding thrust vector control terms.

$$\begin{aligned}\dot{p} &= \frac{L + M_{x_{tvc}} + I_{zx}\dot{r} - qr(I_{zz} - I_{yy}) + I_{zx}pq}{I_{xx}} \\ \dot{q} &= \frac{M + M_{y_{tvc}} - rp(I_{xx} - I_{zz}) - I_{zx}(p^2 - r^2)}{I_{yy}} \\ \dot{r} &= \frac{N + M_{z_{tvc}} + I_{zx}\dot{p} - pq(I_{yy} - I_{xx}) - I_{zx}qr}{I_{zz}}\end{aligned}\tag{4.4}$$

Calculation of aerodynamic moments and moments that comes from thrust vector control are given as (3.25) and (3.31), respectively.

$$\begin{aligned}
\dot{p} &= \frac{QS_{ref}l_{ref}C_l}{I_{xx}} + \frac{-Tl_y \sin \theta_T \cos \psi_T - Tl_z \sin \psi_T}{I_{xx}} \\
&\quad + \frac{I_{zx}\dot{r} - qr(I_{zz} - I_{yy}) + I_{zx}pq}{I_{xx}} \\
\dot{q} &= \frac{QS_{ref}l_{ref}C_m}{I_{yy}} + \frac{Tl_z \cos \theta_T \cos \psi_T + Tl_x \sin \theta_T \cos \psi_T}{I_{yy}} \\
&\quad + \frac{-rp(I_{xx} - I_{zz}) - I_{zx}(p^2 - r^2)}{I_{yy}} \\
\dot{r} &= \frac{QS_{ref}l_{ref}C_n}{I_{zz}} + \frac{-Tl_y \cos \theta_T \cos \psi_T + Tl_x \sin \psi_T}{I_{zz}} \\
&\quad + \frac{I_{zx}\dot{p} - pq(I_{yy} - I_{xx}) - I_{zx}qr}{I_{zz}}
\end{aligned} \tag{4.5}$$

Since the idea of NFL is to bring the system in the form of (3.44), the above equations should be written such that it has two parts: one depending on the input (in this case, fin deflection) and one independent of the input. The aerodynamic database is regulated such that the effect of input can be extracted and expressed separately from flight parameters.

$$\begin{aligned}
\dot{p} &= \frac{QS_{ref}l_{ref} \left( C_{l_\delta}(\delta_A) \right)}{I_{xx}} \\
&\quad + \frac{-Tl_y \sin \theta_T(\delta_T) \cos \psi_T(\delta_T) - Tl_z \sin \psi_T(\delta_T)}{I_{xx}} \\
&\quad + \frac{QS_{ref}l_{ref} \left( C_{l_0} + C_{l_p} \frac{l_{ref}p}{2V} \right)}{I_{xx}} \\
&\quad + \frac{I_{zx}\dot{r} - qr(I_{zz} - I_{yy}) + I_{zx}pq}{I_{xx}}
\end{aligned} \tag{4.6}$$

$$\begin{aligned}
\dot{q} = & \frac{QS_{ref}l_{ref} \left( C_{m\delta}(\delta_A) + \frac{x_{cg}}{l_{ref}} C_{Z\delta}(\delta_A) \right)}{I_{yy}} \\
& + \frac{+Tl_z \cos \theta_T(\delta_T) \cos \psi_T(\delta_T) + Tl_x \sin \theta_T(\delta_T) \cos \psi_T(\delta_T)}{I_{yy}} \\
& + \frac{QS_{ref}l_{ref} \left( C_{m_0} + C_{m_q} \frac{l_{ref}q}{2V} + C_{m\dot{\alpha}} \frac{l_{ref}\dot{\alpha}}{2V} + \frac{x_{cg}}{l_{ref}} C_{Z_0} \right)}{I_{yy}} \\
& + \frac{(-rp(I_{xx} - I_{zz}) - I_{zx}(p^2 - r^2))}{I_{yy}}
\end{aligned} \tag{4.7}$$

$$\begin{aligned}
\dot{r} = & \frac{QS_{ref}l_{ref} \left( C_{n\delta}(\delta_A) - \frac{x_{cg}}{l_{ref}} C_{Y\delta}(\delta_A) \right)}{I_{zz}} \\
& + \frac{-Tl_y \cos \theta_T(\delta_T) \cos \psi_T(\delta_T) + Tl_x \sin \psi_T(\delta_T)}{I_{zz}} \\
& + \frac{QS_{ref}l_{ref} \left( C_{n_0} + C_{n_r} \frac{l_{ref}r}{2V} + C_{n\dot{\beta}} \frac{l_{ref}\dot{\beta}}{2V} - \frac{x_{cg}}{l_{ref}} C_{Y_0} \right)}{I_{zz}} \\
& + \frac{I_{zx}\dot{p} - pq(I_{yy} - I_{xx}) - I_{zx}qr}{I_{zz}}
\end{aligned} \tag{4.8}$$

In the equations (4.6), (4.7), and (4.8), angular rates of the missile are written in most detail by explicitly showing all the terms that is related with the missile's dynamic motion. With the help of these equations, the inner loop can be written in the following compact form (4.9) by defining  $A_{i_{aero}}$ ,  $b_{i_{aero}}$ ,  $A_{i_{tvc}}$ ,  $b_{i_{tvc}}$ . The elements of these matrices are given in (4.10) and (4.11).

$$\begin{bmatrix} \dot{p} \\ \dot{q} \\ \dot{r} \end{bmatrix} = A_{i_{aero}} C_{M_A} + b_{i_{aero}} + A_{i_{tvc}} C_{M_T} + b_{i_{tvc}}$$

$$C_{M_A} = \begin{bmatrix} C_{l_\delta}(\delta) \\ C_{m_\delta}(\delta) + C_{z_\delta}(\delta) \frac{x_{cg}}{l_{ref}} \\ C_{n_\delta}(\delta) - C_{y_\delta}(\delta) \frac{x_{cg}}{l_{ref}} \end{bmatrix}, C_{M_T} = \begin{bmatrix} \cos \theta_T(\delta) \cos \psi_T(\delta) \\ \sin \psi_T(\delta) \\ -\sin \theta_T(\delta) \cos \psi_T(\delta) \end{bmatrix} \quad (4.9)$$

$$A_{i_{aero}} = QS_{ref} l_{ref} \begin{bmatrix} 1/I_{xx} & 0 & 0 \\ 0 & 1/I_{yy} & 0 \\ 0 & 0 & 1/I_{zz} \end{bmatrix}$$

$$b_{i_{aero}} = \begin{bmatrix} \frac{QS_{ref} l_{ref} \left( C_{l_0} + C_{l_p} \frac{p}{V} \right) + I_{zx} \dot{r} - qr(I_{zz} - I_{yy}) + I_{zx} pq}{I_{xx}} \\ QS_{ref} l_{ref} \left( C_{m_0} + C_{m_q} \frac{q}{V} + C_{m_\alpha} \frac{\dot{\alpha}}{V} + \frac{x_{cg}}{l_{ref}} (C_{z_0}) \right) - rp(I_{xx} - I_{zz}) - I_{zx}(p^2 - r^2) \\ \frac{I_{yy}}{I_{zz}} \\ QS_{ref} l_{ref} \left( C_{n_0} + C_{n_r} \frac{r}{V} + C_{n_\beta} \frac{\dot{\beta}}{V} - \frac{x_{cg}}{l_{ref}} (C_{y_0}) \right) + I_{zx} \dot{p} - pq(I_{yy} - I_{xx}) - I_{zx} qr \end{bmatrix} \quad (4.10)$$

$$A_{i_{tvc}} = T \begin{bmatrix} 0 & -l_z & l_y \\ l_z & 0 & -l_x \\ -l_y & l_x & 0 \end{bmatrix} \quad (4.11)$$

$$b_{i_{tvc}} = \begin{bmatrix} 0 \\ 0 \\ 0 \end{bmatrix}$$

The inner loop developed here assumes instantaneous control is applied, ignoring the actuator dynamics. Therefore, angular rates can be directly replaced by virtual control inputs as in (4.12).

$$\begin{bmatrix} v_p \\ v_q \\ v_r \end{bmatrix} = \begin{bmatrix} \dot{p} \\ \dot{q} \\ \dot{r} \end{bmatrix} \quad (4.12)$$

If the coast phase of the flight is considered, the system can be easily inverted, and a controller can be designed using the virtual control input part. However, for the boost phase, inverting the system is not straightforward since the superposition of aerodynamic moments and moments originated from thrust vector control as shown in (4.9) results in a more complex form. This issue will be addressed a little further in this chapter after the controller design subject is touched in order to move forward step by step.

#### 4.1.2.1 Coast Phase

In the coast phase, the terms related to thrust vector control cancel out since there exists no thrust. Therefore, the system given in (4.9) can be feedback linearized as follows.

$$\begin{bmatrix} C_{l\delta_{cgcom}}(\delta_A) \\ C_{m\delta_{cgcom}}(\delta_A) \\ C_{n\delta_{cgcom}}(\delta_A) \end{bmatrix} = A_{i_{aero}}^{-1} \left( -b_{i_{aero}} + \begin{bmatrix} v_p \\ v_q \\ v_r \end{bmatrix} \right) \quad (4.13)$$

Once the aerodynamic coefficient needed for the desired command is figured out, the desired control deflections can be found by inverting the aerodynamic database.

$$\delta_{A_{com}} = \begin{bmatrix} \delta_{A_a} \\ \delta_{A_e} \\ \delta_{A_r} \end{bmatrix} = \begin{bmatrix} C_{l\delta_{cg}}^{-1} \left( C_{l\delta_{cgcom}} \right) \\ C_{m\delta_{cg}}^{-1} \left( C_{m\delta_{cgcom}} \right) \\ C_{n\delta_{cg}}^{-1} \left( C_{n\delta_{cgcom}} \right) \end{bmatrix} \quad (4.14)$$

Reference model with PI controller based on the tracking error is used to design the virtual control input. The reference model aims to convert the command to a reference that is achievable to track by the missile. As illustrated in Figure 5, reference model is modelled as a second-order transfer function in Laplace domain with natural frequencies  $\omega_{rm_p}, \omega_{rm_q}, \omega_{rm_r}$  for roll, pitch and yaw channels respectively and damping ratio  $\zeta_{rm}$ .

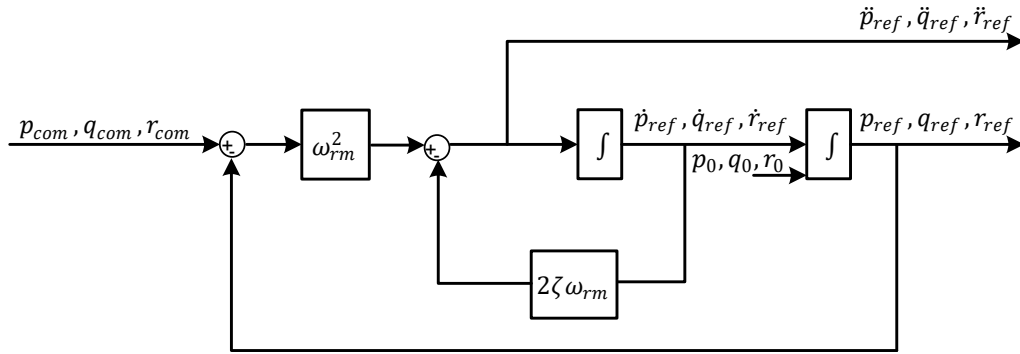


Figure 5 Reference Model

$$\begin{aligned}
 \ddot{p}_{ref} &= \omega_{rm_p}^2 (p_{com} - p_{ref}) - 2\zeta_{rm}\omega_{rm_p}\dot{p}_{ref} \\
 \ddot{q}_{ref} &= \omega_{rm_q}^2 (q_{com} - q_{ref}) - 2\zeta_{rm}\omega_{rm_q}\dot{q}_{ref} \\
 \ddot{r}_{ref} &= \omega_{rm_r}^2 (r_{com} - r_{ref}) - 2\zeta_{rm}\omega_{rm_r}\dot{r}_{ref}
 \end{aligned} \tag{4.15}$$

Noting that;

$$\omega_{rm} = \begin{bmatrix} \omega_{rm_p} \\ \omega_{rm_q} \\ \omega_{rm_r} \end{bmatrix}$$

The derivative of the reference command is given above, which should also be used for the reference model tracking. Taking the Laplace transform of the equations above carries us to find the reference command in terms of the measured state and commanded signal.

$$p_{ref} = \frac{\omega_{rm_p}^2}{s^2 + 2\zeta_{rm}\omega_{rm_p}s + \omega_{rm_p}^2} p_{com} \quad (4.16)$$

The same idea is extended for the pitch and yaw roll angular velocities, i.e., their corresponding reference signal is found with the same idea. After designing the reference model, PI controller is designed for the angular rates. The inner loop process for the coast phase is illustrated in Figure 6.

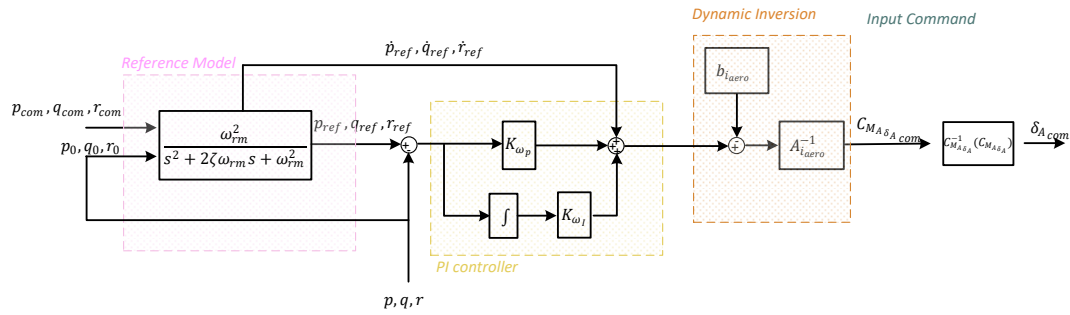


Figure 6 Inner Loop Schematic for the Coast Phase

By defining the virtual control input as described in (4.12), it can be designed with different approaches. Just as it is said, PI controller is found suitable. For other approaches, one can refer [49]. Using this control structure, gains need to be calculated. In Figure 7, a perfect dynamic inversion is described.

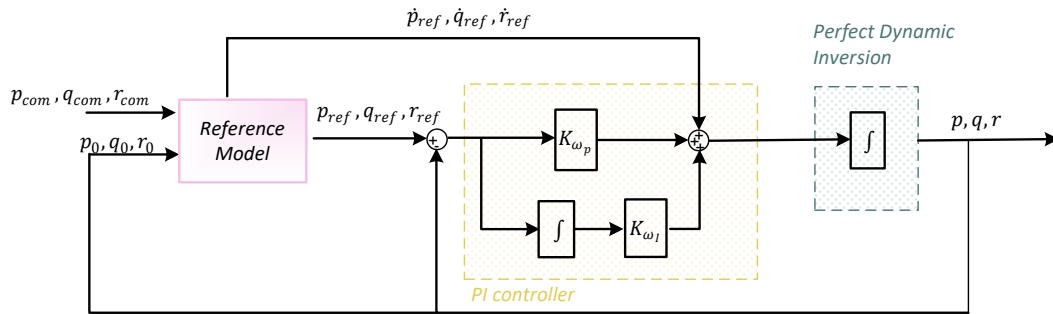


Figure 7 Perfect Dynamic Inversion Visualization

However, there will be errors in the inversion process. Let us put together all the dynamic inversion errors in the roll channel into a variable  $err_{inv}$ , and find the gains of roll channel. The differential equation for the roll channel will be:

$$\dot{p} = \dot{p}_{ref} + K_{pp}(p_{ref} - p) + K_{Ip} \int (p_{ref} - p) + err_{inv} \quad (4.17)$$

Upon careful examination of Figure 7, the transfer function from inversion error to tracking error will be transfer function of PI controller subpart:

$$TF = -\frac{1}{s^2 + K_{pp}s + K_{Ip}} \quad (4.18)$$

By equating the characteristic equation of this transfer function to the characteristic equation of the reference model given in (4.16), the PI gains can be decided. Also, by applying same idea in the pitch and yaw channel, overall gains of the inner loop are written as follows.

$$\begin{aligned} K_{pp} &= 2\zeta_{rm}\omega_{rm_p}, K_{Ip} = \omega_{rm_p}^2 \\ K_{pq} &= 2\zeta_{rm}\omega_{rm_q}, K_{Iq} = \omega_{rm_q}^2 \\ K_{pr} &= 2\zeta_{rm}\omega_{rm_r}, K_{Ir} = \omega_{rm_r}^2 \end{aligned} \quad (4.19)$$

Consequently, the virtual control input is designed as in the following equation.

$$\begin{bmatrix} v_p \\ v_q \\ v_r \end{bmatrix} = \begin{bmatrix} K_{pp} & K_{pI} & 0 & 0 & 0 & 0 \\ 0 & 0 & K_{qp} & K_{qI} & 0 & 0 \\ 0 & 0 & 0 & 0 & K_{rp} & K_{rI} \end{bmatrix} \begin{bmatrix} p_{ref} - p \\ \int p_{ref} - p \\ q_{ref} - q \\ \int q_{ref} - q \\ r_{ref} - r \\ \int r_{ref} - r \end{bmatrix} + \begin{bmatrix} \dot{p}_{ref} \\ \dot{q}_{ref} \\ \dot{r}_{ref} \end{bmatrix} \quad (4.20)$$

## 4.1.2.2 Boost Phase

### 4.1.2.2.1 Case 1: Mechanically Coupled Control Surfaces

The autopilot design process is a bit more complicated for the boost phase. Equations (4.9) and (4.12) still will be combined, but finding the input command from (4.21) needs some numerical process since the equation cannot be inverted directly with the analytical methods.

$$\begin{bmatrix} v_p \\ v_q \\ v_r \end{bmatrix} = A_{i_{aero}} C_{M_A} + b_{i_{aero}} + A_{i_{tvc}} C_{M_T} + b_{i_{tvc}} \quad (4.21)$$

In chapter 3.1.4.3.1, it is already mentioned that the fins used for thrust vector control and the aerodynamic fins moving together are in favor of the system design. So as to achieve that, it is seen input vector ( $\delta = [\delta_e \delta_r \delta_a]^T$ ) needs to be extracted from (4.21) such that it includes both AC inputs ( $\delta_A$ ) and TVC inputs ( $\delta_T$ ). The virtual control inputs are designed same as in the coast phase with (4.20). From there, the right-hand side of the (4.21) is solved for input with a numerical method in negligible tolerance. The details of this numerical process are given in Appendix B.

### 4.1.2.2.2 Case 2: Separately Actuated Control Surfaces

Another approach to this dual control situation might be allocating the total control requirement. The virtual control input found like (4.21) can be met by allocating total moment to aerodynamic control and thrust vector control. A way to distribute the virtual control is considering the effectiveness of aerodynamic moment over the moment generated by TVC which is referred as  $E$  and calculated dynamically in the simulation depending on the flight conditions for each channel as in (4.22).

$$E = \frac{\text{moment produced by TVC per unit } \delta_T}{\text{moment produced by AC per unit } \delta_A} \quad (4.22)$$

It is clear that, at the beginning of the flight, since the velocity is quite low, there is little dynamic pressure for aerodynamic forces to be created. Therefore, using TVC to control the attitude would be more reasonable in this region. However, as velocity increases, after some point, aerodynamic forces will get effective.

$$v = v_0 + v_\delta = \underbrace{b_{i_{aero}} + b_{i_{tvc}}}_{v_0} + \underbrace{v_{aero} + v_{tvc}}_{v_\delta}$$

$$v_{aero} = \left( \frac{1}{E+1} \right) v_\delta = A_{i_{aero}} C_{M_A}$$

$$v_{tvc} = \left( \frac{E}{E+1} \right) v_\delta = A_{i_{tvc}} C_{M_T}$$
(4.23)

In Figure 8 the allocation is illustrated. The aim of control allocation done here is to demand total desired moment from aerodynamic control deflections and jet vane deflections separately. Therefore, while allocating the control first the decoupling matrices  $b_{i_{aero}}$  and  $b_{i_{tvc}}$  is subtracted from virtual input since those consists of body's contribution without the deflection commands.

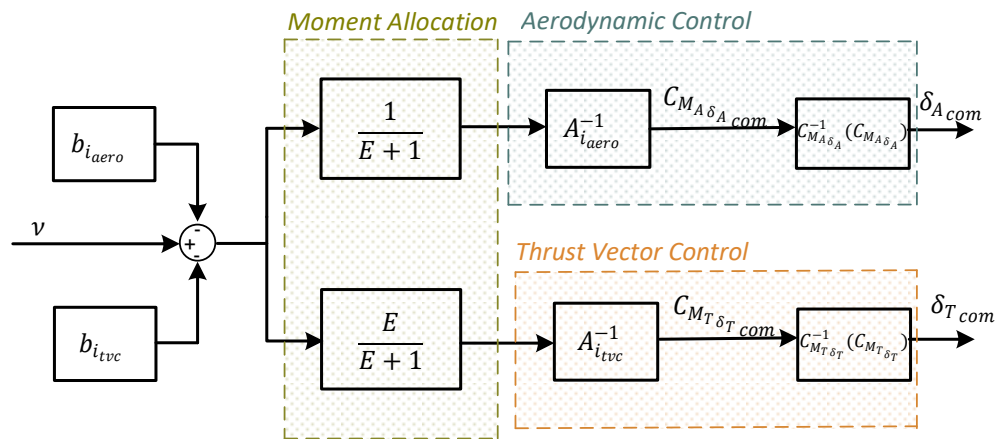


Figure 8 Virtual Input Allocation to AC and TVC

Once the effective fin deflections are found either by imposing a mechanical coupling or sharing the control, the true fin deflections can be decided using (3.30).

This completes the inner loop design for attitude autopilot. The formulation given throughout 4.1.2 describes a way to effectuate angular rate commands with fin deflections.

### 4.1.3 Outer Loop Design

The outer loop takes the commands for the Euler angles and creates angular rate commands for the inner loop to realize the demanded control with the fin commands.

Outer Loop formulation can be easily drawn from (3.3) firstly by writing the relation between Euler angular rates and angular velocities as in (4.24).

$$\begin{bmatrix} \dot{\phi} \\ \dot{\theta} \\ \dot{\psi} \end{bmatrix} = \begin{bmatrix} 1 & \sin \phi \tan \theta & \cos \phi \tan \theta \\ 0 & \cos \phi & -\sin \phi \\ 0 & \sin \phi \sec \theta & \cos \phi \sec \theta \end{bmatrix} \begin{bmatrix} p \\ q \\ r \end{bmatrix} \quad (4.24)$$

Similar to the idea used for the inner loop, Euler angle rates are selected as virtual control inputs in (4.25) to linearize the feedback.

$$\begin{bmatrix} v_\phi \\ v_\theta \\ v_\psi \end{bmatrix} = \begin{bmatrix} \dot{\phi} \\ \dot{\theta} \\ \dot{\psi} \end{bmatrix} \quad (4.25)$$

Then by merging (4.24) and (4.25) the outer loop can be written in the form of (3.39) as in (4.26).

$$\begin{bmatrix} v_\phi \\ v_\theta \\ v_\psi \end{bmatrix} = A_o \omega + b_o \quad (4.26)$$

$$A_o = \begin{bmatrix} 1 & \sin \phi \tan \theta & \cos \phi \tan \theta \\ 0 & \cos \phi & -\sin \phi \\ 0 & \sin \phi \sec \theta & \cos \phi \sec \theta \end{bmatrix}, b_o = \begin{bmatrix} 0 \\ 0 \\ 0 \end{bmatrix}$$

For the outer loop, again the commands are passed through a second-order reference model, and reference command is given to the system to be followed. The PI controller structure is implemented as it is described in detail in 4.1.2. Therefore, virtual control is designed as (4.27), and the procession of calculations of gains is the same as explained in 4.1.2.

$$\omega_{com} = A_o^{-1} \left( -b_o + K_{Euler} \begin{bmatrix} \phi_{ref} - \phi \\ \int \phi_{ref} - \phi \\ \theta_{ref} - \theta \\ \int \theta_{ref} - \theta \\ \psi_{ref} - \psi \\ \int \psi_{ref} - \psi \end{bmatrix} + \begin{bmatrix} \dot{\phi}_{ref} \\ \dot{\theta}_{ref} \\ \dot{\psi}_{ref} \end{bmatrix} \right) \quad (4.27)$$

$$K_{Euler} = \begin{bmatrix} K_{\phi_P} & K_{\phi_I} & 0 & 0 & 0 & 0 \\ 0 & 0 & K_{\theta_P} & K_{\theta_I} & 0 & 0 \\ 0 & 0 & 0 & 0 & K_{\psi_P} & K_{\psi_I} \end{bmatrix}$$

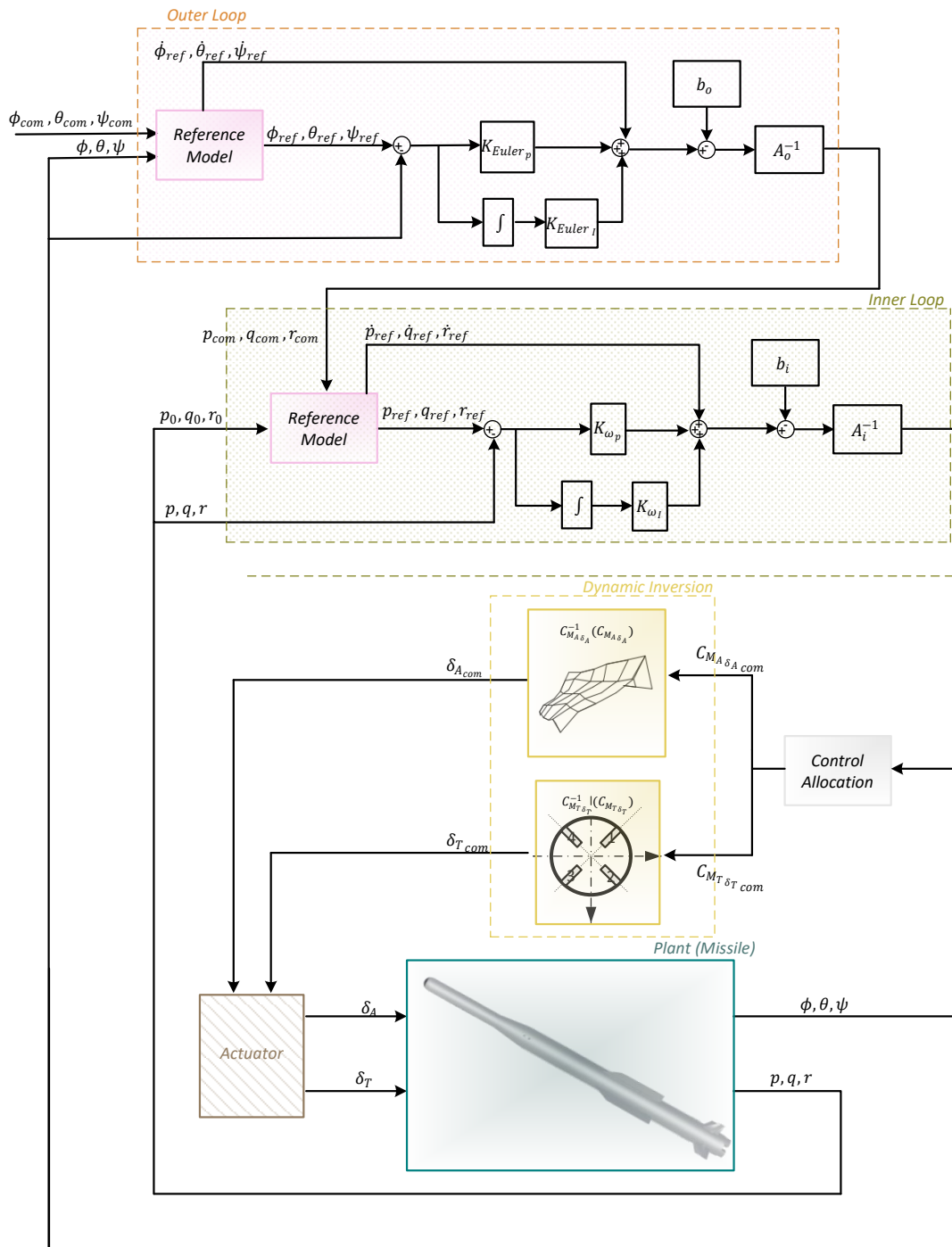


Figure 9 Attitude Autopilot Scheme

#### **4.1.4 Evaluation of Nominal Attitude Autopilot**

After presenting the attitude autopilot, a set of simulation studies are carried on within the nominal conditions, i.e., with no uncertainties or disturbances in the system and assumed as all the required measurements can be done perfectly. As an example, the commands that are evaluated as challenging for this system are applied to all three channels throughout a flight regime that consists of multiple phases boost & coast, and all responses are displayed in a normalized form, where the value used for normalization is specified on the corresponding figures. In Figure 10, control performance presented with the close capture of the result in yaw channel.

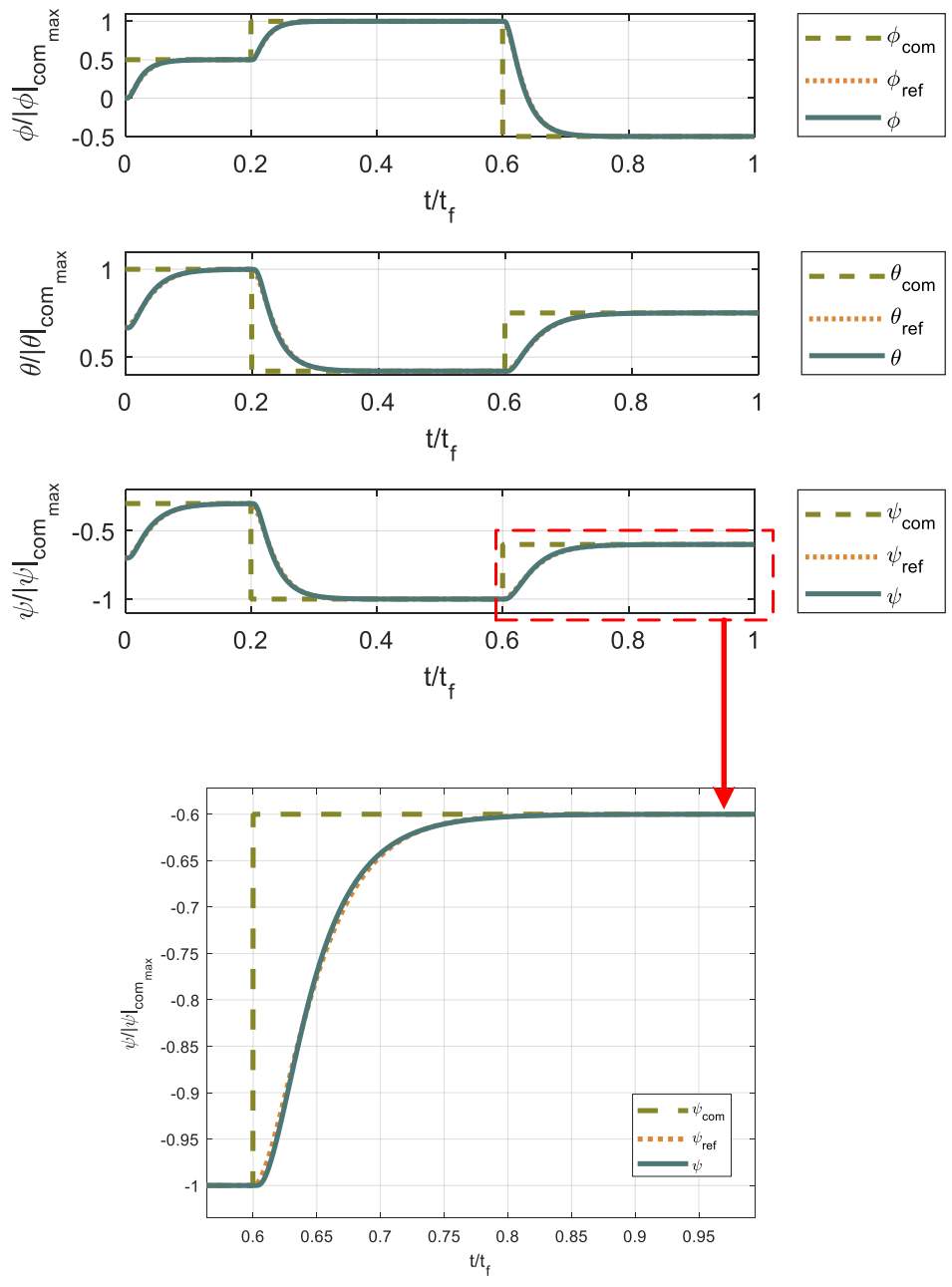


Figure 10 Normalized Euler Angle Tracking Performance of Attitude Autopilot

As explained before, the commands are converted to a reference signal that the missile should follow. In Figure 10, although the missile is under the highly coupled dynamics due to the selected command set, as expected, all of the

responses follow their reference commands successfully, thanks to the nonlinear nature of the autopilot design.

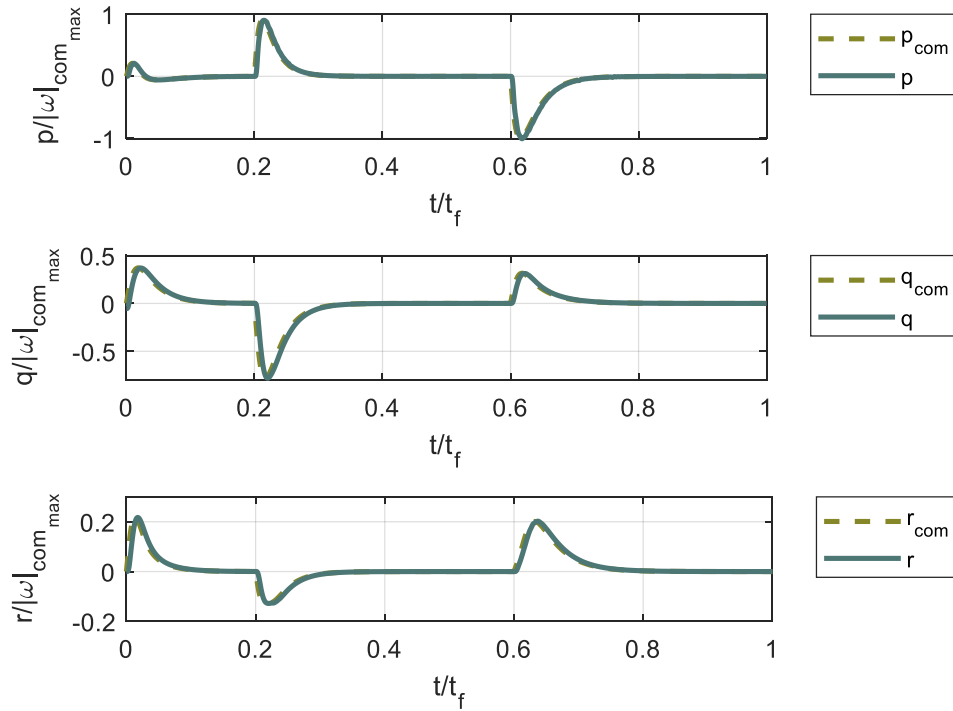


Figure 11 Normalized Angular Rate Tracking Performance of Attitude Autopilot

The outer loop assumes that the inner loop controls the angular rates much faster than the outer loop and creates the corresponding commands for the inner loop. While the outer loop realizes the Euler angle commands, the inner loop controls the angular rates in a faster fashion as it is observed from Figure 11.

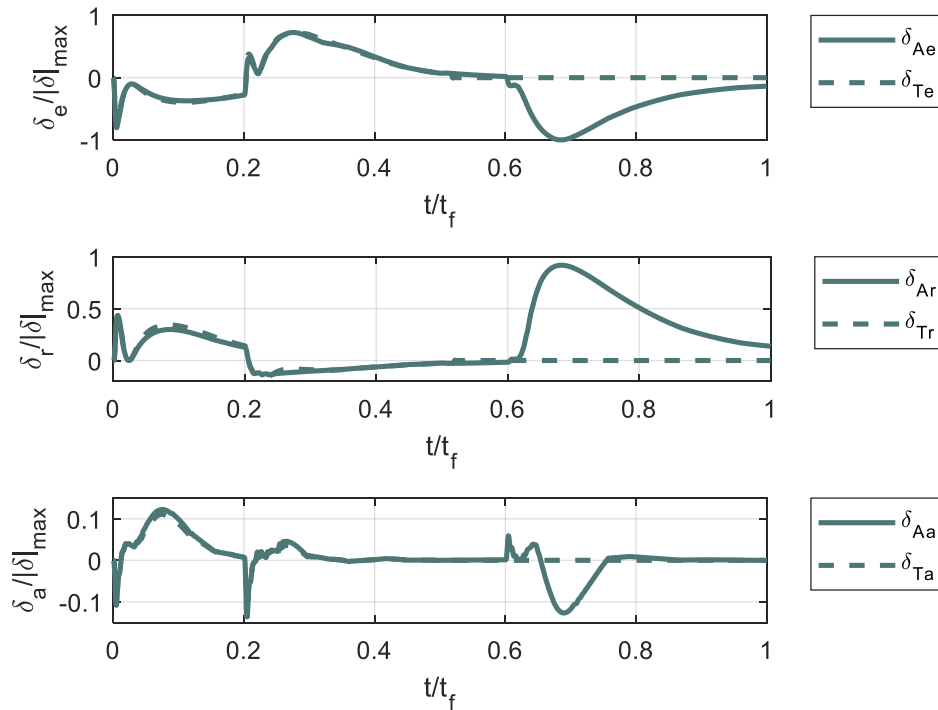


Figure 12 Normalized Effective Fin Deflections with Attitude Autopilot

Autopilot designed here converts angular rate commands to fin deflection commands in coast phase or aerodynamic and jet vane commands for the boost phase. Since the investigated missile has two flight phases, jet vanes cannot produce any command after the boost phase. As it is mentioned in 3.1.4.4, in the system, there are four fins for AC and four jet vanes for TVC. The effective fin commands pass through the actuator dynamics then they are distributed to the actual fins. Then again, effective fin deflections are calculated and plotted in Figure 12.

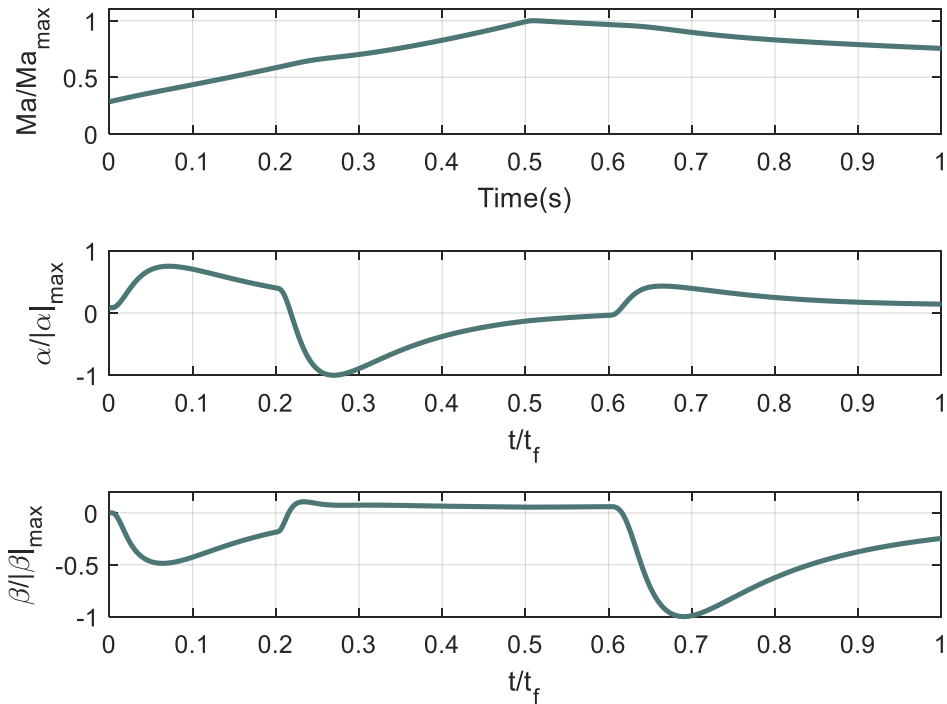


Figure 13 Normalized Values of Mach Number, Angle of Attack and Angle of Sideslip with Attitude Autopilot

For the flight condition of the example, it is seen that speed decreases after the boost phase due to drag and gravity as illustrated in Figure 13. Also, to realize the commanded angles, the missile is exposed to both the angle of attack and the sideslip angles to a considerable level, as expected from an air defense system.

## 4.2 Acceleration Autopilot

Acceleration autopilots aim to realize the commanded acceleration signal which is usually the output of the guidance algorithm. The control of accelerations in the pitch and yaw channels with the roll angle control are included in this part leading to a total approach to the control of the missile's acceleration in 6-DOF. Reducing the plant model to a linear system by choosing state variables according to their impact on control variables is a well-known approach but has drawbacks with the

high angle of attack dynamics. To overcome the weaknesses of such an approach and utilize the system's abilities more precisely, NFL control was adopted to the problem. However, the NFL is not suitable for the non-minimum phase systems due to its inversion process. Therefore, output redefinition is applied to overcome this issue.

#### 4.2.1 Problem Formulation

The translational dynamics of the missile are written as (3.8). Firstly, the state vector with system's output and input is described, similar to the way followed for attitude autopilot. The states of acceleration dynamics include angular rates in three axes ( $p, q, r$ ), angle of attack ( $\alpha$ ) and sideslip angle ( $\beta$ ), lateral and longitudinal accelerations of the missile ( $a_y, a_z$ ), and lastly, the roll angle ( $\phi$ ) to deal with the dynamics in three axes as a whole. Again, the control vector is chosen as effective fin deflections ( $\delta_e, \delta_r, \delta_a$ ) for this tail-controlled missile. Although it is intended to control the missile's acceleration of center of gravity ( $cg$ ), the output vector is taken as accelerations according to a point in front of  $cg$ . The details of this point ( $p$ ) and the control approach has been mentioned in depth in 4.2.2. This approach is known as output redefinition in literature.

$$\vec{x}_i = \begin{bmatrix} p \\ q \\ r \end{bmatrix}, \vec{x}_o = \begin{bmatrix} \alpha \\ \beta \\ \phi \\ a_{p_y} \\ a_{p_z} \end{bmatrix}, \vec{y} = \begin{bmatrix} \phi \\ a_{p_y} \\ a_{p_z} \end{bmatrix}, \vec{u} = \begin{bmatrix} \delta_e \\ \delta_r \\ \delta_a \end{bmatrix} \quad (4.28)$$

Angular rates are much faster than the angle of attack and the acceleration dynamics. Therefore, those are controlled in the inner loop and assumed as they reach steady state much faster than the accelerations which compose the outer loop's controlled variables. As the theory of the NFL suggests, this cascaded structure works as follows: by inverting the outer loop, the required command of

the inner loop can be calculated, and the inner loop actualizes this command by generating a control surface command. The process is given in (4.2) and (4.3) with newly defined system variables.

#### **4.2.2 Minimum Phase Output Definition**

In order to create a force in a particular direction for a tail-controlled missile in the air, firstly, an angle of attack towards that direction should be created in order to increase the lift force. To point the nose of the missile in the relevant direction, control surfaces deflect such that it creates a force in the opposite direction. Since the tails are behind the center of gravity, the opposite force aims to create a teetering effect. However, when this situation occurs, since the total force on the missile body in the relevant direction decreases momentarily, the missile moves to the opposite direction first, until the force on the other side prevails with the angle of attack. This phenomenon is known as the non-minimum phase behavior of aerodynamic tail-controlled missiles. Mathematical representation of such systems results in open-loop right half plane zeros in the s-domain. Due to the nature of the aerodynamic tail-controlled missiles, transfer functions from control surface deflection to accelerations have open-loop zeros at the right half-plane, as one can see an example of it in Appendix A.

Nonlinear dynamic inversion is a method that finds the required command for a system by inverting the open-loop dynamics. The zeros of the system become poles with this inversion process. Therefore, right half plane zero can cause undesirable transient dynamics or even an instability issue. In order to avoid this problem, there are studies as in [45] such that the angle of attack is chosen as the control output of the second loop, and a third loop is suggested to control the acceleration. Another approach is to redefine output, including the angle of attack in the output [24]. However, the accurate measurement of the aerodynamic angles is not feasible in real systems. A physically motivated approach is presented in [34], which defines the output according to IMU position to overcome this non-minimum phase issue.

However, IMU location is the result of the whole design process, and the transfer function from control surface deflection to acceleration calculated at IMU location does not always have to result in a minimum phase system. Therefore, the author proposed a more novel approach by defining the acceleration output at the center of percussion [33].

Center of Percussion (*cop*): If a bar is hit from a point besides its center of gravity(*cg*), it will produce a torque around its *cg*, and a rotational motion in addition to a translational motion will be produced. Moreover, there is a location on the bar called the center of oscillation or equivalently center of percussion such that forward translational and backward rotational velocity becomes equal in magnitude and opposite in direction [6]. In fact, the center of percussion can be defined as a point at which the forces acting on an extended object are recovered by rotational acceleration. This definition adapted to non-minimum phase missiles in [33], and the output redefinition in this study is made in accordance with it. In (4.29), the acceleration created by fin is equated to fin induced rotational acceleration in the pitch channel where  $x_{cop/cg}$  shows the distance from *cop* to *cg* along  $x_B$ . In Figure 42 the center of percussion illustrated.

$$x_{cop/cg} \frac{QS_{ref}l_{ref}C_{m\delta_e}}{I_{yy}} = \frac{QS_{ref}}{m}C_{z\delta_e} \quad (4.29)$$

Center of percussion should be along center of gravity and its distance from the *cg* in vector form can be defined as in (4.30).

$$\vec{x}_{cop} = [x_{cop/cg} \ 0 \ 0]^T \quad (4.30)$$

By taking the derivation of above position vector two times, acceleration at the *cop* can be found. In (4.31)  $\vec{a}_{cop/I}^B$  is missile's acceleration at the *cop* with respect to inertial frame written in body frame,  $\vec{a}_{cg/I}^B$  is missile's acceleration at the *cg* with

respect to inertial frame written in body frame and the other parameters are as described in 3.

$$\begin{aligned}
\vec{a}_{cop/1}^B &= \vec{a}_{cg/1}^B + \left. \frac{d^2 \vec{x}_{cop}}{dt^2} \right|_I \\
&= \vec{a}_{cg/1}^B + \ddot{\vec{x}}_{cop} + \dot{\vec{\omega}}_{B/1}^B \times \vec{x}_{cop} + 2\vec{\omega}_{B/1}^B \times \dot{\vec{x}}_{cop} + \vec{\omega}_{B/1}^B \\
&\quad \times (\vec{\omega}_{B/1}^B \times \vec{x}_{cop})
\end{aligned} \tag{4.31}$$

By neglecting the change in center of gravity, the above equation is simplified as in (4.32).

$$\vec{a}_{cop/1}^B = \vec{a}_{cg/1}^B + \begin{bmatrix} -x_{cop/cg}(q^2 + r^2) \\ x_{cop/cg}(\dot{r} + pq) \\ x_{cop/cg}(-\dot{q} + pr) \end{bmatrix} \tag{4.32}$$

In this study, acceleration output is defined at a point  $p$  which equated to the  $cop$  location as described in (4.33), which is found dynamically according to the flight condition.

$$x_p = x_{cop/cg} \tag{4.33}$$

For a given flight condition (constant speed and altitude) Figure 43 in Appendix A. shows the change in zeros of the system with  $x_p$ . The poles of the system do not change with this newly defined output.

Linear accelerations of point  $p$  and the  $cg$  with respect to the inertial frame is defined as  $\vec{a}_{p/1}^B$  and  $\vec{a}_{cg/1}^B$  respectively. Scalar components of these vectors are defined as in (4.34).

$$\vec{a}_{p/1}^B = \begin{bmatrix} a_{p_x} \\ a_{p_y} \\ a_{p_z} \end{bmatrix}, \vec{a}_{cg/1}^B = \begin{bmatrix} a_{cg_x} \\ a_{cg_y} \\ a_{cg_z} \end{bmatrix} \tag{4.34}$$

The output vector  $\vec{y}$  of the acceleration autopilot and its components are shown in (4.35).

$$\vec{y} = \begin{bmatrix} \phi \\ a_{p_y} \\ a_{p_z} \end{bmatrix} = \begin{bmatrix} \int (p + (q \sin \phi + r \cos \phi) \tan \theta) dt \\ a_{cgy} + x_p(\dot{r} + pq) \\ a_{cgz} + x_p(-\dot{q} + pr) \end{bmatrix} \quad (4.35)$$

Note that the roll dynamic may also be written in terms of aerodynamic angles. However, since it is already controlled in the attitude autopilot, the idea is adapted here as well.

### 4.2.3 Inner Loop Design

Angular rates control for boost and coast phase with two structural cases (aerodynamic and thrust vector control with same and different actuators) are explained in detail in 4.1.2 for the attitude autopilot. This inner loop strategy is directly implemented here as well. Therefore, reader can refer to 4.1.2 for the inner loop design.

### 4.2.4 Outer Loop Design

The outer loop seeks to follow the reference acceleration commands via generating angular rate commands for the inner loop to follow. The equations given as (3.3) and (3.8) are used to control roll angle, lateral and longitudinal accelerations, respectively. The gravitational and centrifugal acceleration is neglected.

Normal force components are included in (3.24) and (3.32). In order to bring the equation into a compatible format with the nonlinear dynamic inversion method, the components of the forces tried to be written in two parts as the part depends on

inputs, and the part does not depend on the inputs i.e. decoupling matrix. The accelerations in yaw and pitch channel are tabulated in (4.36) with all the parameters described in detail.

$$\begin{aligned}
a_{cg_y} &= \frac{Y}{m} \\
a_{cg_z} &= \frac{Z}{m} \\
Z &= QC_Z S_{ref} + F_{T_z} \\
Y &= QC_Y S_{ref} + F_{T_y} \\
C_Z &= C_Z(\alpha, \beta, Ma, \delta_A) \\
&= C_{Z_0}(\alpha, \beta, Ma) + C_{Z_q}(Ma, x_{cg}) \frac{ql_{ref}}{2V} \\
&\quad + C_{Z_{\delta_A}}(\alpha, \beta, Ma, \delta_A) \\
C_Y &= C_Y(\alpha, \beta, Ma, \delta_A) \\
&= C_{Y_0}(\alpha, \beta, Ma) + C_{Y_r}(Ma, x_{cg}) \frac{rl_{ref}}{2V} \\
&\quad + C_{Y_{\delta_A}}(\alpha, \beta, Ma, \delta_A) \\
F_{T_z} &= -T \sin \theta_T(\delta_{T_e}) \cos \psi_T(\delta_{T_r}) \\
F_{T_y} &= T \sin \psi_T(\delta_{T_r})
\end{aligned} \tag{4.36}$$

As it is explained earlier the acceleration outputs redefined in (4.37) as described in 4.2.2.

$$\begin{aligned}
a_{p_y} &= a_{cg_y} + x_p(\dot{r} + pq) \\
a_{p_z} &= a_{cg_z} + x_p(-\dot{q} + pr)
\end{aligned} \tag{4.37}$$

By taking the derivative of (4.37), similar representation to (3.44) is obtained in (4.38) as it is looked for.

$$\dot{a}_{p_y} = \dot{a}_{cg_y} + x_p(\ddot{r} + \dot{p}q + p\dot{q}) \tag{4.38}$$

$$\dot{a}_{p_z} = \dot{a}_{c_{g_z}} + x_p(-\ddot{q} + \dot{p}r + p\dot{r})$$

From this point on, control variables dynamics are derived as in (4.39). Dynamic equations of angular accelerations are inserted as they are already defined with equation (4.4).

Change of aerodynamic coefficients with respect to Mach and fin deflections, derivatives of dynamic coefficients, higher-order terms are ignored since those terms are small compared to the angle of attack and angle of sideslip dynamics.

$$\begin{aligned} \dot{\phi} &= p + (q \sin \phi + r \cos \phi) \tan \theta \\ \dot{a}_{p_y} &= \frac{QS_{ref}}{m} \left( \frac{\partial C_{Y_0}}{\partial \alpha} \dot{\alpha} + \frac{\partial C_{Y_0}}{\partial \beta} \dot{\beta} \right) + \frac{x_p QS_{ref} l_{ref}}{I_{zz}} \left( \frac{\partial C_{n_0}}{\partial \alpha} \dot{\alpha} + \frac{\partial C_{n_0}}{\partial \beta} \dot{\beta} \right) \\ &\quad + x_p \left( \frac{QS_{ref} l_{ref} C_l + M_{x_{tvc}} - qr(I_{zz} - I_{yy})}{I_{xx}} q \right. \\ &\quad \left. + \frac{QS_{ref} l_{ref} C_m + M_{y_{tvc}} - rp(I_{xx} - I_{zz})}{I_{yy}} p \right) \\ \dot{a}_{p_z} &= \frac{QS_{ref}}{m} \left( \frac{\partial C_{Z_0}}{\partial \alpha} \dot{\alpha} + \frac{\partial C_{Z_0}}{\partial \beta} \dot{\beta} \right) - \frac{x_p QS_{ref} l_{ref}}{I_{yy}} \left( \frac{\partial C_{m_0}}{\partial \alpha} \dot{\alpha} + \frac{\partial C_{m_0}}{\partial \beta} \dot{\beta} \right) \\ &\quad + x_p \left( \frac{QS_{ref} l_{ref} C_l + M_{x_{tvc}} - qr(I_{zz} - I_{yy})}{I_{xx}} r \right. \\ &\quad \left. + \frac{QS_{ref} l_{ref} C_n + M_{z_{tvc}} - pq(I_{yy} - I_{xx})}{I_{zz}} p \right) \end{aligned} \quad (4.39)$$

Note that partial derivatives can be calculated as (4.40) where  $h$  is a sufficiently small step size.

$$\frac{\partial C_{i_j}(x_1, \dots, x_k, \dots, x_n)}{\partial x_k} = \frac{C_{i_j}(x_1, \dots, x_k + h, \dots, x_n) - C_{i_j}(x_1, \dots, x_k, \dots, x_n)}{h} \quad (4.40)$$

In (4.39),  $\dot{\alpha}$  and  $\dot{\beta}$  terms should be calculated. This will be done by taking the derivatives of the equations given in (4.41).

$$\begin{aligned}\tan \beta &= \frac{v}{u} \\ \tan \alpha &= \frac{w}{u}\end{aligned}\tag{4.41}$$

The formal definitions of aerodynamic angles are defined in 3.1.4.4. Above equations can be arranged as in (4.42).

$$\begin{aligned}\tan^2 \alpha + \tan^2 \beta + 1 &= \frac{v^2 + w^2 + u^2}{u^2} \\ u &= V/\sqrt{\tan^2 \alpha + \tan^2 \beta + 1} \\ v &= u \tan \beta \\ w &= u \tan \alpha\end{aligned}\tag{4.42}$$

Following derivations in (4.43) and (4.44) are obtained from (3.27), and (3.28).

$$\begin{aligned}\dot{\alpha} &= \frac{1}{1 + \left(\frac{w}{u}\right)^2} \frac{\dot{w}u - w\dot{u}}{u^2} \\ \dot{\beta} &= \frac{1}{1 + \left(\frac{v}{u}\right)^2} \frac{\dot{v}u - v\dot{u}}{u^2}\end{aligned}\tag{4.43}$$

Using the arrangements from (4.42), and substituting  $\dot{w}$  and  $\dot{u}$  from (3.8) only with neglecting the gravitational effects, angle of attack and angle of sideslip dynamics can be written.

$$\begin{aligned}\dot{\alpha} &= q - (p \cos \alpha + r \sin \alpha) \cos \alpha \tan \beta + \frac{(a_{cg_z} \cos \alpha - a_{cg_x} \sin \alpha) \cos \alpha}{V/\sqrt{1 + \tan^2 \alpha + \tan^2 \beta}} \\ \dot{\beta} &= -r + (p \cos \beta + q \sin \beta) \cos \beta \tan \alpha + \frac{(a_{cg_y} \cos \beta - a_{cg_x} \sin \beta) \cos \beta}{V/\sqrt{1 + \tan^2 \alpha + \tan^2 \beta}}\end{aligned}\tag{4.44}$$

By inserting these into (4.39) outer loop can be written in matrix form depending on the inner loop control variables as in (4.45).

$$\dot{y} = f(p, q, r) = A_o \begin{bmatrix} p \\ q \\ r \end{bmatrix} + b_o$$

$$\begin{bmatrix} \dot{\phi} \\ \dot{a}_{p/I_y}^B \\ \dot{a}_{p/I_z}^B \end{bmatrix} = \begin{bmatrix} A_{o11} & A_{o12} & A_{o13} \\ A_{o21} & A_{o22} & A_{o23} \\ A_{o31} & A_{o32} & A_{o33} \end{bmatrix} \begin{bmatrix} p \\ q \\ r \end{bmatrix} + \begin{bmatrix} b_{o1} \\ b_{o2} \\ b_{o3} \end{bmatrix} \quad (4.45)$$

The terms in  $A_o$  matrix are calculated in (4.46).

$$A_{o11} = 1$$

$$A_{o12} = \sin \phi \tan \theta$$

$$A_{o13} = \cos \phi \tan \theta$$

$$A_{o21} = \left( \frac{QS_{ref}}{m} \left( -\frac{\partial C_{Y_0}}{\partial \alpha} \cos^2 \alpha \tan \beta + \frac{\partial C_{Y_0}}{\partial \beta} \cos^2 \beta \tan \alpha \right) \right.$$

$$+ \frac{x_p QS_{ref} l_{ref}}{I_{zz}} \left( -\frac{\partial C_{n_0}}{\partial \alpha} \cos^2 \alpha \tan \beta + \frac{\partial C_{n_0}}{\partial \beta} \cos^2 \beta \tan \alpha \right)$$

$$\left. + \frac{x_p QS_{ref} l_{ref} C_m}{I_{yy}} \right)$$

$$A_{o22} = \left( \frac{QS_{ref}}{m} \left( \frac{\partial C_{Y_0}}{\partial \alpha} + \frac{\partial C_{Y_0}}{\partial \beta} \sin \beta \cos \beta \tan \alpha \right) \right.$$

$$+ \frac{x_p QS_{ref} l_{ref}}{I_{zz}} \left( \frac{\partial C_{n_0}}{\partial \alpha} + \frac{\partial C_{n_0}}{\partial \beta} \sin \beta \cos \beta \tan \alpha \right)$$

$$\left. + \frac{x_p QS_{ref} l_{ref} C_l}{I_{xx}} \right) \quad (4.46)$$

$$A_{o23} = \left( \frac{QS_{ref}}{m} \left( -\frac{\partial C_{Y_0}}{\partial \alpha} \sin \alpha \cos \alpha \tan \beta - \frac{\partial C_{Y_0}}{\partial \beta} \right) \right.$$

$$\left. + \frac{x_p QS_{ref} l_{ref}}{I_{zz}} \left( -\frac{\partial C_{n_0}}{\partial \alpha} \sin \alpha \cos \alpha \tan \beta - \frac{\partial C_{n_0}}{\partial \beta} \right) \right)$$

$$\begin{aligned}
A_{o_{31}} &= \left( \frac{QS_{ref}}{m} \left( -\frac{\partial C_{Z_0}}{\partial \alpha} \cos^2 \alpha \tan \beta + \frac{\partial C_{Z_0}}{\partial \beta} \cos^2 \beta \tan \alpha \right) \right. \\
&\quad \left. - \frac{x_p QS_{ref} l_{ref}}{I_{yy}} \left( -\frac{\partial C_{m_0}}{\partial \alpha} \cos^2 \alpha \tan \beta + \frac{\partial C_{m_0}}{\partial \beta} \cos^2 \beta \tan \alpha \right) \right. \\
&\quad \left. + \frac{x_p QS_{ref} l_{ref} C_n}{I_{zz}} \right) \\
A_{o_{32}} &= \left( \frac{QS_{ref}}{m} \left( \frac{\partial C_{Z_0}}{\partial \alpha} + \frac{\partial C_{Z_0}}{\partial \beta} \sin \beta \cos \beta \tan \alpha \right) \right. \\
&\quad \left. - \frac{x_p QS_{ref} l_{ref}}{I_{yy}} \left( \frac{\partial C_{m_0}}{\partial \alpha} + \frac{\partial C_{m_0}}{\partial \beta} \sin \beta \cos \beta \tan \alpha \right) \right) \\
A_{o_{33}} &= \left( \frac{QS_{ref}}{m} \left( -\frac{\partial C_{Z_0}}{\partial \alpha} \sin \alpha \cos \alpha \tan \beta - \frac{\partial C_{Z_0}}{\partial \beta} \right) \right. \\
&\quad \left. - \frac{x_p QS_{ref} l_{ref}}{I_{yy}} \left( -\frac{\partial C_{m_0}}{\partial \alpha} \sin \alpha \cos \alpha \tan \beta - \frac{\partial C_{m_0}}{\partial \beta} \right) \right. \\
&\quad \left. + \frac{x_p QS_{ref} l_{ref} C_l}{I_{xx}} \right)
\end{aligned}$$

The terms in  $b_o$  matrix are calculated in (4.47).

$$\begin{aligned}
b_{o_1} &= 0 \\
b_{o_2} &= QS_{ref} \left( \left( \frac{1}{m} \frac{\partial C_{Y_0}}{\partial \alpha} + \frac{x_p l_{ref}}{I_{zz}} \frac{\partial C_{n_0}}{\partial \alpha} \right) \frac{(a_{cgz} \cos \alpha - a_{cgx} \sin \alpha) \cos \alpha}{V/\sqrt{1 + \tan^2 \alpha + \tan^2 \beta}} \right. \\
&\quad \left. + \left( \frac{1}{m} \frac{\partial C_{Y_0}}{\partial \beta} + \frac{x_p l_{ref}}{I_{zz}} \frac{\partial C_{n_0}}{\partial \beta} \right) \frac{(a_{cgy} \cos \beta - a_{cgx} \sin \beta) \cos \beta}{V/\sqrt{1 + \tan^2 \alpha + \tan^2 \beta}} \right) \quad (4.47) \\
b_{o_3} &= QS_{ref} \left( \left( \frac{1}{m} \frac{\partial C_{Z_0}}{\partial \alpha} - \frac{x_p l_{ref}}{I_{yy}} \frac{\partial C_{m_0}}{\partial \alpha} \right) \frac{(a_{cgz} \cos \alpha - a_{cgx} \sin \alpha) \cos \alpha}{V/\sqrt{1 + \tan^2 \alpha + \tan^2 \beta}} \right. \\
&\quad \left. + \left( \frac{1}{m} \frac{\partial C_{Z_0}}{\partial \beta} - \frac{x_p l_{ref}}{I_{yy}} \frac{\partial C_{m_0}}{\partial \beta} \right) \frac{(a_{cgy} \cos \beta - a_{cgz} \sin \beta) \cos \beta}{V/\sqrt{1 + \tan^2 \alpha + \tan^2 \beta}} \right)
\end{aligned}$$

Similar to the idea followed for attitude autopilot, virtual control inputs for the given system is selected as rates of the outputs as given in (4.48).

$$\begin{bmatrix} v_\phi \\ v_{a_y} \\ v_{a_z} \end{bmatrix} = \begin{bmatrix} \dot{\phi} \\ \dot{a}_{p_y} \\ \dot{a}_{p_z} \end{bmatrix} \quad (4.48)$$

Then a second-order reference model and a PI controller are implemented again. For the design methodology of virtual control and the calculation of the gains, one can refer to 4.1.2 since the same idea is extended as well for the loop described here.

$$\omega_{com} = A_o^{-1} \left( -b_0 + K_{acc} \begin{bmatrix} \phi_{ref} - \phi \\ \int \phi_{ref} - \phi \\ a_{p_y ref} - a_{p_y} \\ \int a_{p_y ref} - a_{p_y} \\ a_{p_z ref} - a_{p_z} \\ \int a_{p_z ref} - a_{p_z} \end{bmatrix} + \begin{bmatrix} \dot{\phi}_{ref} \\ \dot{a}_{p_y ref} \\ \dot{a}_{p_z ref} \end{bmatrix} \right) \quad (4.49)$$

$$K_{acc} = \begin{bmatrix} K_{\phi_P} & K_{\phi_I} & 0 & 0 & 0 & 0 \\ 0 & 0 & K_{a_{yP}} & K_{a_{yI}} & 0 & 0 \\ 0 & 0 & 0 & 0 & K_{a_{zP}} & K_{a_{zI}} \end{bmatrix}$$

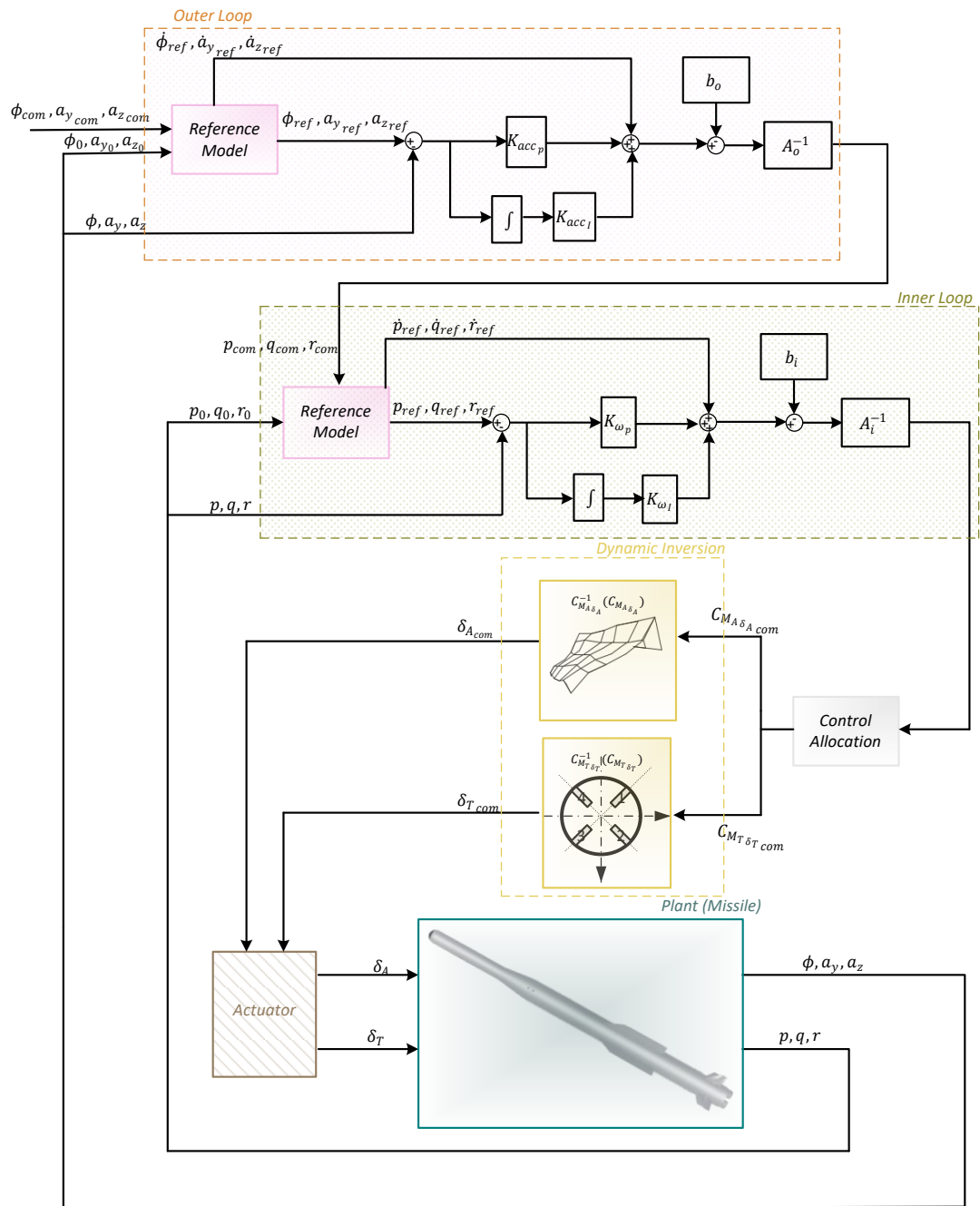


Figure 14 Acceleration Autopilot Scheme

#### **4.2.5 Evaluation of Nominal Acceleration Autopilot**

The results are given in comparison with another autopilot designed with MFC in order to see if the performance is acceptable compared to the MFC method that is already available for the system under consideration. Moreover, to see the superiority of the NDI method described here due to coupled effects, two example scenarios are generated such that for the first scenario no roll angle is expected from missile and acceleration commands in pitch and yaw dynamics are comparatively small, for the second scenario, cross-coupling effects are higher due to expectations on roll control and higher acceleration commands. These cases are referred to as ‘scenario 1’ and ‘scenario 2’ respectively through the explanations below.

Again, as in 4.1.4 all the responses are displayed in a normalized form, and the values used for normalization are given in the figures.

### 4.2.5.1 Scenario 1

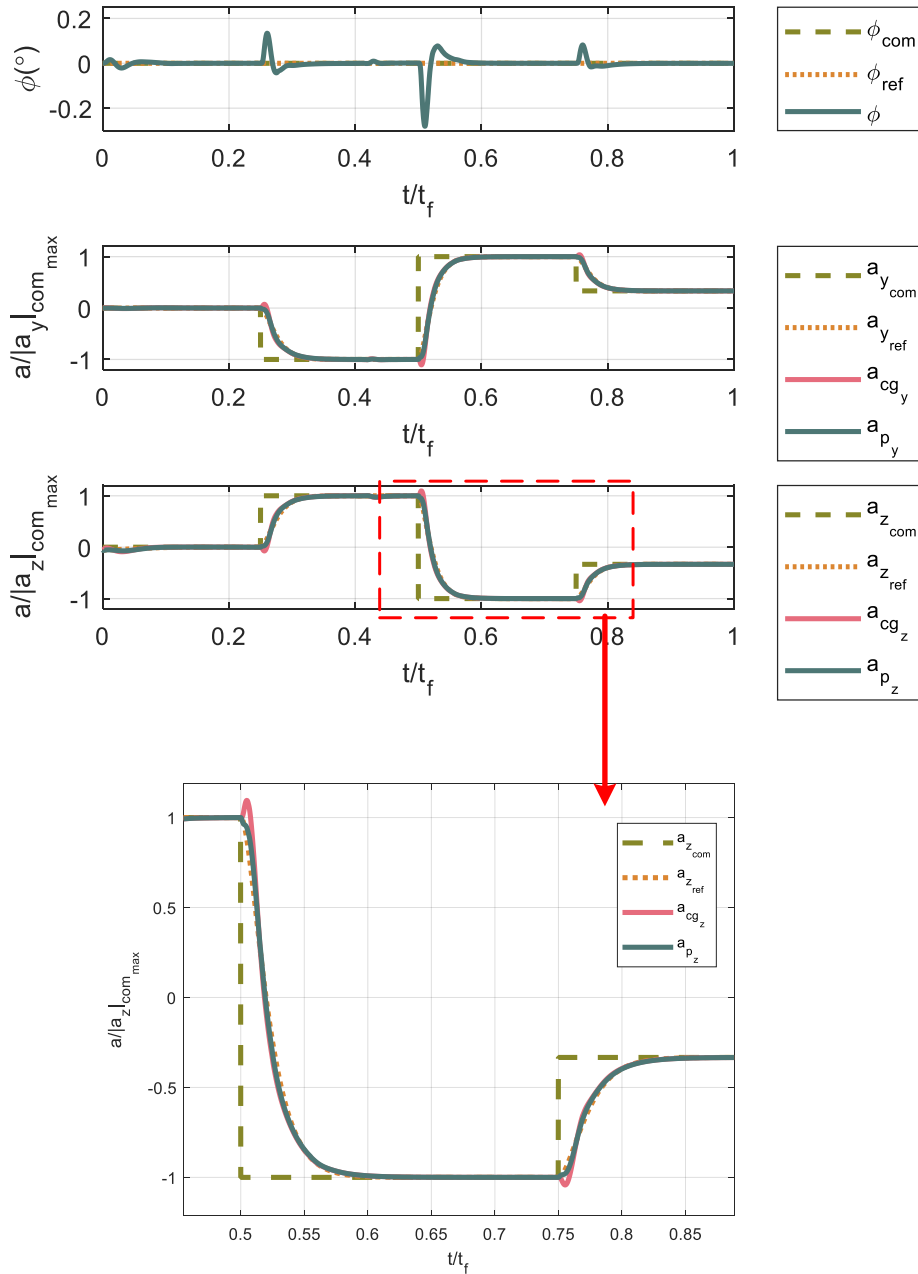


Figure 15 Normalized Acceleration Tracking Performance for Scenario 1

It is seen in Figure 15, the acceleration on the *cop* follows the reference command, which is produced by reference model. However, when the acceleration of the

center of gravity ( $cg$ ) is considered, it first produces acceleration to the opposite side, which is mentioned as non-minimum phase behavior, and then it also follows the reference. The roll angle sets itself according to changing dynamics in the pitch and yaw channels.

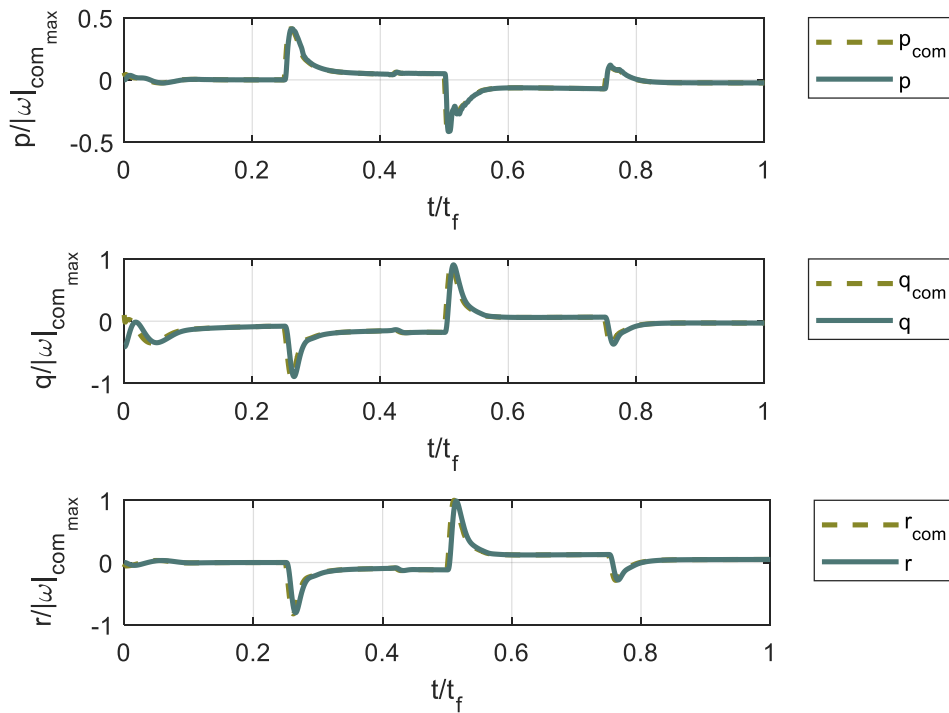


Figure 16 Normalized Angular Rate Tracking Performance for Scenario 1

It is seen in Figure 16, the inner loop controllers realize the angular rate commands of the outer loop successfully.

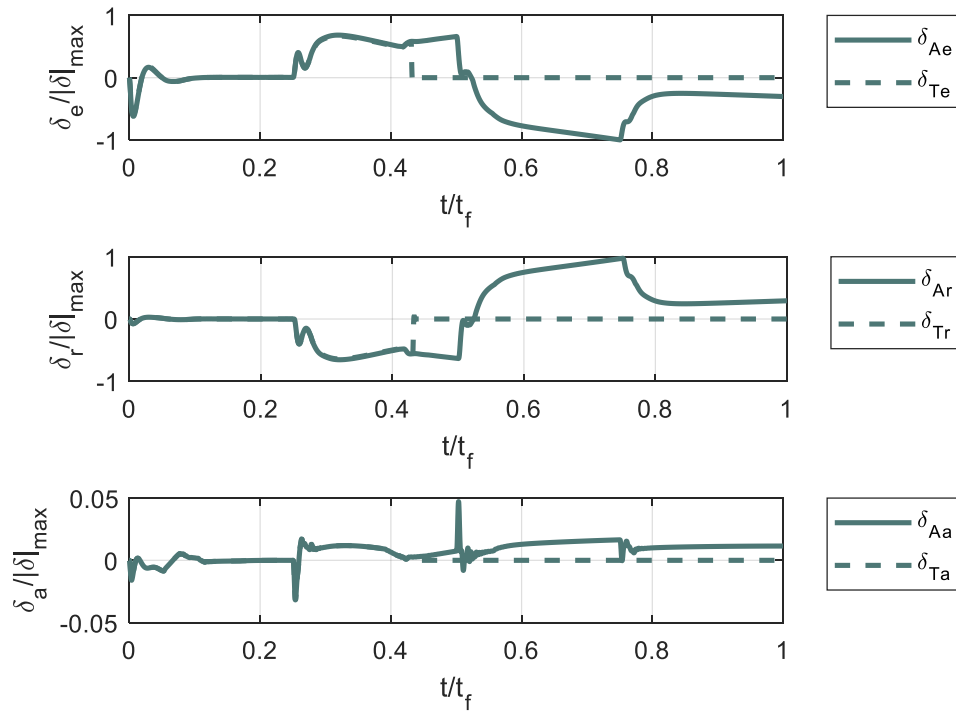


Figure 17 Normalized Effective Fin Deflections for Scenario 1

Corresponding fin commands are tabulated for the given commands in Figure 17. Jet vane deflections are not available after the boost phase, and the aileron command is much less than the commands in the other channels due to zero command in the roll channel.

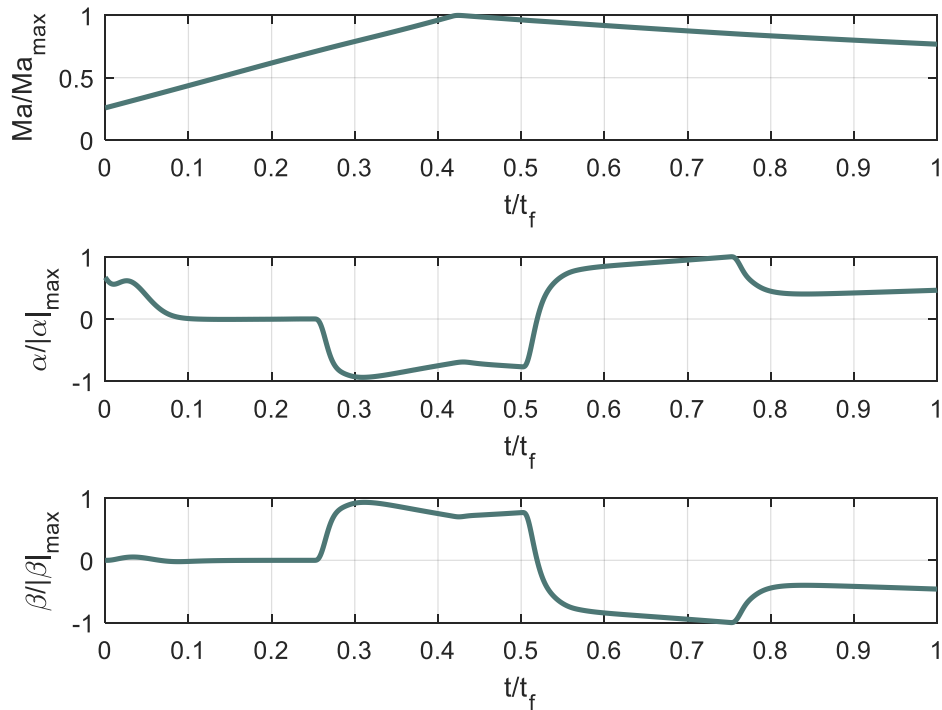


Figure 18 Normalized Values of Mach Number, Angle of Attack, and Angle of Sideslip for Scenario 1

Due to similar commands on yaw and pitch channel, angle of attack and sideslip angle displays similar behavior as it is seen in Figure 18. When the outputs are compared with the baseline autopilot, Figure 19 shows that although some performance degradation occurs for the baseline autopilot, such as small fluctuations in acceleration and some separation from roll command, it also works quite well.

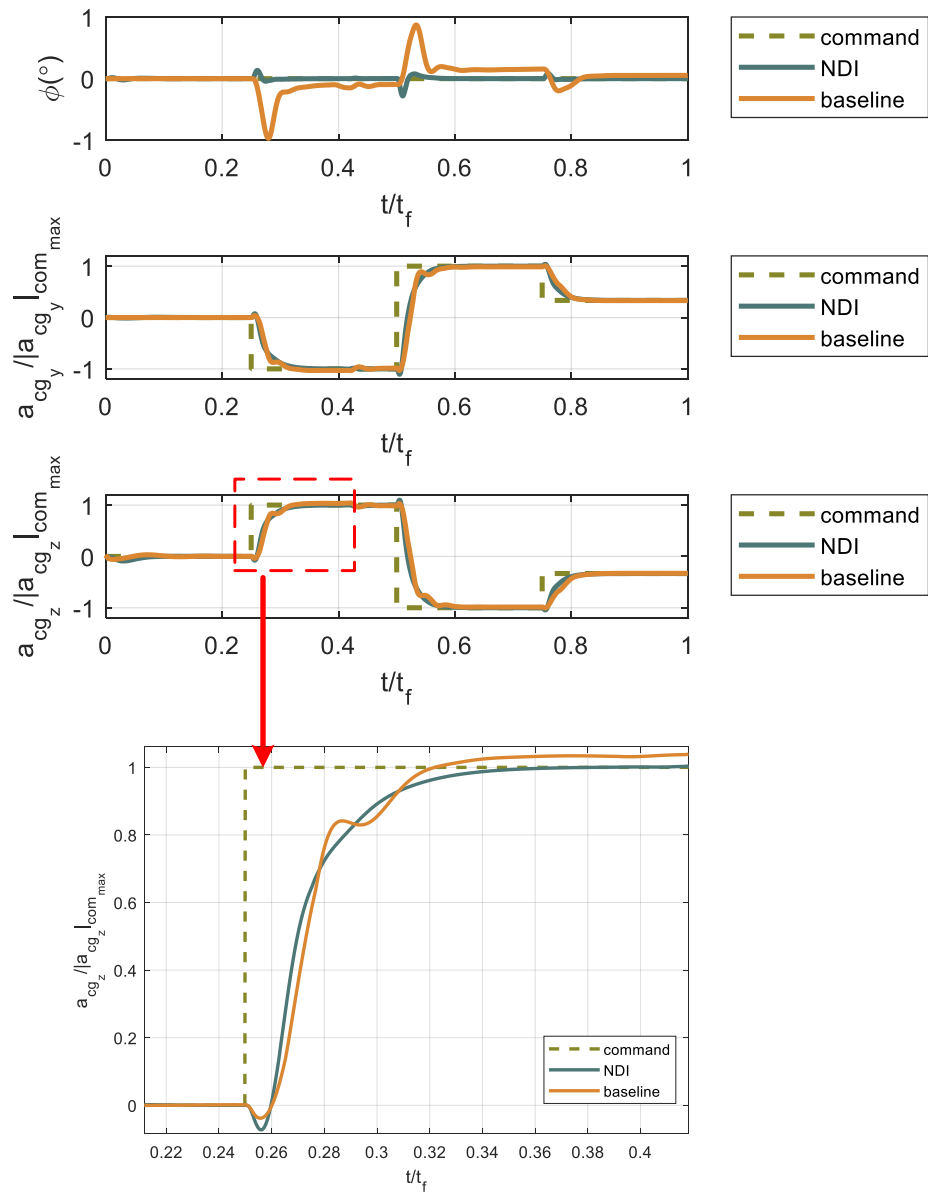


Figure 19 Normalized Acceleration Tracking Performance in Comparison with the Baseline Autopilot for Scenario 1

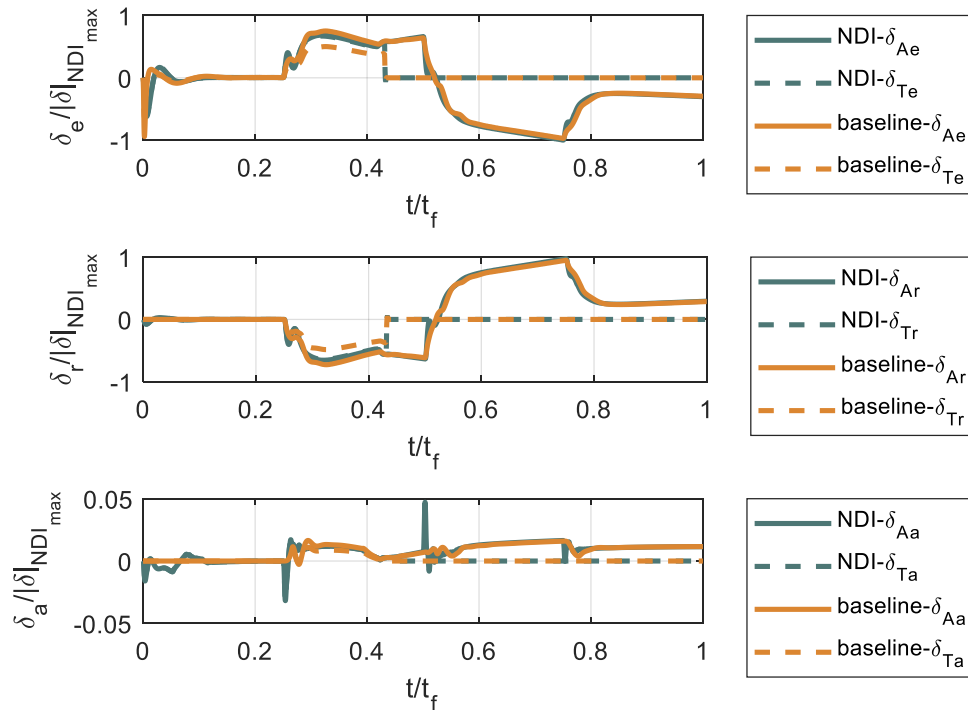


Figure 20 Normalized Effective Fin Deflections in Comparison with Baseline Autopilot for Scenario 1

From the effective fin deflections in Figure 20, it is seen that baseline autopilot applies very small deflection in the roll channel, which explains the poor roll angle control.

#### 4.2.5.2 Scenario 2

As mentioned before, a more challenging scenario is generated for this scenario with higher control demands and as a result more cross couplings occur. All the results are tabulated in normalized, and normalization values specified on the figures form again. Figure 21 shows the performance of the NDI autopilot at both the designed *cop* point and at the *cg* in all three axes with close capture of performance in the pitch axis included.

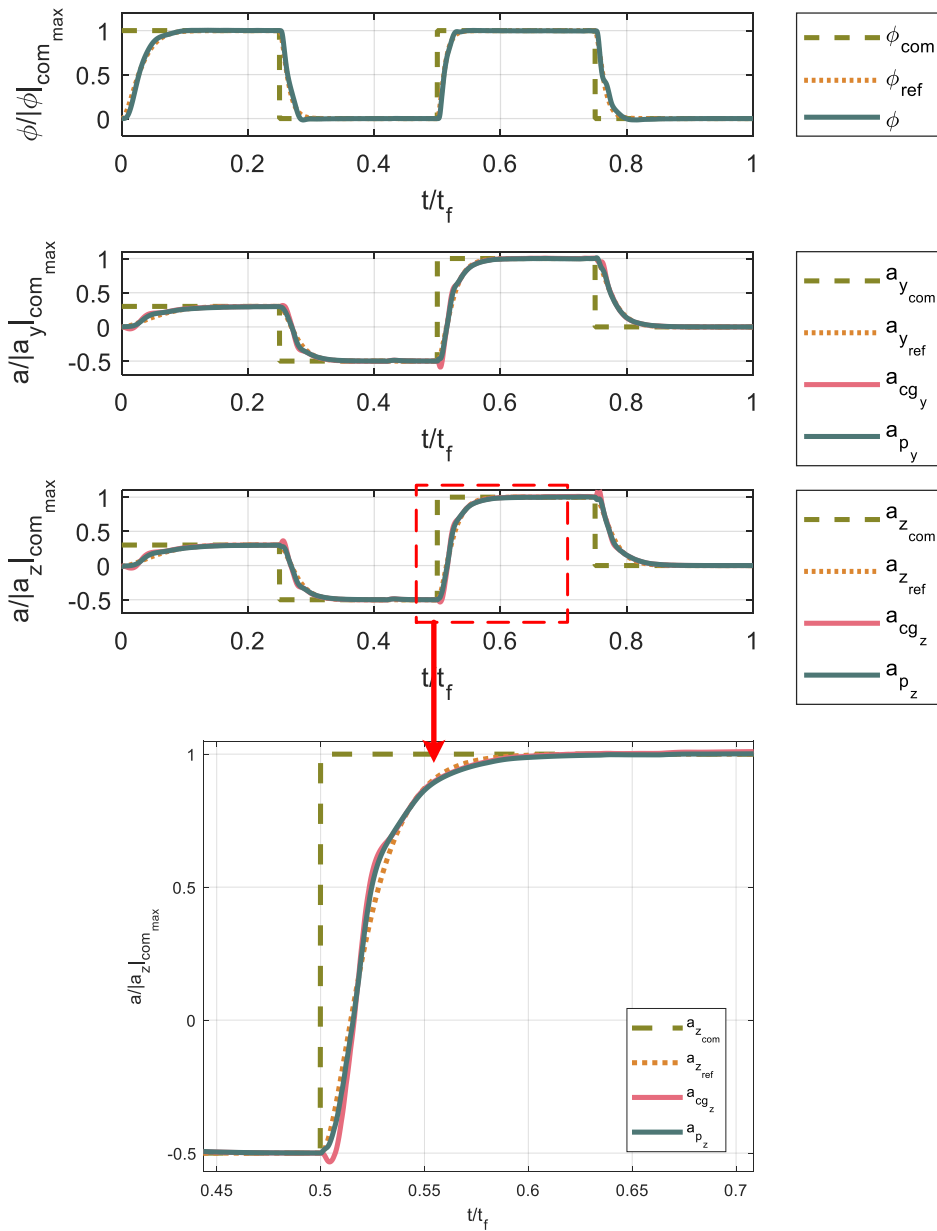


Figure 21 Normalized Acceleration Tracking Performance for Scenario 2

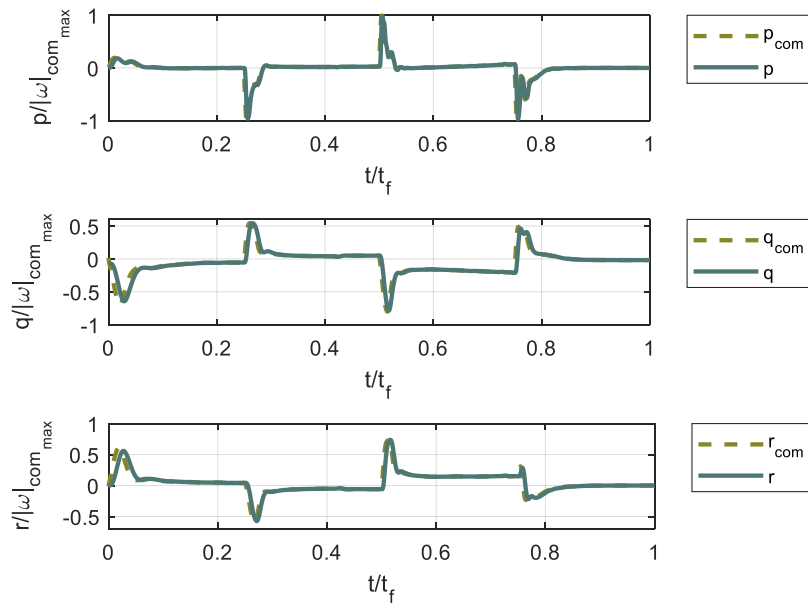


Figure 22 Normalized Angular Rate Tracking Performance for Scenario 2

Figure 22 and Figure 23 display angular rate performances and corresponding fin deflections, respectively.

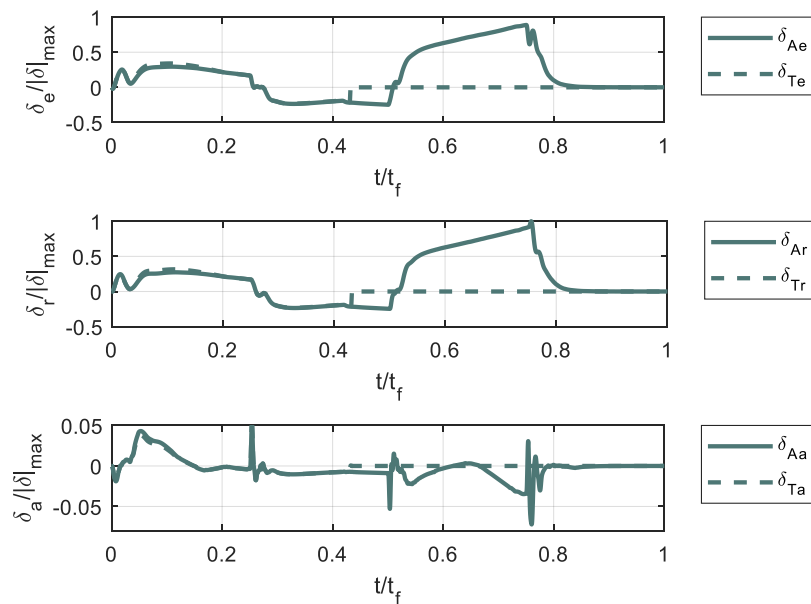


Figure 23 Normalized Effective Fin Deflections for Scenario 2

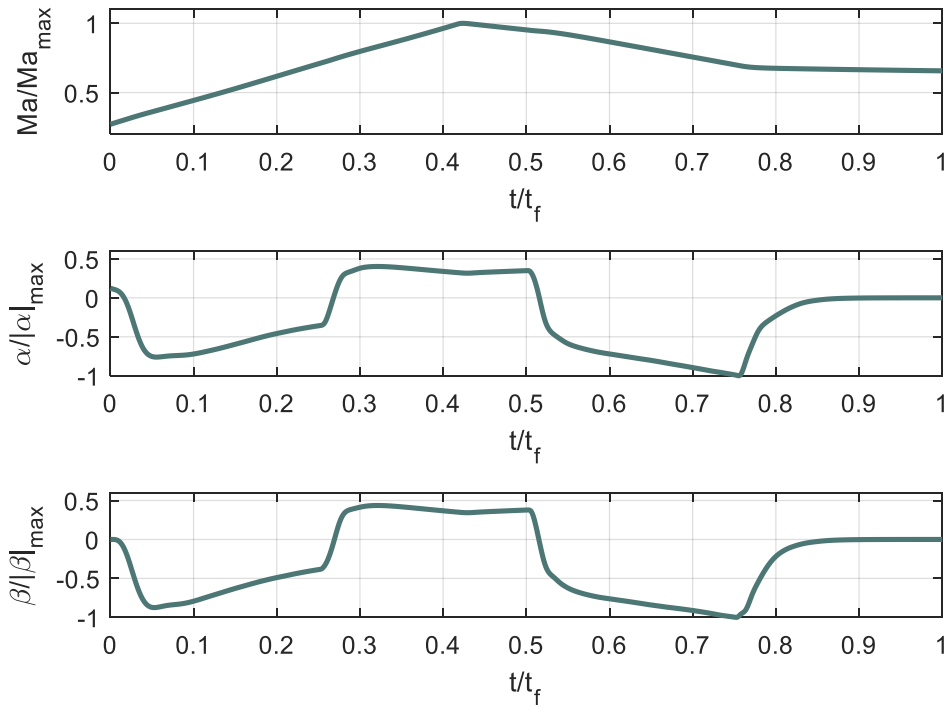


Figure 24 Normalized Values of Mach Number, Angle of Attack and Angle of Sideslip for Scenario 2

In order to preserve the integrity of the given analysis throughout the thesis, Mach and aerodynamic angles are given in Figure 24. When they are compared with the Figure 18 of scenario 1, it can be seen that the angle of sideslip is dominant than the angle of attack for scenario 2 due to the command in roll channel. This effect results in an increase in the nonlinearity, and the baseline autopilot performs in a way that approves this in Figure 25. In the figure, while the baseline autopilot exhibits prominent performance degradation, the NDI autopilot handles the situation.

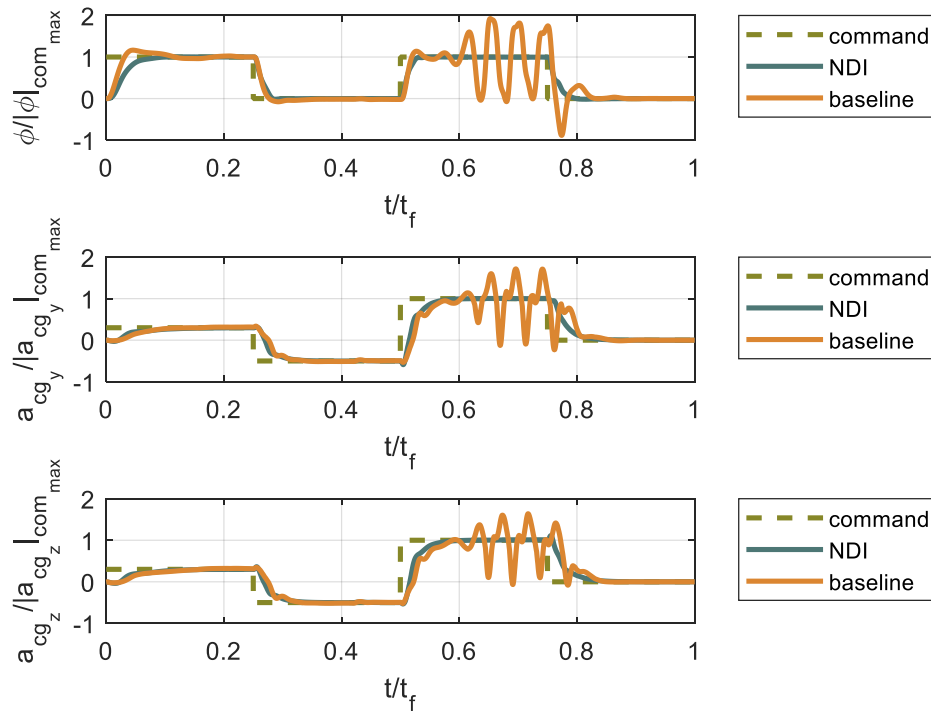


Figure 25 Normalized Acceleration Tracking Performance in Comparison with the Baseline Autopilot for Scenario 2

In the above Figure 26 fin deflections are compared for scenario 2. The reflection of performance worsening to fin deflections is observed in the figure.

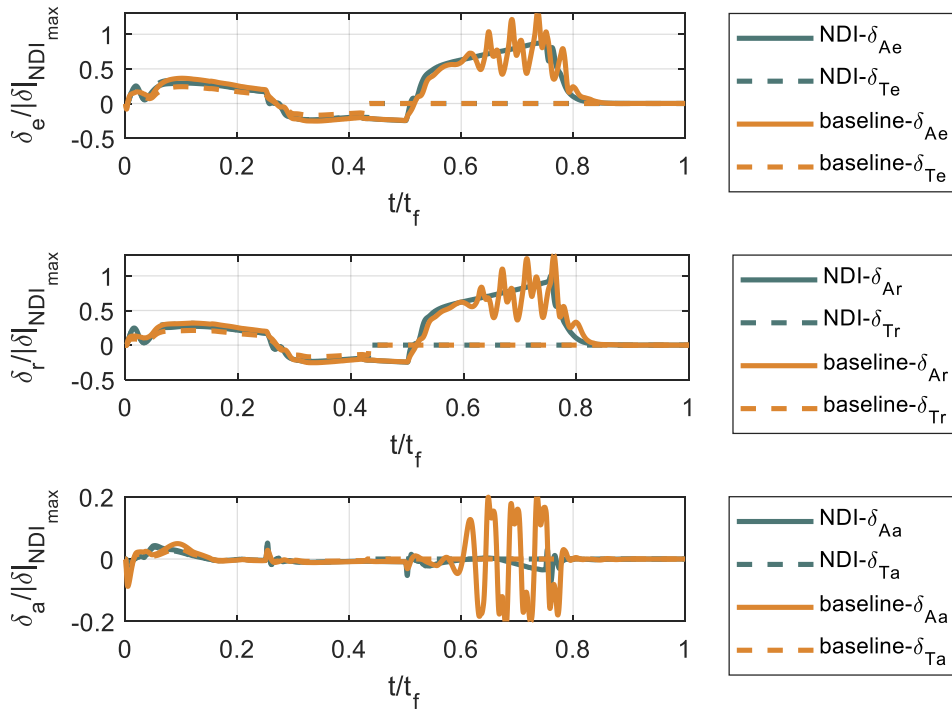


Figure 26 Normalized Effective Fin Deflections in Comparison with Baseline Autopilot for Scenario 2

### 4.3 Sensitivity Analysis

The control algorithm suggested uses different kinds of information such as physical parameters of the missile, aerodynamic parameters, and flight conditions. Some of these parameters can be measured with sensors, whereas some need to be estimated or approximated. In order to get an idea of how much the control algorithm can tolerate uncertainty on this information that we cannot measure, a sensitivity analysis with predefined four cases is carried out.

In Table 3, uncertainty percentages are set for the parameters that the algorithm relies on, and sensors do not measure. These uncertainties are decided realistically by considering the design and manufacturing process of such a missile system.

Table 3 Uncertainties for Sensitivity Analysis

Variable	Symbol	Uncertainty (%)	Case -1	Case-2	Case-3	Case-4
Mass	$m$	1	+	+	+	-
Inertia	$I$	5	+	+	-	-
Center of Gravity	$x_{cg}$	3	+	-	-	-
Non-dimensional Force Coefficients	$C_X, C_Y, C_Z$	25	+,+,+	-,,-	+,+,+	-,,-
Non-dimensional Dynamic Force Coefficients	$C_{X_d}, C_{Y_d}, C_{Z_d}$	25	+,+,+	-,,-	+,+,+	-,,-
Non-dimensional Moment Coefficients	$C_l, C_m, C_n$	25	+,+,+	-,,-	+,+,+	-,,-
Non-dimensional Dynamic Moment Coefficients	$C_{l_d}, C_{m_d}, C_{n_d}$	25	+,+,+	-,,-	+,+,+	-,,-
Thrust Force	$T$	10	+	+	-	+
Thrust Deflection Angles	$\theta_T, \psi_T$	5	+,+	-,	-,	+,+
Aerodynamic Angles	$\alpha, \beta$	10	+,+	-,	+,	-,
Dynamic Pressure	$Q$	5	+	+	-	-
Mach Number	$M$	5	+	-	+	-

In the table (+) sign means that the defined variable is extra in the real-world model of the simulation as much as the uncertainty percentage, i.e., the autopilot used the value of that parameter less as much as the uncertainty percentage. For the (-) sign, this is vice versa.

For this sensitivity analysis, the prescribed challenging cases in 4.1.4 and scenario 2 in 4.2.5.2 are used.

### 4.3.1 Sensitivity Analysis for Attitude Autopilot

First, the results of sensitivity analysis for the attitude autopilot are tabulated. It is observed in Figure 27 that although some fluctuations occur in the transient dynamics, tracking performance remains quite well.

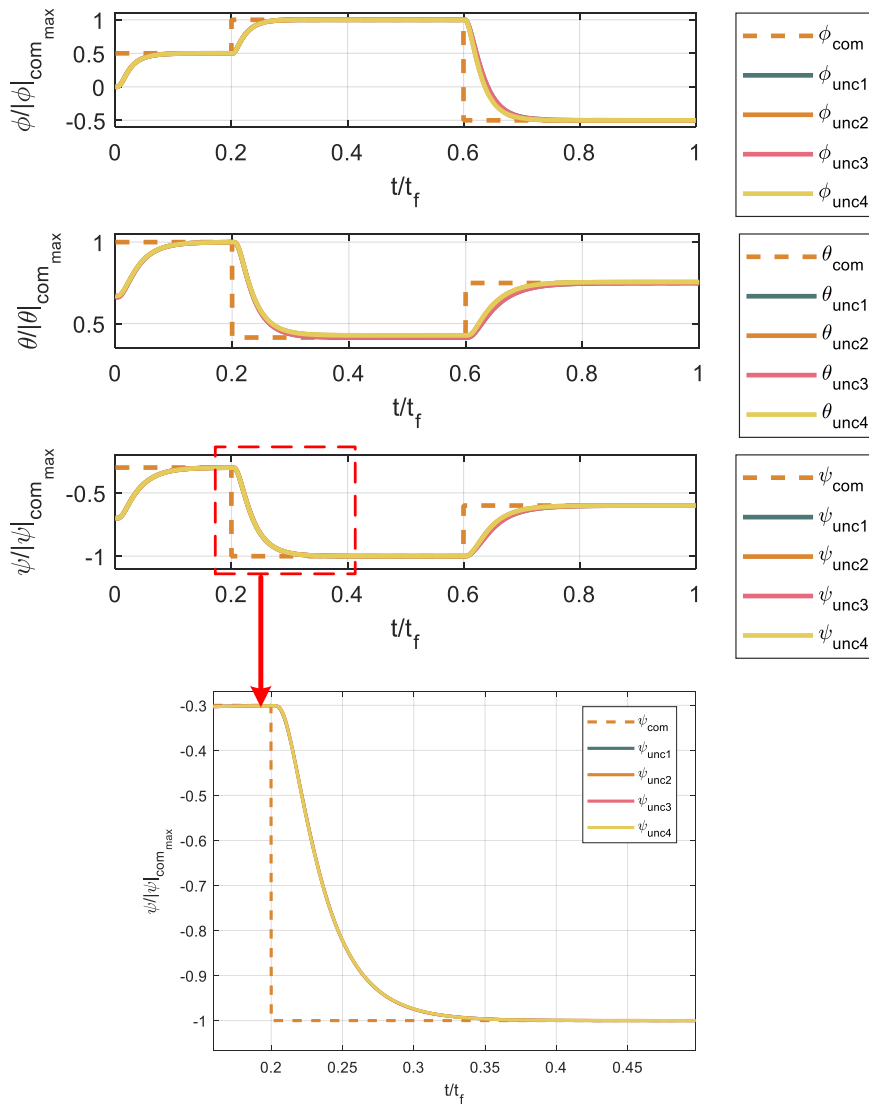


Figure 27 Normalized Euler Angle Tracking Performance of Attitude Autopilot under Uncertainties

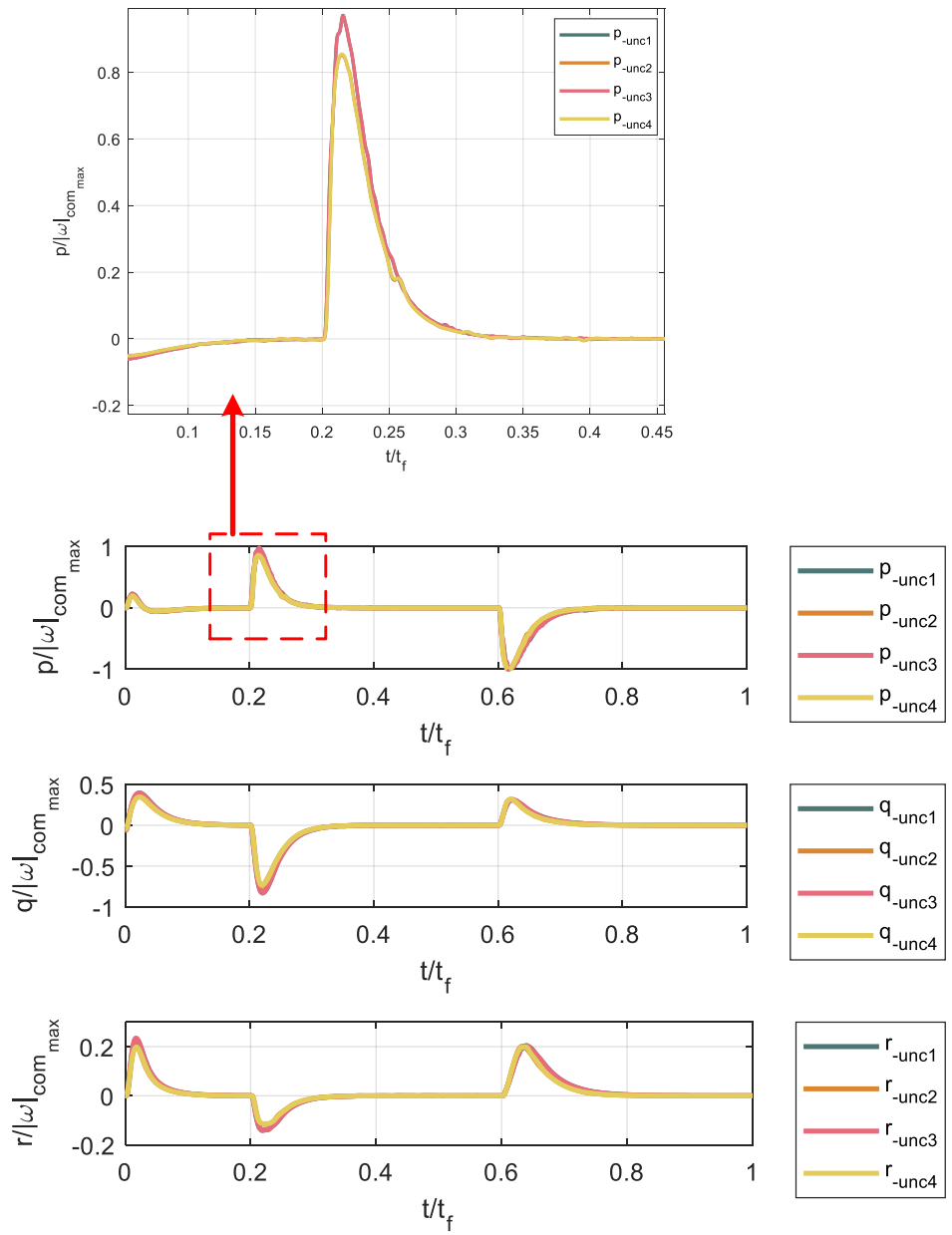


Figure 28 Normalized Angular Rates of Attitude Autopilot under Uncertainties

Figure 28 shows the variation of inner loop parameters in time with uncertainties. The system seems to have some fast responses in angular velocity dynamics. The corresponding inputs to the system are shown in Figure 29 and Figure 30.

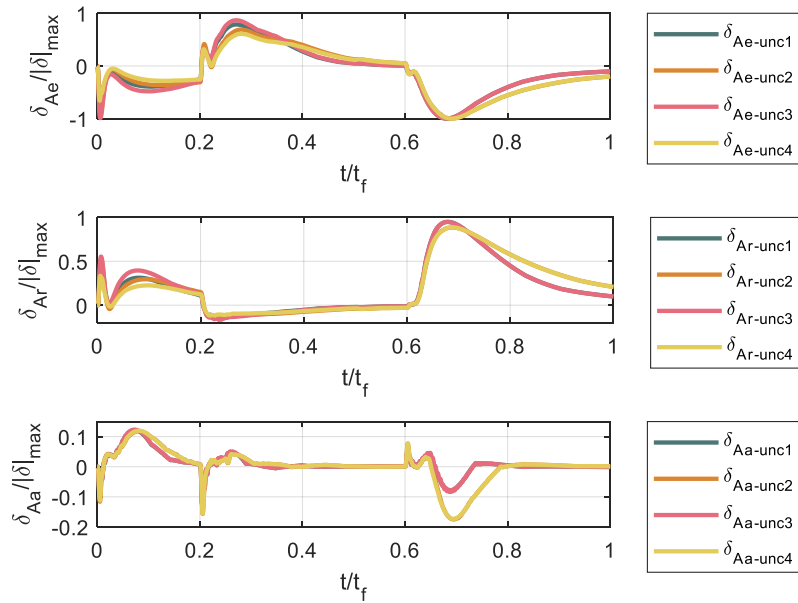


Figure 29 Normalized Effective Aerodynamic Fin Deflections with Attitude Autopilot under Uncertainties

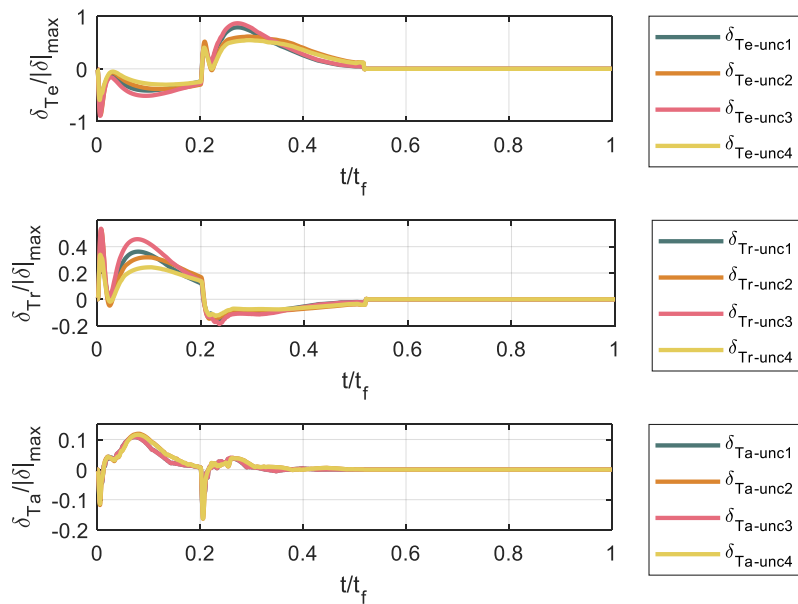


Figure 30 Normalized Effective Jet Vane Deflections with Attitude Autopilot under Uncertainties

### 4.3.2 Sensitivity Analysis for Acceleration Autopilot

Secondly, sensitivity analysis with the same uncertainties is repeated, and the results are listed.

The normalized accelerations shown in the below Figure 31 are the accelerations at the center of gravity. Again, it is seen that there is no significant decrease in the acceleration tracking performance of the missile.

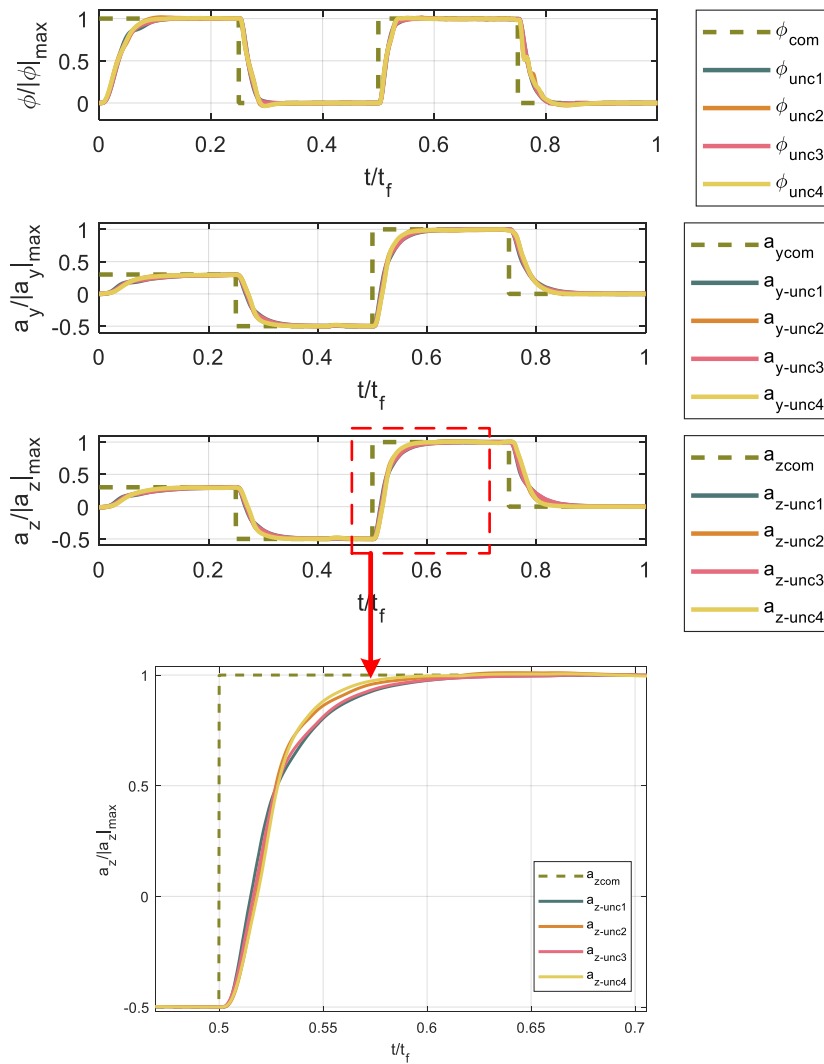


Figure 31 Normalized Acceleration Tracking Performance for Scenario 2 under Uncertainties

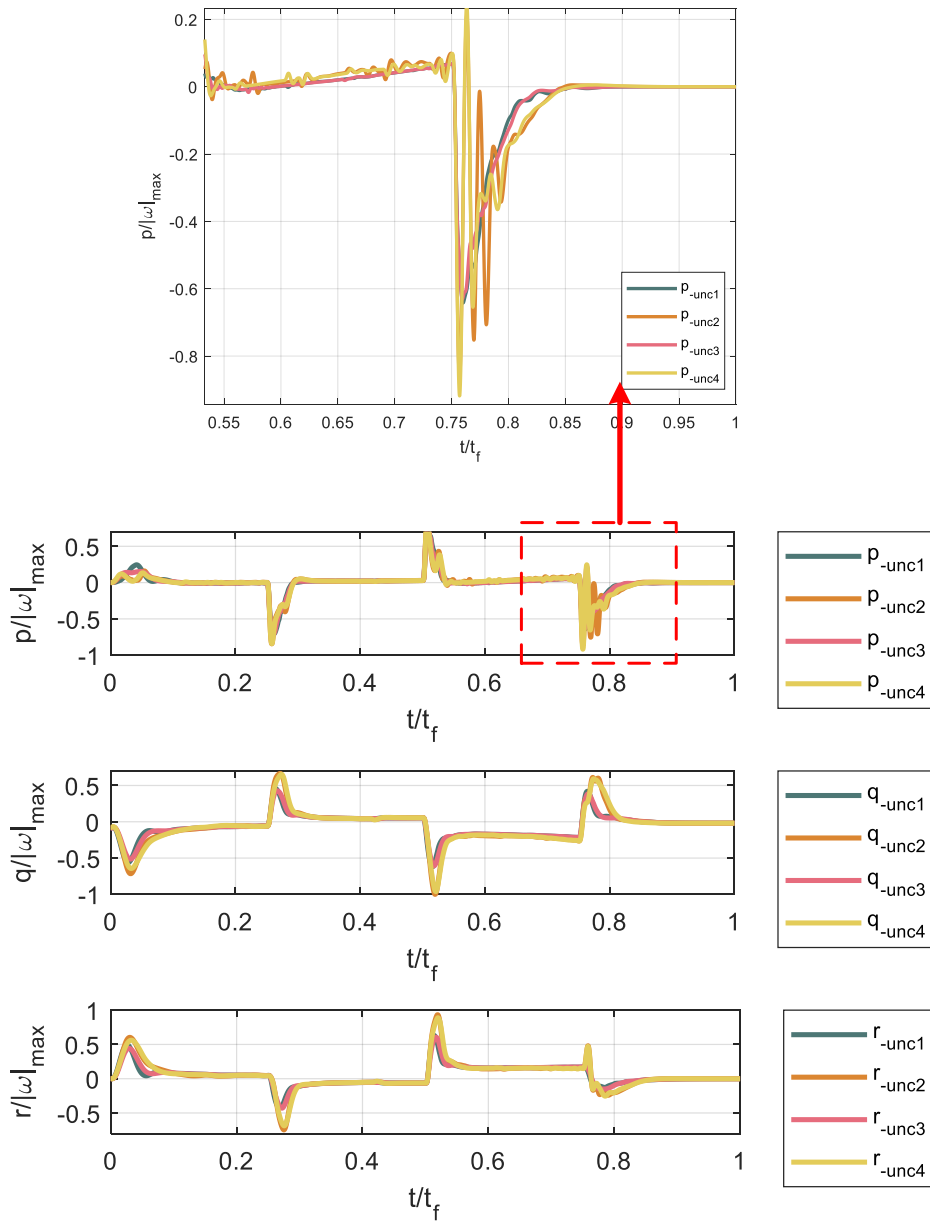


Figure 32 Normalized Angular Rates for Scenario 2 under Uncertainties

Although there may be some distortions due to the high amount of uncertainties, the overall performance seems to be ensured by the rapid control of the inner loop, as shown in Figure 32.

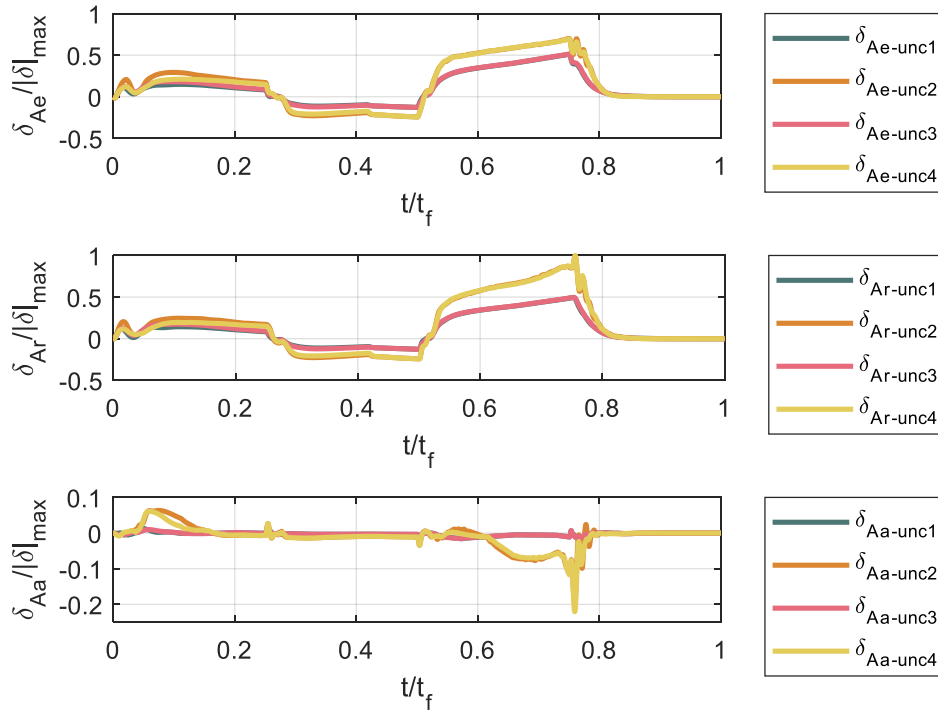


Figure 33 Normalized Effective Aerodynamic Fin Deflections for Scenario 2 under Uncertainties

Figure 33 and Figure 34 put on view the effective fin deflections under the effects of the uncertainties. Obviously, the closed-loop feedback system handles the uncertainties.

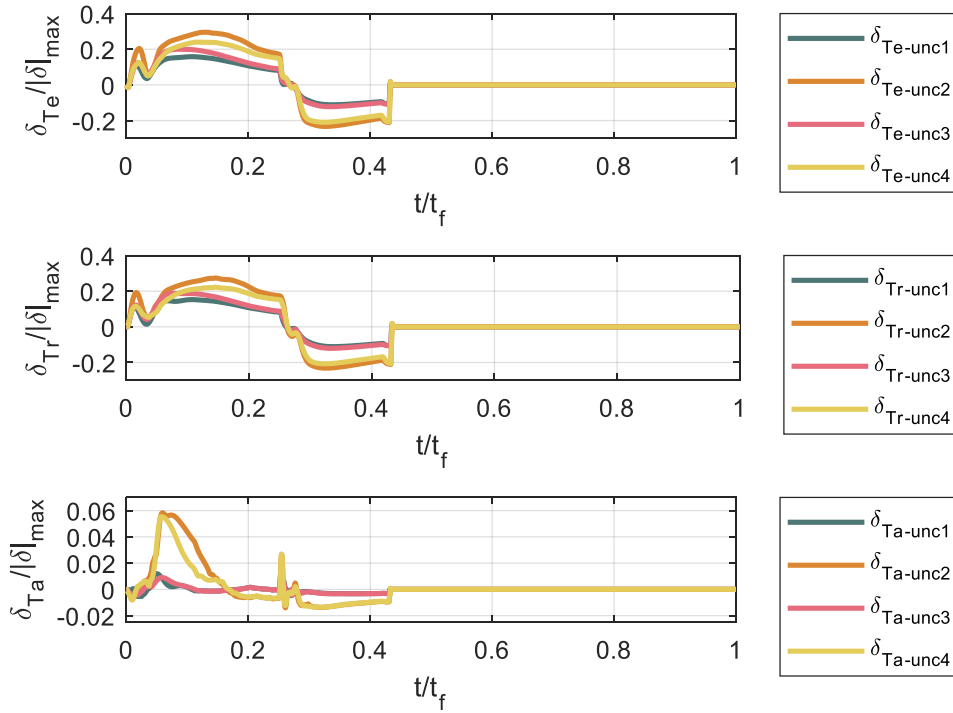


Figure 34 Normalized Effective Jet Vane Deflections for Scenario 2 under Uncertainties

#### 4.4 Realistic Nonlinear Simulation Scenario

In this analysis, a simulation of a possible engagement is examined for a guided scenario without the knowledge of aerodynamic angles which are laborious to obtain in application. Also, a realistic IMU model is used for the guided case. The rates of angular velocities are obtained by calculating virtual control input as in (4.9).

Pure proportional navigation (PPN) guidance is used with effective navigation gain  $N' = 5$ . The algorithm is adopted from [42] for further information, one may refer to it.

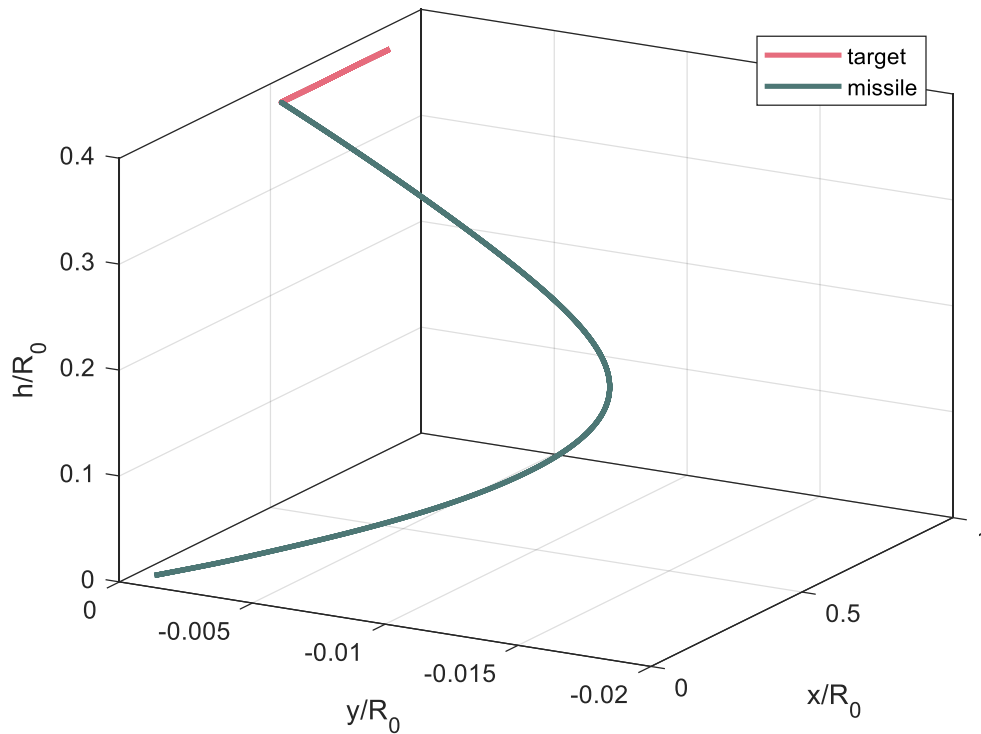


Figure 35 Normalized Trajectories of the Missile, and Target for Guided Scenario ( $R_0$ : initial range between missile and target)

The simulation is stopped when the range between the missile and the target becomes less than 1 meters. It is noticeable in Figure 35 that a challenging engagement scenario for the missile is captured, such that the target moves behind the launch point of the missile. In Figure 35, the nondimensionalization value  $R_0$  represents the initial range between the target and the missile.

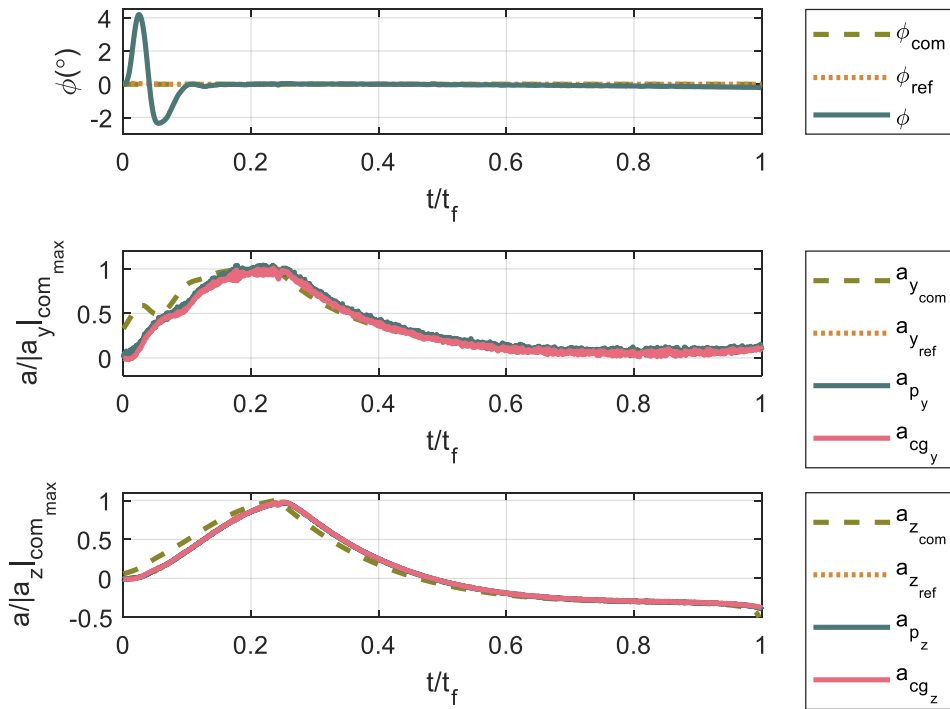


Figure 36 Normalized Acceleration Tracking Performance for Guided Scenario

The roll command is zero since a skid-to-turn guidance approach is applied. The Euler angles can be calculated by the integration of the gyro outputs. Noting that, gyro measurements have errors as described in 3.1.4.5.2. Measurement errors in the model are included as well as the initialization errors in Euler angles. As a result, in Figure 36 a tracking error has occurred in the roll channel, but this error did not hinder the engagement success. The acceleration commands are tracked with outstanding performance in Figure 36 when the results are observed at the center of percussion (*cop*). However, minor tracking errors occurred at the center of gravity, not affecting the closed loop's overall performance.

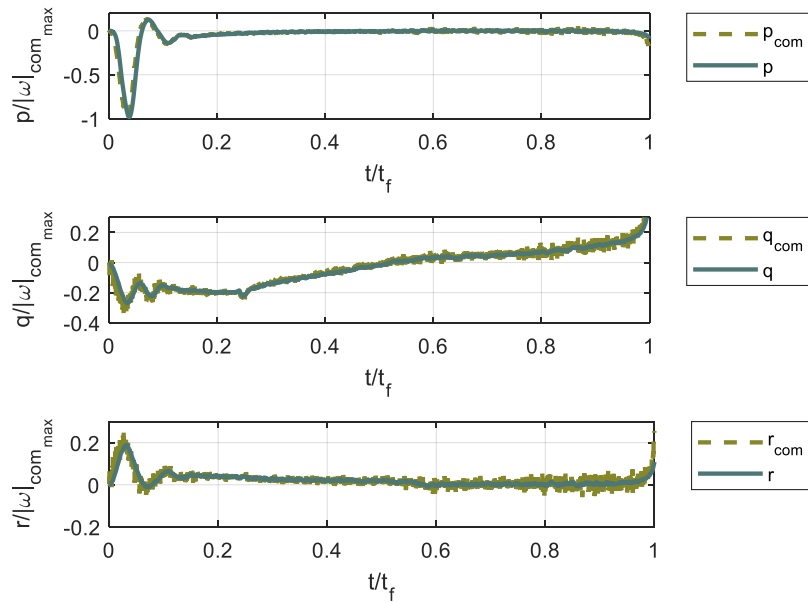


Figure 37 Normalized Angular Rates for Guided Scenario

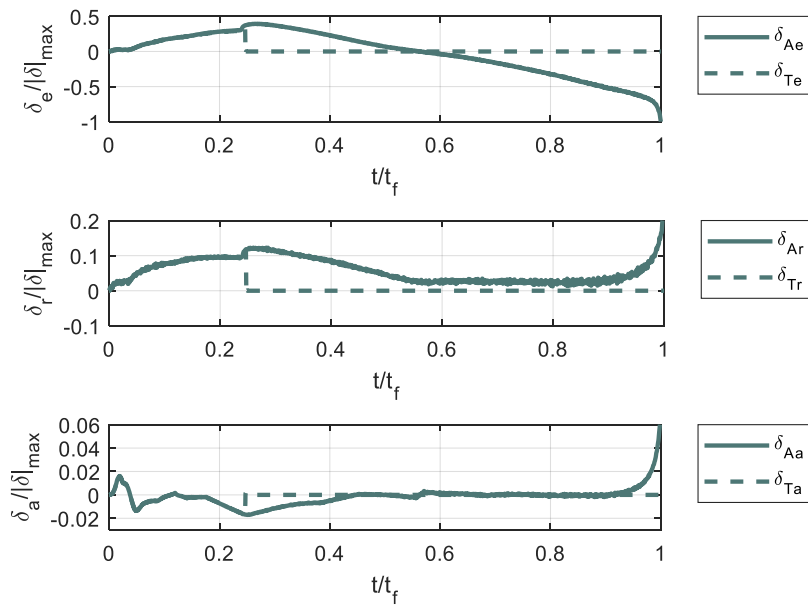


Figure 38 Normalized Effective Fin Deflections for Guided Scenario

The above two figures, Figure 37 and Figure 38 is added to provide analysis integrity by showing the inner loop behavior and the related normalized fin angles.

It should be reminded that the scenario consists of a boost and a coast phase. In the latter, jet vanes do not provide control. Therefore, after the boost phase, aerodynamic fin deflections are increased.

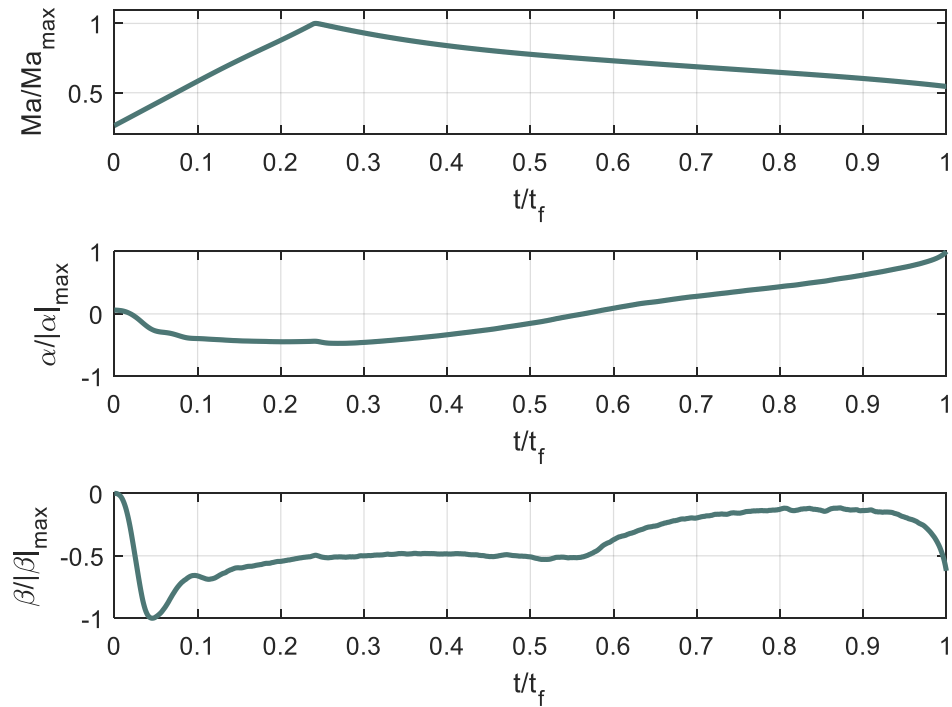


Figure 39 Normalized Values of Mach Number, Angle of Attack and Angle of Sideslip for Guided Scenario

In Figure 39, the trends in aerodynamic angles and Mach number are given for completeness of the analysis.



## CHAPTER 5

### DISCUSSION AND CONCLUSION

This study is inspired by the idea of an autopilot that can handle the control of an agile air defense missile through all flight regimes without any performance loss. Therefore, the NDI method is applied to avoid performance losses due to the neglects in the linearization process. However, there are some difficulties associated with the application of this control method. Those can be listed as a hybrid control mechanism of the missile in the boost phase, non-minimum phase behavior of aerodynamic tail control, high performance requirement while maintaining its robustness, as expected from an air defense system. This study addresses these issues and mainly focuses on the detailed application of NDI autopilot design on such plants. In the thesis, attitude and acceleration autopilots are designed and reference models are used to have a better command profiles, which are given in (4.16), Two loop cascaded structure with second-order reference models is used both for attitude and acceleration autopilots and the characteristics of the reference models are described in (4.19), where the faster reference model is used at higher dynamic pressure. In order to have a standard performance all over the flight, the damping ratio  $\zeta_{rm}$  and natural frequency  $\omega_{rm}$  of the reference models are arranged according to the operating point.

After clarifying this, the performance of the autopilots may be criticized. Since particular observations are added to simulation results throughout the chapters, in this part the results can be summarized. First, the autopilots are tested in a nominal condition such that all the required feedback terms are available and there are no uncertainties on the system parameters. Both attitude and acceleration autopilots have satisfactory results in the nominal case overcoming the aforementioned problems of the system. Moreover, a comparison with baseline autopilot is carried

on showing that it can be deduced that the nonlinear approach has better the performance.

The NDI method without an adaptive augmentation is usually commented as highly dependent on the precise knowledge of flight, physical and aerodynamic parameters. Therefore, sensitivity analyses are done. Although the overall performances degrade from the nominal cases, the levels of this degradation is acceptable for such uncertainty rates. Even though this analyses gives an idea of autopilots' sensitivity, it is limited and still, further analyses are required to ensure robustness.

The missile autopilots in application are run on an on-board computer with the discrete and erroneous measurements of the sensors. Moreover, some data required for NDI autopilots such as aerodynamic angles, Euler angles, angular velocity rates cannot be measured directly with the sensors. Last, a target-missile engagement scenario is generated, and the autopilots run in the simulation with feedbacks from IMU model, calculation of Euler angle using gyro model, and without the knowledge of aerodynamic angles to test the designed autopilot under such perfectness. Considering the results, the method proves itself to be feasible in applications.

## REFERENCES

- [1] Ansari, U., & Bajodah, A. H. (2017). Robust launch vehicle's generalized Dynamic Inversion Attitude Control. *Aircraft Engineering and Aerospace Technology*, 89(6), 902–910. <https://doi.org/10.1108/aeat-06-2015-0149>
- [2] Bayoğlu, T. (2016). *Aerodynamic Parameter Estimation of a Supersonic Missile with Rapid Speed Variation By Using Kalman Filtering* (thesis). Retrieved October 10, 2021, from <https://open.metu.edu.tr/handle/11511/25956>.
- [3] Bıyıklı, R., Tekin, R., & Yavrucuk, İ. (2022). Control Allocation Strategies for a Hybrid Controlled Missile with NDI Autopilot. *The 13<sup>th</sup> Asian Control Conference (ASCC 2022)*. Manuscript submitted for publication.
- [4] Bıyıklı, R., Tekin, R., & Yavrucuk, İ. (2022). Nonlinear Dynamic Inversion Autopilot for a Thrust Vector and Aerodynamic Controlled Missile. *CEAS EuroGNC 2022 Conference on Guidance, Navigation and Control*. Manuscript submitted for publication.
- [5] Cao, S., Shen, L., Zhang, R., Yu, H., & Wang, X. (2019). Adaptive Incremental Nonlinear Dynamic Inversion Control based on Neural Network for UAV maneuver. *2019 IEEE/ASME International Conference on Advanced Intelligent Mechatronics (AIM)*. <https://doi.org/10.1109/aim.2019.8868510>
- [6] Center of Percussion. (n.d.). Retrieved December 28, 2021, from <https://sciencedemonstrations.fas.harvard.edu/presentations/center-percussion>
- [7] Chai, R., Tsourdos, A., Savvaris, A., Chai, S., Xia, Y., & Philip Chen, C. L. (2021). Review of Advanced Guidance and control algorithms for space/aerospace vehicles. *Progress in Aerospace Sciences*, 122, 100696. <https://doi.org/10.1016/j.paerosci.2021.100696>
- [8] Chapra, S. C., & Canale, R. P. (2006). Chapter 5 Bracketing Methods. In *Numerical methods for engineers: Steven C. Chapra, Raymond P. Canale* (pp. 124–132). essay, McGraw-Hill.
- [9] Chen, F., Qian, C., Jiang, Y., & Xu, Y. (2021). Hybrid nonlinear control for fighter with center of gravity perturbation and aerodynamic parameter uncertainty. *IEEE Access*, 9, 139315–139327. <https://doi.org/10.1109/access.2021.3118545>

- [10] Chen, W.-H. (2003). Nonlinear disturbance observer-enhanced dynamic inversion control of missiles. *Journal of Guidance, Control, and Dynamics*, 26(1), 161–166. <https://doi.org/10.2514/2.5027>
- [11] Elshafei, A. L. (2020). *L11 Feedback Linearization Overview*. YouTube. Retrieved December 27, 2021, from <https://www.youtube.com/watch?v=2bO2JtHpBj4>.
- [12] Elshafei, A. L. (2020). *L13 Input-Output Linearization*. YouTube. Retrieved December 27, 2021, from <https://www.youtube.com/watch?v=418mCXvicUo&t=1051s>.
- [13] Etkin, B. (1972). Reference Frames and Transformations, General Equations of Unsteady Motion. In *Dynamics of Atmospheric Flight* (pp. 104–189). essay, John Wiley & Sons, Inc.
- [14] Etkin, B., & Reid, L. D. (1996). *Dynamics of flight: Stability and control*. John Wiley & Sons.
- [15] Fleeman, E. L. (2006). *Tactical missile design*. American Institute of Aeronautics and Astronautics.
- [16] Fu-Kuang Yeh, Hsiuan-Hau Chien, & Li-Chen Fu. (2002). Nonlinear optimal sliding mode midcourse controller with thrust vector control. *Proceedings of the 2002 American Control Conference (IEEE Cat. No.CH37301)*. <https://doi.org/10.1109/acc.2002.1023208>
- [17] Gambhire, S. J., Kishore, D. R., Londhe, P. S., & Pawar, S. N. (2020). Review of sliding mode based control techniques for control system applications. *International Journal of Dynamics and Control*, 9(1), 363–378. <https://doi.org/10.1007/s40435-020-00638-7>
- [18] Gezer, R. B. (2014). *Fourier Series Based Model Reference Adaptive Control* (thesis). METU, Ankara. Retrieved December 28, 2021, from <https://open.metu.edu.tr/handle/11511/57913>.
- [19] Gezer, R. B., & Kutay, A. T. (2014). Robust model following control design for Missile Roll Autopilot. *2014 UKACC International Conference on Control (CONTROL)*. <https://doi.org/10.1109/control.2014.6915107>
- [20] Gui, H., Sun, R., Lu, Q., & Zhou, G. (2021). Improved backstepping control with adaptive estimation for Nonlinear Missile Systems. *Journal of Spacecraft and Rockets*, 1–10. <https://doi.org/10.2514/1.a34860>

- [21] *HG1930 inertial measurement unit*. Aerospace. (n.d.). Retrieved December 27, 2021, from <https://aerospace.honeywell.com/us/en/learn/products/sensors/hg1930-inertial-measurement-unit>
- [22] Hill, P. G., & Peterson, C. R. (1992). Chapter 12 Chemical Rocket Propellants: Combustion and Expansion. In *Mechanics and thermodynamics of propulsion* (pp. 599–601). essay, Addison-Wesley Publishing Company, Inc.
- [23] Hindman, R., & Shell, W. M. (2005). Design of a missile autopilot using adaptive nonlinear dynamic inversion. *Proceedings of the 2005, American Control Conference, 2005*. <https://doi.org/10.1109/acc.2005.1469954>
- [24] Hong, J.-H., & Lee, C.-H. (2020). Nonlinear autopilot design for endo- and Exoatmospheric Interceptor with Thrust Vector Control. *IEEE Transactions on Aerospace and Electronic Systems*, 56(1), 796–810. <https://doi.org/10.1109/taes.2019.2921181>
- [25] Huang, B., Liu, Y., & Xu, A. (2021). Dynamic Inversion Controller Design for BTT missile based on Sliding Mode Control. *2021 IEEE 4th Advanced Information Management, Communicates, Electronic and Automation Control Conference (IMCEC)*. <https://doi.org/10.1109/imcec51613.2021.9482013>
- [26] *Keyword Analysis & Research: HG1930*. free tracking. (n.d.). Retrieved December 27, 2021, from <https://www.eigolink.net/find/hg1930>
- [27] Khalil, H. K. (2002). 13 Feedback Linearization. In *Nonlinear systems* (pp. 505–551). essay, Prentice Hall.
- [28] Lane, S. H., & Stengel, R. F. (1986). Flight control design using nonlinear inverse dynamics. *1986 American Control Conference*. <https://doi.org/10.23919/acc.1986.4789006>
- [29] Lee, C.-H., Jun, B.-E., Shin, H.-S., & Tsourdos, A. (2017). Nonlinear acceleration controller for exo-atmospheric and endo-atmospheric interceptors with TVC. *2017 25th Mediterranean Conference on Control and Automation (MED)*. <https://doi.org/10.1109/med.2017.7984110>
- [30] McFarland, M. B., & Calise, A. J. (2000). Adaptive nonlinear control of agile antiair missiles using neural networks. *IEEE Transactions on Control Systems Technology*, 8(5), 749–756. <https://doi.org/10.1109/87.865848>

- [31] McFarland, M., & Hoque, S. (2000). Robustness of a nonlinear missile autopilot designed using dynamic inversion. *AIAA Guidance, Navigation, and Control Conference and Exhibit*. <https://doi.org/10.2514/6.2000-3970>
- [32] Özgören M. Kemal. (2020). 3.8 Expression of a Transformation Matrix in Terms of Euler Angles. In *Kinematics of general spatial mechanical systems* (pp. 42–46). essay, Wiley.
- [33] Peter, F. U. (2018). *Nonlinear and adaptive missile autopilot design* (thesis). Retrieved September 20, 2021, from <https://mediatum.ub.tum.de/doc/1416304/1416304.pdf>.
- [34] Peter, F., Leitão, M., & Holzapfel, F. (2012). Adaptive augmentation of a new baseline control architecture for tail-controlled missiles using a nonlinear reference model. *AIAA Guidance, Navigation, and Control Conference*. <https://doi.org/10.2514/6.2012-5037>
- [35] R., F. C. M. (2004). 5 Gravity. In *Solid earth an introduction to Global Geophysics* (pp. 197–205). essay, Cambridge Univ. Press.
- [36] Schumacher, C. J., & Khargonekar, P. P. (1998). Stability Analysis of a missile control system with a dynamic inversion controller. *Proceedings of the 1998 American Control Conference. ACC (IEEE Cat. No.98CH36207)*. <https://doi.org/10.1109/acc.1998.707303>
- [37] Slotine, J.-J. (2018). *11 Feedback Linearization*. YouTube/MIT. Retrieved December 27, 2021, from <https://www.youtube.com/watch?v=KgTFOGeQQDo>.
- [38] Slotine, J.-J. E., & Li, W. (1991). Part 2 : Nonlinear Control Systems Design. In *Applied Nonlinear Control: An introduction* (pp. 191–392). essay, Prentice-Hall.
- [39] Stevens, B. L., Lewis, F. L., & Johnson, E. N. (2016). 5 Modern Design Techniques. In *Aircraft Control and Simulation: Dynamics, controls design, and Autonomous Systems* (pp. 337–452). essay, John Wiley & Sons.
- [40] Taur, D.-R., Chern, J.-S., Taur, D.-R., & Chern, J.-S. (1997). Optimal Thrust Vector Control of tactical missiles. *Guidance, Navigation, and Control Conference*. <https://doi.org/10.2514/6.1997-3475>
- [41] Tekin, R. (2010). *Design, Modeling, Guidance and Control of a Vertical Launch Surface to Air Missile* (thesis). Retrieved September 20, 2021, from <https://open.metu.edu.tr/bitstream/handle/11511/19885/index.pdf?sequence=1>.

- [42] Tekin, R., & Erer, K. S. (2015). Considerations on boost phase modeling and guidance command generation. *AIAA Guidance, Navigation, and Control Conference*. <https://doi.org/10.2514/6.2015-0862>
- [43] Tekin, R., Atesoglu, Ö., & Leblebicioglu, K. (2010). Modeling and vertical launch analysis of an aero- and thrust vector controlled surface to air missile. *AIAA Atmospheric Flight Mechanics Conference*. <https://doi.org/10.2514/6.2010-7639>
- [44] Tipán, S., Thai, S., Proff, M., & Theodoulis, S. (2020). Nonlinear dynamic inversion autopilot design for dual-spin guided projectiles. *IFAC-PapersOnLine*, 53(2), 14827–14832. <https://doi.org/10.1016/j.ifacol.2020.12.1926>
- [45] Tiryaki Kutluay, K. (2010). *Adaptive Control of Guided Missiles* (thesis). Retrieved September 20, 2021, from <http://etd.lib.metu.edu.tr/upload/12613083/index.pdf>.
- [46] van 't Veld, R., Van Kampen, E.-J., & Chu, Q. P. (2018). Stability and robustness analysis and improvements for incremental nonlinear dynamic inversion control. *2018 AIAA Guidance, Navigation, and Control Conference*. <https://doi.org/10.2514/6.2018-1127>
- [47] Wang, J., Holzapfel, F., & Peter, F. (2013). Comparison of Nonlinear Dynamic Inversion and Backstepping Controls with Application to a Quadrotor. *2nd CEAS Specialist Conference on Guidance, Navigation & Control*. Delft.
- [48] Wang, X., Van Kampen, E.-J., Chu, Q. P., & Lu, P. (2018). Stability Analysis for Incremental Nonlinear Dynamic Inversion Control. *2018 AIAA Guidance, Navigation, and Control Conference*. <https://doi.org/10.2514/6.2018-1115>
- [49] Zhang, F., & Holzapfel, F. (2015). Flight control using physical dynamic inversion. *AIAA Guidance, Navigation, and Control Conference*. <https://doi.org/10.2514/6.2015-1758>
- [50] Zipfel, P. H. (2007). Chapter 8. Three-Degrees-of\_freedom Simulations. In *Modeling and simulation of Aerospace Vehicle Dynamics (2nd edition)* (pp. 265–276). essay, American Institute of Aeronautics and Astronautics.



## APPENDICES

### A. Non-minimum Phase Inspection with Linear Analysis

In this section, the non-minimum phase characteristic of the aerodynamic tail-controlled missile will be investigated in pitch channel by writing the transfer function from elevator input  $\delta_e$  to acceleration output ( $a_{cgz}$ ). Starting from the force equation, acceleration can be written as in (A.1).

$$\vec{a}_{B/I}^B = \begin{bmatrix} a_{cgx} \\ a_{cgy} \\ a_{cgz} \end{bmatrix} = \begin{bmatrix} \dot{u} \\ \dot{v} \\ \dot{w} \end{bmatrix} + \begin{bmatrix} p \\ q \\ r \end{bmatrix} \times \begin{bmatrix} u \\ v \\ w \end{bmatrix} \quad (\text{A.1})$$

Since the analysis will be carried out only for pitch dynamics, the effect of yaw and roll will be ignored. Also, gravitational effects are neglected in the equations. By making some arrangements, angle of attack dynamics can be written as in (A.2) where  $V$  is the magnitude of the missile's velocity vector and other parameters previously described throughout the study.

$$\begin{aligned} a_{cgz} &= \dot{w} - qu \\ \alpha &= \tan\left(\frac{w}{u}\right) \approx \frac{w}{u} \\ \dot{w} &= \dot{\alpha}u \\ a_{cgz} &= u(\dot{\alpha} - q) \approx V(\dot{\alpha} - q) \\ \dot{\alpha} &= \frac{a_{cgz}}{V} + q \end{aligned} \quad (\text{A.2})$$

The normal acceleration is the result of normal force, and it is defined linear as in (A.3) with respect to aerodynamic parameters.

$$a_{cgz} = \frac{Z}{m} = \frac{QS_{ref}}{m} C_z \quad (\text{A.3})$$

$$\frac{Z}{mV} = Z_\alpha \alpha + Z_q q + Z_{\delta_e} \delta_e$$

Using the angle of attack dynamics given in (A.2) and introducing non-dimensional force moment coefficients first state variable equation can be generated as in (A.4).

$$\begin{aligned} \dot{\alpha} &= Z_\alpha \alpha + Z_q q + Z_{\delta_e} \delta_e + q \\ Z_\alpha &= \frac{QS_{ref}}{mV} C_{z\alpha}, Z_q = \frac{QS_{ref}l_{ref}}{2mV^2} C_{zq}, Z_{\delta_e} = \frac{QS_{ref}}{mV} C_{z\delta_e} \end{aligned} \quad (A.4)$$

From the moment equation, the rest of the pitch dynamics can be written by following a similar process as in (A.5).

$$\begin{aligned} \dot{q} &= \frac{M}{I_{yy}} = \frac{QS_{ref}l_{ref}}{I_{yy}} C_m \\ \frac{M}{I_{yy}} &= M_\alpha \alpha + M_q q + M_{\delta_e} \delta_e \\ \dot{q} &= M_\alpha \alpha + M_q q + M_{\delta_e} \delta_e \\ M_\alpha &= \frac{QS_{ref}l_{ref}}{I_{yy}} C_{m\alpha}, M_q = \frac{QS_{ref}l_{ref}^2}{2VI_{yy}} C_{mq}, M_{\delta_e} = \frac{QS_{ref}l_{ref}}{I_{yy}} C_{m\delta_e} \end{aligned} \quad (A.5)$$

Then the overall pitch dynamics of the missile are written with the state variable and output equations as in (A.6).

$$\begin{aligned} \begin{bmatrix} \dot{\alpha} \\ \dot{q} \end{bmatrix} &= \begin{bmatrix} Z_\alpha & Z_q + 1 \\ M_\alpha & M_q \end{bmatrix} \begin{bmatrix} \alpha \\ q \end{bmatrix} + \begin{bmatrix} Z_{\delta_e} \\ M_{\delta_e} \end{bmatrix} \delta_e \\ y = a_{cgz} &= [VZ_\alpha \quad VZ_q] \begin{bmatrix} \alpha \\ q \end{bmatrix} + [VZ_{\delta_e}] \delta_e \end{aligned} \quad (A.6)$$

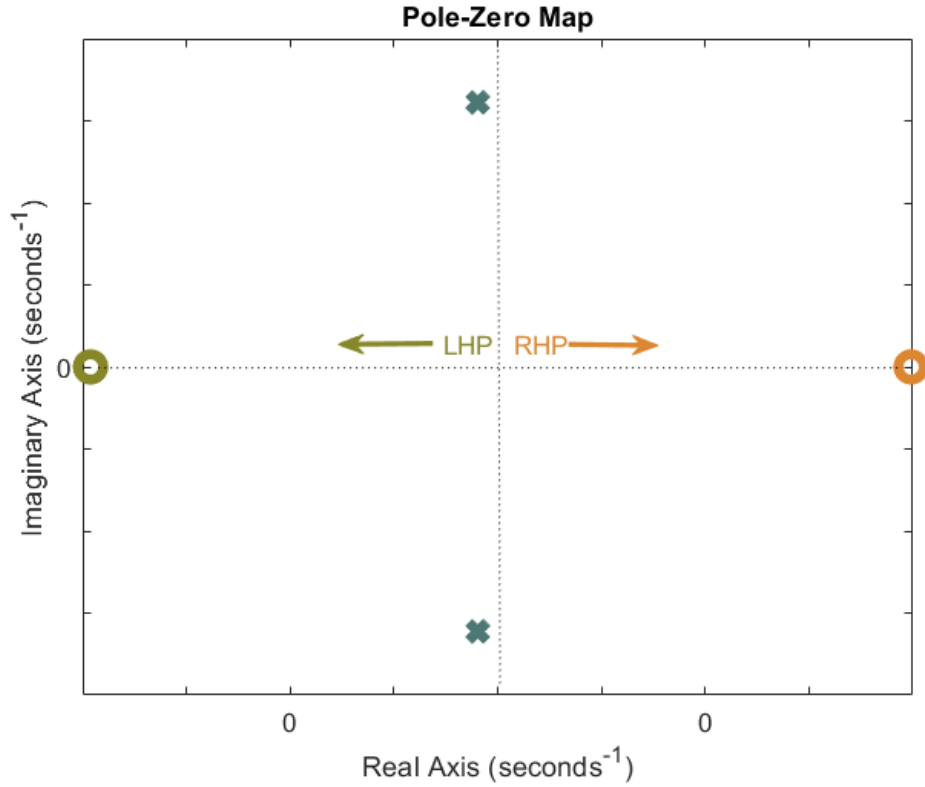


Figure 40 Pole-Zero Map for the Transfer Function from  $\delta_e$  to  $a_{cg_z}$

For a given flight condition pole-zero map of the system is obtained. Consistent with the physical working principle of tail control, the above system results in a system with zeros at RHP.

Now, if the output is defined with respect to another point  $p$  ahead of the center of percussion is calculated similarly to (4.32) ( $x_p > x_{cop/cg}$ ), the new system can be written as (A.7), i.e., state variable equations remain the same whereas the output equation changes.

The component of  $\vec{a}_{p/l}^B$  on  $z_B$  axis is defined as  $a_{p_z}$ .

$$\begin{aligned}
 a_{p_z} &= -Vq + V\dot{\alpha} - x_p\dot{q} \\
 y &= a_{p_z} \\
 &= -Vq + V(Z_\alpha\alpha + Z_qq + Z_{\delta_e}\delta_e + q) - x_p(M_\alpha\alpha + M_qq + M_{\delta_e}\delta_e)
 \end{aligned} \tag{A.7}$$

$$a_{p_z} = [(VZ_\alpha - x_p M_\alpha) \quad (VZ_q - x_p M_q)] \begin{bmatrix} \alpha \\ q \end{bmatrix} + [(VZ_{\delta_e} - x_{cg,p} M_{\delta_e})] \delta_e$$

When the pole-zero map of the newly defined system is investigated, it is seen that the zeros are at the LHP, and the poles is remained the same.

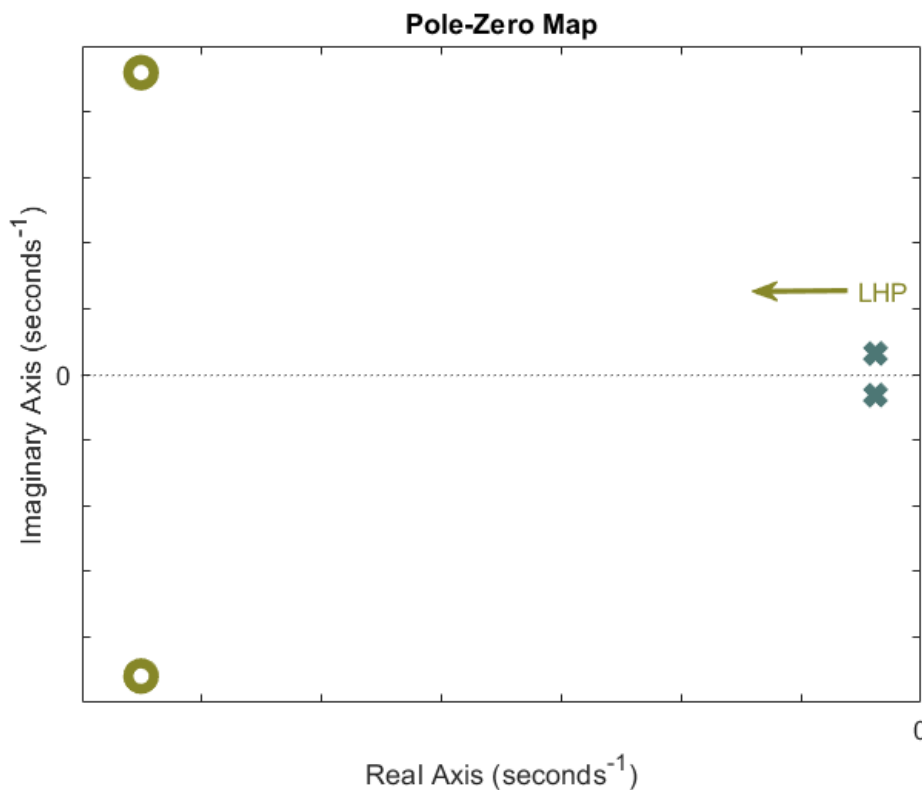


Figure 41 Pole-Zero Map for the Transfer Function from  $\delta_e$  to  $a_{p_z}$

Clearly, it is seen from Figure 41 the location of zeros is dependent on the selection of the point. In order to see the movement of the zeros with this selection, the system's pole-zero maps for different  $p$  locations is obtained in Figure 43. Where  $p$  is now chosen as a point ahead of the center of gravity.

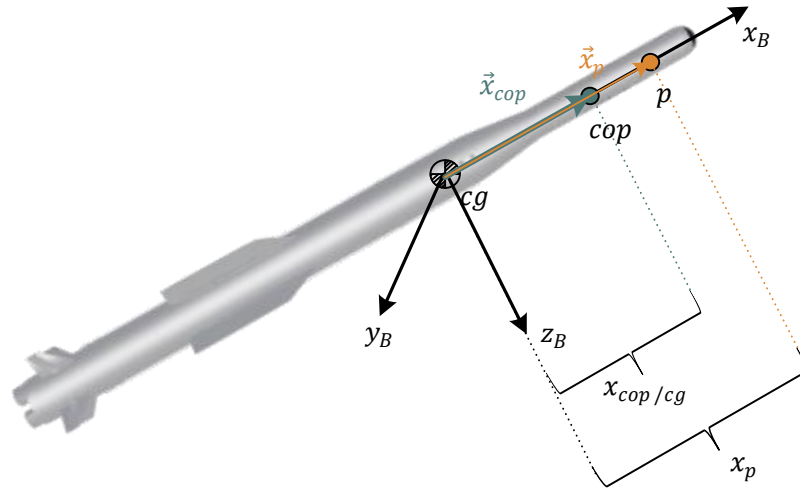


Figure 42 Center of Percussion on the Missile

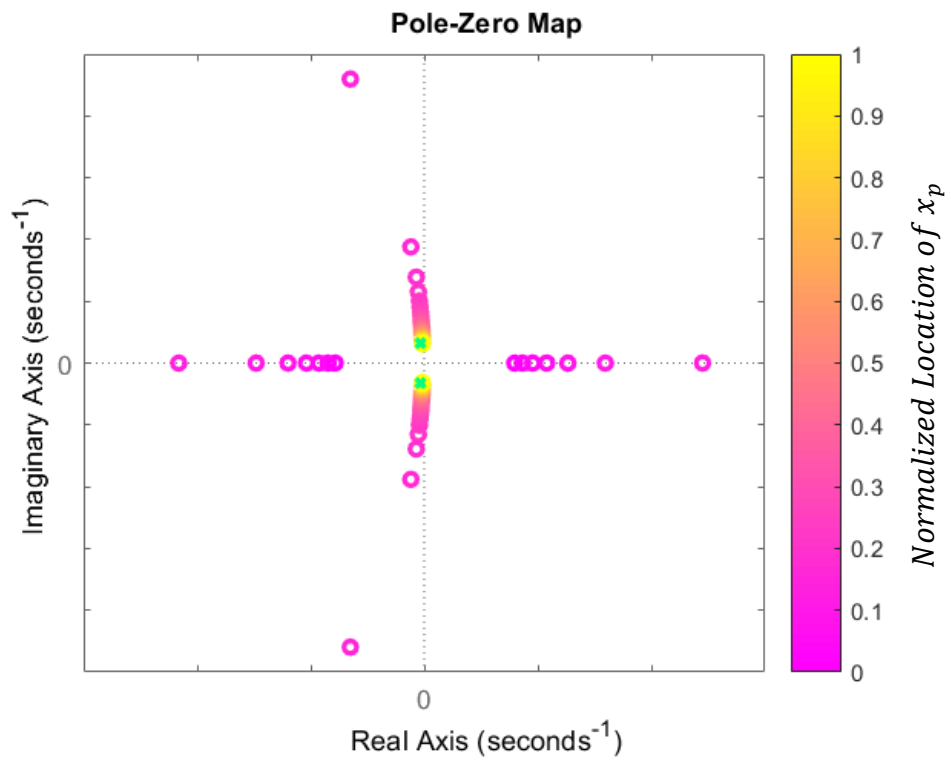


Figure 43 Movements of Zeros on Pole-Zero Maps with Normalized Location of  $x_p$

It is observed from Figure 43 that after some distance ahead of the  $cg$ , zeros move to the LHP. In the LHP, as the distance of location that the output is calculated is increasing, the magnitude of real parts and imaginary parts of the zeros are decreasing with this system. The zeros become poles at the inversion process, so choosing the distance much ahead of  $cop$  may cause trouble due to the very fast dynamics of zeros there.

## B. Solution for Mechanically Coupled Control Surfaces

It is previously mentioned that for some designs, it is preferable to drive the aerodynamic control fins and thrust vector fins with the same actuator. The missile design considered here has four aerodynamic control fins referred as  $\delta_{A_{1,2,3,4}}$  and four jet vanes referred as  $\delta_{T_{1,2,3,4}}$  in cross configuration. After reminding this, let us define a mechanical relation between these fins such that control in the boost phase is always applied as:

$$m\delta_{A_n} = \delta_{T_n} \quad (n = 1, \dots, 4) \quad (\text{B.1})$$

This relation basically means TVC jet vane is deflected  $m$  times of AC fin deflection. In this case (4.21) should be solved with a condition on it and it can be rewritten as in (B.2).

$$\begin{bmatrix} v_p \\ v_q \\ v_r \end{bmatrix} = \underbrace{\frac{A_{i_{aero}} C_{M_A}(\delta_A) + b_{i_{aero}}}{\text{A nonlinear equation}}}_{\text{depending on aerodynamic database}} + \underbrace{\frac{A_{i_{tvc}} C_{M_T}(\delta_T) + b_{i_{tvc}}}{\text{A nonlinear equation}}}_{\text{depending on thrust deflection angles}} \quad (\text{B.2})$$

As a reminder, the above equation is in terms of effective elevator, rudder and aileron inputs of AC fins and jet vanes given in (B.3).

$$\delta_A = \begin{bmatrix} \delta_{A_e} \\ \delta_{A_r} \\ \delta_{A_a} \end{bmatrix}, \delta_T = \begin{bmatrix} \delta_{T_e} \\ \delta_{T_r} \\ \delta_{T_a} \end{bmatrix} \quad (\text{B.3})$$

Using this (3.29) for a given AC  $\delta_A$ ,  $\delta_n$  can be calculated and by imposing the condition given on (B.1)  $\delta_{T_n}$  can be found and using (3.30), then it can be converted to effective jet vane inputs  $\delta_T$ . This process summarized in Figure 44.

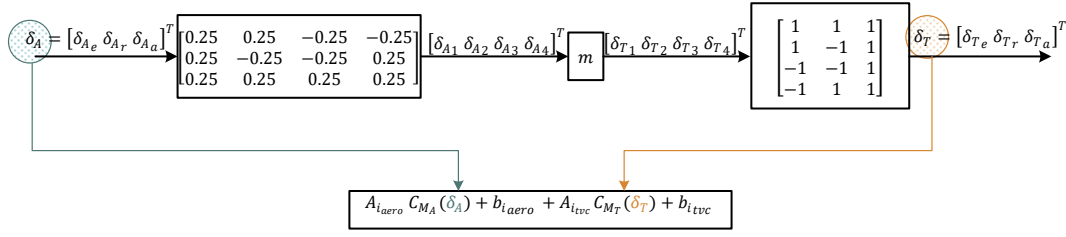


Figure 44 Conversion of Effective Deflections to Real Deflections

This process helps us to calculate the right-hand side of the (B.2) with condition (B.1). Defining this calculation with a new nonlinear function  $h(\delta)$  since all other inputs depend on  $\delta$  with new condition and selecting an initial condition for it as  $\delta_k$  bisection method that solves (B.2) such that  $v = h(\delta)$  is described. For a detailed discussion on this numerical method, one may refer to [8]. The bisection method is found suitable for the current problem since for a given time instant, inner loop nonlinear system matrices are constant and moment coefficient of the system for the case here is monotonically decreasing with  $\delta$ , and continuous function.

$$h(\delta) = A_{i_{aero}} C_{M_A}(\delta_A) + b_{i_{aero}} + A_{i_{tvc}} C_{M_T}(\delta_T) + b_{i_{tvc}}$$

$$\delta_k = C_{M_A}^{-1} \left( (v - b_{i_{aero}}) A_{i_{aero}}^{-1} \right) \quad (B.1)$$

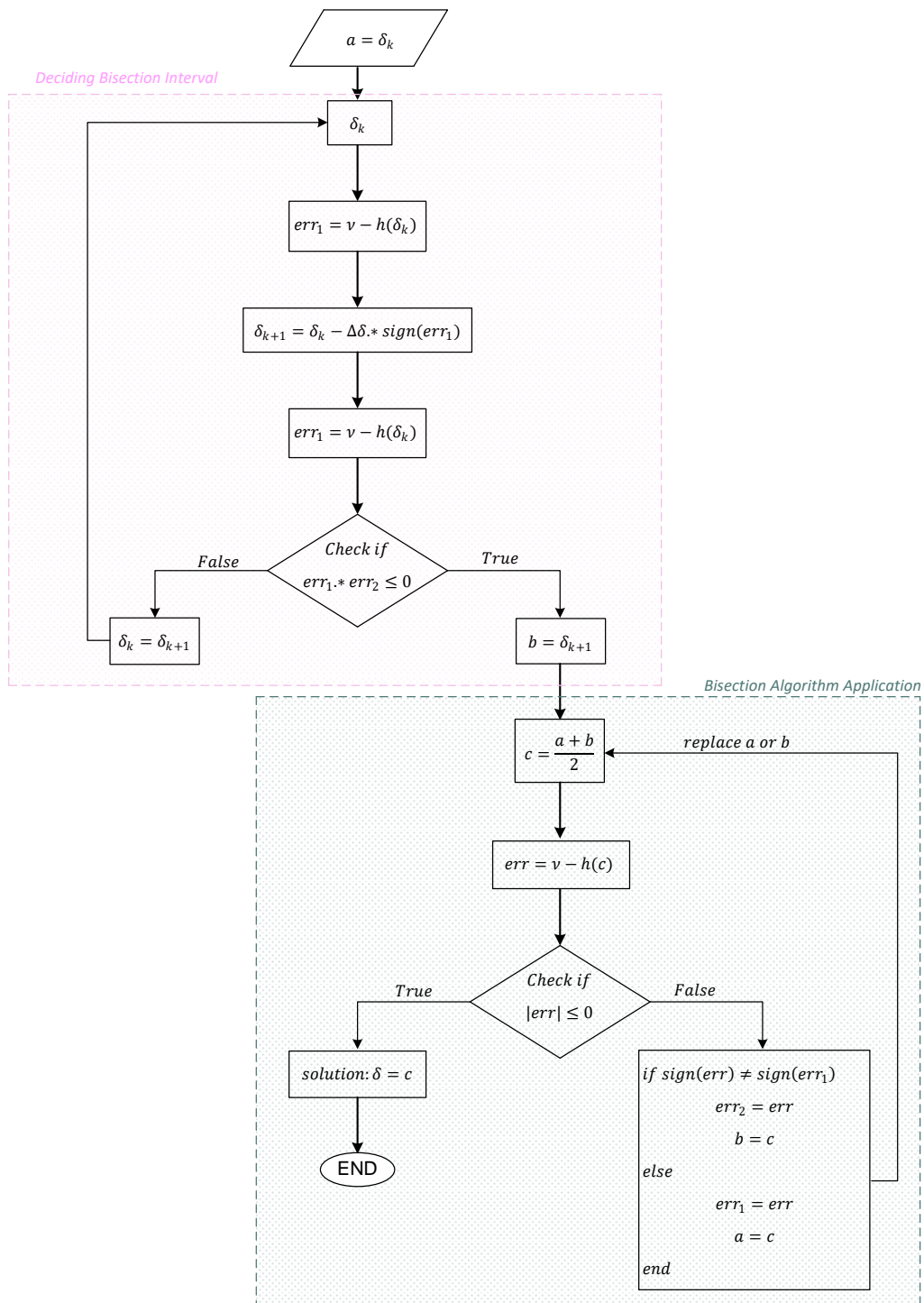


Figure 45 Algorithm Scheme for Imposing Mechanical Coupling to Autopilot Design

This algorithm finds a solution with a tolerance  $\varepsilon$ .

The result with this condition for a selected  $m$  is tabulated below. The results are compared with the highly coupled cases shown before in Figure 46-50, noting that TVC is only valid in the boost phase. Therefore, results are restricted to the boost phase.

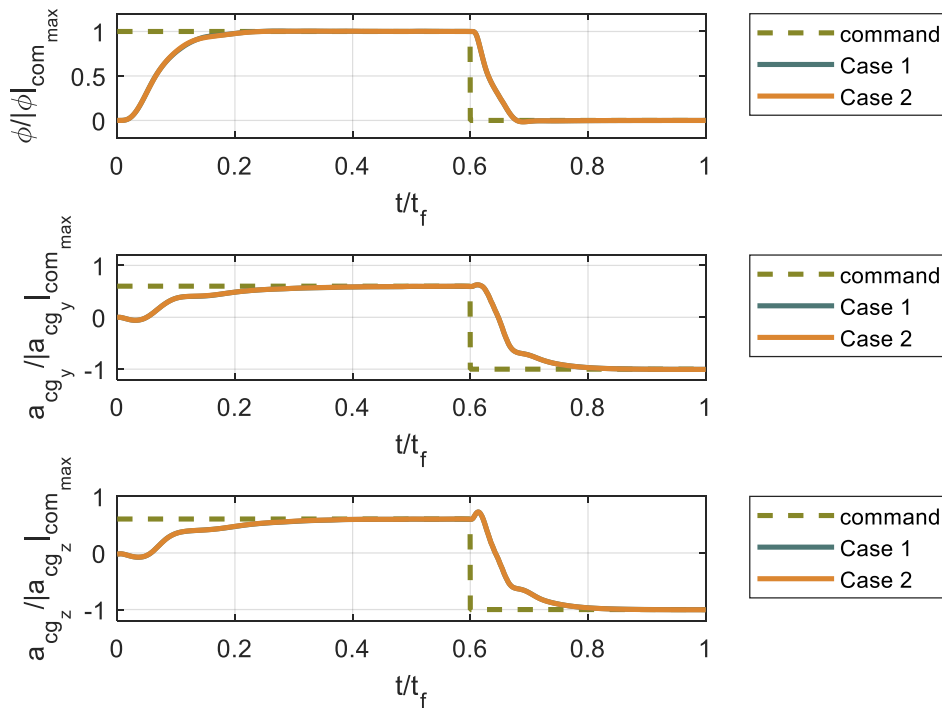


Figure 46 Normalized Acceleration Tracking Performance Comparison for Case 1 and Case 2

In Figure 48 it is seen that the ratio between fins are imposed as in described algorithm.

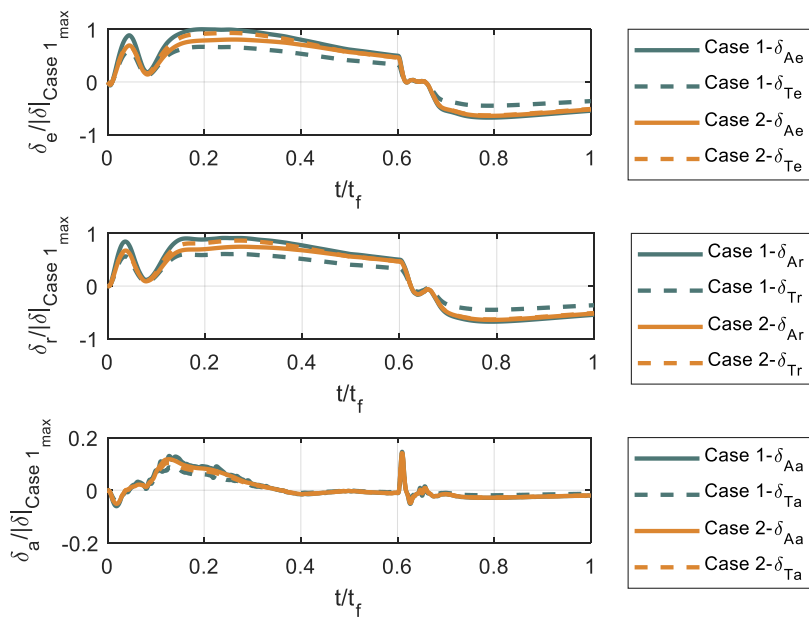


Figure 47 Normalized Effective Fin Deflection Comparison for Case 1 and Case 2

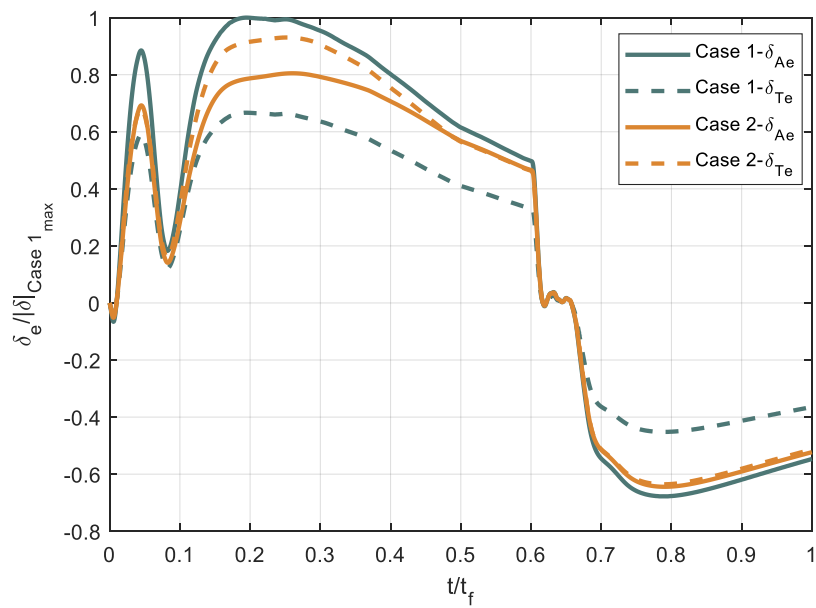


Figure 48 Normalized Elevator Deflection Comparison for Case 1 and Case 2

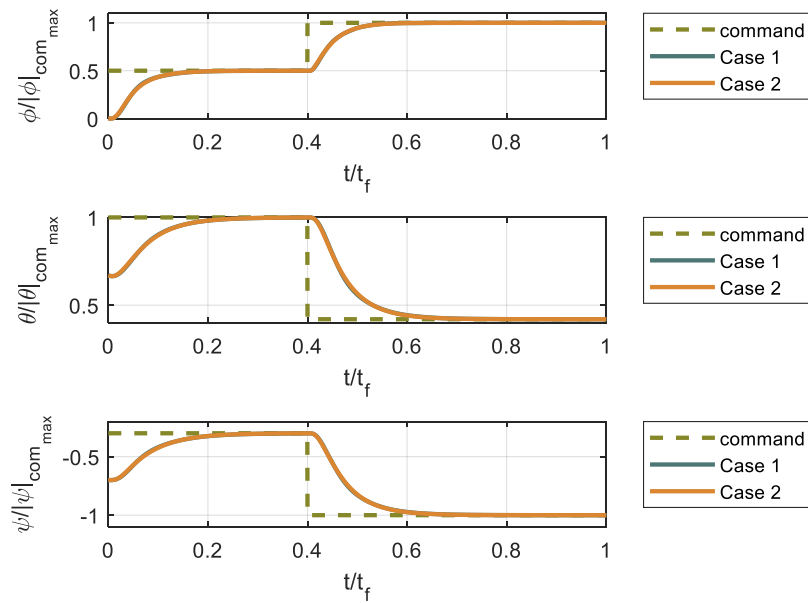


Figure 49 Normalized Euler Angle Tracking Performance Comparison for Case 1 and Case 2 for Attitude Autopilots

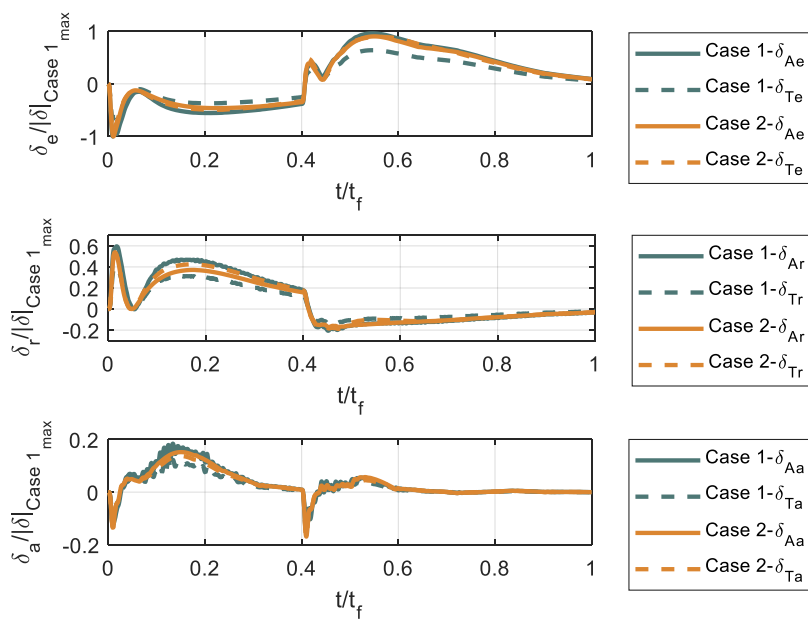


Figure 50 Normalized Effective Fin Deflection Comparison for Case 1 and Case 2 for Attitude Autopilot

It is observed that, although effective control commands vary evidently in Figure 50, mechanical coupling on the fins does not have a significant effect on the control performance as seen in Figure 46. Even this restriction may be better for the autopilot design since it is seen that the control commands are higher with the control allocation method. For higher commands, on the control variables these fin deflections tend to saturate faster compared to the mechanically coupled case. Saturation on fin deflection may cause performance degradation, which could be a future work.